UNIVERSIDAD NACIONAL AUTÓNOMA DE MEXICO
PROGRAMA DE POSGRADO EN ASTROFÍSICA
INSTITUTO DE ASTRONOMÍA
ASTROFÍSICA TEÓRICA

EVOLUCIÓN TÉRMICA DE ESTRELLAS DE NEUTRONES EN LA TEORÍA DE GRAVEDAD MODIFICADA $f(R) = R + aR^2$

TESIS

QUE PARA OPTAR POR EL GRADO DE:
MAESTRO EN CIENCIAS (ASTROFÍSICA)

PRESENTA:
MARTIN JAVIER NAVA CALLEJAS

TUTOR
DR. DANY PIERRE PAGE ROLLINET
INSTITUTO DE ASTRONOMÍA - UNAM

CIUDAD UNIVERSITARIA, CDMX, ENERO 2021.

To my family, for their unconditional love and support: my mom and dad, for their patience, wisdom advisement and encouragement to give always my best and make this a better world; my sister, for her observations and advisements, to Prof. Dany, for his invaluable support and mentorship, and for confirming my impressions that neutron stars are the most fascinating objects in the universe, to my friend Cristian, for discussing mathematics and introducing me into philosophy, and to Macarena, for her support and friendship.

Acknowledgements

I thank to my advisor Dr. Dany Page, for his support in the realization of this thesis and his mentorship in the study of the cooling process in neutron stars; to Drs. Margarita Rosado and Sergio Mendoza for being part of my Academic Comitee. Special thanks to: Dr. Mikhail Beznogov, for his help with Mathematica, and to Drs. Luisa Jaime and Sergio Mendoza for discussions and observations regarding the modified theories of gravity.

This work is part of the projects "Física y Astrofísica de Estrellas de Neutrones", CB-2014-1 No. 240512 financed by CONACYT, and "Física y Astrofísica de Estrellas de Neutrones" financed by UNAM-DGAPA, No. PAPIIT-IN109520, both under the direction of Dr.Dany Pierre Page Rollinet.

Contents

Abstract

The purpose of this thesis was to analyze the cooling process of NSs, under the assumption that their structure is described by a static, spherically symmetric metric and the gravity model $f(R) = R + \alpha R^2$, where $\alpha = 2.78 \times 10^X$ cm^2 with $X = 9, 10, 11, 12$. The energy and heat-transport equations can be incorporated into this scheme without further modifications.

For describing the composition of NSs, APR, MS-A1, MS-B1 and MS-C1 were the EoS chosen. The field equations were solved implementing a 4th Order Runge Kutta method in FORTRAN 77, while for the thermal evolution the relativistic code *NSCool* was employed.

Adressing in separate experiments the thickness of the light-elements envelope and superfluidity, it was possible to show that their role in the cooling process for this gravity model is practically the same as in GR, i.e. increasing the effective temperature and enhancing cooling at later times respectively. The Direct Urca gravitational mass-threshold is slightly modified even for $X = 12$, implying that the cooling of a 2 $M_\odot$ star as a 1.4 $M_\odot$ one is an EoS-dependent effect.

On the other hand, certain configurations of light-elements envelope and superfluidity allow to explain most of the observational data which this work is contrasted with, for the EoS chosen and $X \leq 12$, leaving them as viable models. Additionally, for $X = 9$ the results are numerically indistinguishable between both gravity models.

Resumen

El propósito de esta tesis fue analizar el proceso de enfriamiento de estrellas de neutrones, considerando que su estructura esta descrita por una métrica estática y esfericamente simétrica en el modelo de gravedad $f(R) = R + \alpha R^2$, donde $\alpha = 2.78 \times 10^X$ cm^2, con $X = 9, 10, 11, 12$. Las ecuaciones de energía y transporte de calor pueden ser incorporadas a este esquema sin mayores modificaciones.

Para describir la composición de las estrellas de neutrones, las ecuaciones de estado APR, MS-A1, MS-B1 y MS-C1 fueron seleccionadas e incorporadas en forma tabulada al conjunto de ecuaciones de estructura, las cuales se resolvieron implementando un método Runge-Kutta de Orden 4 en FORTRAN77. Por otra parte, la evolución térmica de los modelos estelares fue posible mediante el código relativista *NSCool*.

Considerando en experimentos separados el cambio en el espesor de elementos ligeros y la superfluidez, fue posible mostrar que su rol en el proceso de enfriamiento es el mismo tanto en αR^2 como en Relatividad General, es decir, incrementar la temperatura efectiva y acelerar el proceso de enfriamiento en etapas tardías, respectivamente. Por otra parte, el límite de masa gravitacional para el que ocurre el proceso de Urca directo (DUrca) es ligeramente modificado en $X = 12$, provocando que el enfriamiento de una estrella de 2 $M_\odot$ se asemeje al de una con 1.4 $M_\odot$, aunque este efecto depende de la Ecuación de Estado elegida.

Por otra parte, ciertas configuraciones de elementos ligeros y modelos de superfluidez permiten explicar una considerable cantidad de los objetos en la muestra considerada, con $X = 12$ y dependiendo además de la Ecuación de Estado seleccionada. Debido a ello, pueden ser calificados como modelos viables. Finalmente, los resultados para $X = 9$ son numéricamente indistinguibles con los predichos por Relatividad General.

Chapter 1

Introduction

The study of neutron stars can be seen as the tale of two cities: on the left, the structure of the spacetime itself, the scenario without which physics would be meaningless; on the right, the composition. The interactions between particles, and the asociated thermodynamic variables. The bridge between them was firmly stablished with the arrival of General Relativity (GR), the most successful theory of gravitation to date. Quoting John A. Wheeler, the physics behind this theory can be summarized as follows: "spacetime tells matter how to move; matter tells spacetime how to curve". Mathematically, these words can be translated into a set of second-order, non-linear differential equations commonly refered as Einstein's field equations,

$$G_{\mu\nu} = \frac{8\pi G}{c^4} T_{\mu\nu} \tag{1.1}$$

where $G = 6.671{\times}10^{-11}$ m^3 kg^{-1} s^{-2} is the universal constant of gravity, $c = 299792458$ m s^{-1} the speed of light in vacuum, $T_{\mu\nu}$ and $G_{\mu\nu}$ are the energy-momentum and Einstein tensors respectively, the first describing the energy-matter, while the second encloses the variations of the metric tensor $g_{\mu\nu}$ with respect to a coordinate system. Once an explicit form of $T_{\mu\nu}$ and a proposal for the metric tensor are given, their substitution in eq. 1.1 returns a set of differential equations which, after numerical or analytical solution, leads to a full knowledge of the structure of matter and space-time, or, more specifically, the star and its surrounding space time for the purpose of this thesis.

Equally important is the fact that Einstein's equation can be derived from a variational principle imposed over the action

$$S[g_{\mu\nu}] = \int_\Omega \sqrt{-g} d^4x \frac{1}{c} \left[\mathcal{L}_G + \mathcal{L}_M\right] \ , \tag{1.2}$$

where $\mathcal{L}_M$, $\mathcal{L}_G$ are the Lagrangian density functionals of the matter-energy and the gravitational field, respectively. The explicit form of the second is

$$\mathcal{L}_G = \frac{c^4}{16\pi G} \left(\Lambda + R\right) \tag{1.3}$$

with R the scalar curvature and Λ the *cosmological constant*, which in the study of neutron stars (NSs) is usually set to zero due to its small value.

Current constraints over Neutron Stars gravitational mass and radius have come from observational data of binary systems, gravitational waves, and from theoretical works on cooling. At the present time, $M_{\text{grav}} \in [1.4, 2.5]M_{\odot}$, $r_* \in [11, 13]$ km. [1, 2, 3]. The average density of a star can be estimated as $\langle\rho\rangle = 3M_{\text{grav}}/4\pi r_*^3 \in [10^{14}, 10^{15}]$ g/cm^3, closer to the symmetric nuclear density ($\sim 2\times10^{14}$ g/cm^3) and far above the neutron drip point ($\sim 10^{11}$ g/cm^3). This has been pointed as suggestive evidence that "exotic" particles such as K, π mesons or even deconfined quarks might exist in the core of the star. Currently, this is a topic of active researching and great interest for constraining the behaviour of matter under extreme conditions of pressure, temperature and magnetic field which are beyond the limits in Earth laboratories.

Let us mention that GR predictions do not limit themselves to just NS: together with black holes (BH) and white dwarfs (WD), they conform a subclass of stellar objects, referred to as *compact*. Observational data have revealed that these objects' gravitational mass and radius quotient GM/c^2r is high in comparison with other stars. Due to these facts, NS, BH and WD are placed in the *strong gravitational regime*. In clear contrast, objects like the Earth or the Sun correspond to the *weak gravitational regime*, where GR field equations *almost* reduce to pure Poisson's equation with the assumption $g_{\mu\nu} = \eta_{\mu\nu} + h_{\mu\nu}$, $|h_{\mu\nu}| \leq 1$, and $\eta_{\mu\nu}$ being Minkowski's metric. Considerable deviations near the surface of the object are expected to appear if the quotient mentioned above is not too little. For example, it is $\sim \mathcal{O}(10^{-10})$ for the Earth, while $\sim \mathcal{O}(10^{-4})$ for the Sun. This small difference with a pure *flat spacetime*, i.e. one that globally obeys Minkowski's metric, has been considered as solid evidence behind Mercury's precession and deviations of light beams from linear trajectories. In addition to these facts, the propagation of *gravitational waves* and their detection have paved the way to consider GR as a theory that successfully adress the weak-field limit.

By retaining the cosmological constant it is possible to study the Universe as an isolated system, where the matter-energy is distributed as follows: $\sim 30\%$ corresponds to baryonic and *dark* matter (DM), while the remaining $\sim 70\%$ is commonly refered as *dark energy* (DE) [4]. The adjective is earned for their absence of electromagnetic interactions, situation which have kept their exact nature as an open question and as a subject of active research. On the other hand, their presence is infered from the gravitational effects over baryonic matter, which can be observed in different wavelengths, thus placing constrains over the DM-DE theoretical models

From the exposition given above, one feels obliged to ask: if GR has succeeded in explaining a vast amount of observational phenomena, why bother looking for an extended or alternative gravitational theory? In first place, from pure scientific spirit a theory cannot be considered as *the right one* based on its correct predictions only. In particular, there could be alternate theories which lead to the same conclusions.

Indeed, experimental evidence must be the rule to measure whether the predictions are allowed or not. If these constrains are not too refined, there exists the possibility of waiting for future measurements which helps improving data.

In second place, an alternative theory of gravitation might help solving the *controversies* of GR, which are now enlisted:

1. A better explanation for DM and DE. GR succeeds explaining the Universe only if DM and DE are provided as sources. An alternative explanation would demand that these are related to pure gravitational aspects, not to a form of unknown energy-matter.

2. Strong-regime deviations. Since Solar Sytem test and gravitational waves belong to the weak-field regime, it has been argued that GR might not be capable of explaining the interior of NS and WD, the early times of the Universe and the exterior of BH. Another aspect to be enlisted is the recent observations of massive NS and BH, in comparison with existent models and data. In the particular case of NS, however, there is an uncertainty with the Equation of State: several proposals have led to an interval of possible masses, among which the observational data fit reasonably well.

3. Compatibility with the quantum regime From a purely theoretical analysis, GR does not belong to the class of renormalizable Lagrangian densities. Although the weak-field limit can be incorporated moderately well, the full Lagrangian is regarded as incomplete for a quantum approach. While this situation is not in conflict with astrophysical sources, GR must be considered as an *effective field theory* only, a point of view which enforces its interpretation as a *low energy theory*, relying in the addition of further terms to explain perturbative calculations for example. Surprisingly, it has been shown that the divergences arising from working with $\mathcal{L}_G \propto R$ only can be eliminated with the presence of higher powers of the scalar curvature.

Due to these facts, $f(R)$-model was introduced as an alternative for GR, usually refered as a "natural" modification for its premise: regarding $\Lambda + R$ as low-energy terms of a power series in R, this model proposes that the gravitational Lagrangian density might be a general function of the scalar curvature,

$$\mathcal{L}_G = \frac{c^4}{16\pi G} f(R) = \frac{c^4}{16\pi G} \sum_{n=0}^{\infty} a_n R^n \ . \tag{1.4}$$

The most immediate extension for compact objects, which has been studied for several years, is $f(R) = R + \alpha R^2$ where α is a free parameter until observational constrains are taken into account. Being an extension based on the scalar curvature only, the imposition of a variational principle yields a different set of equations of motion. While the structure of the stars, arising from numerical solutions, have been intensively studied along the years (in the strong and weak field limits), together with the geodesic equations for particles and even gravitational waves, the cooling

process of such stars is a novelty in the field. From one side, the incorporation of radiative transport equations might seem non-immediate for alternative theories of gravitation, in particular for those admitting non-conservation of the energy-momentum tensor. In addition, modifying the equations of motion for the metric tensor implies that, if numerical precision is desired in the crust and envelope of the star, the cooling code must incorporate these variations due to the fact that the local surface gravity might not be the same in both gravitational theories. In that sense, the $f(R) = R + \alpha R^2$ model (also adressed as quadratic for the rest of this work) offers the advantage of incorporating to its scheme the well-known radiative transport equations in a natural way, and the possibility of working with GR cooling codes due to the numerical proximity of the local surface gravity in both theories. The purpose of the present work is to analyze the cooling process of NSs under the assumption that the quadratic model of gravitation describes the structure of these objects, employing the numerical code `NSCool` [56].

The structure of this work is the following: Chapter 2 describes the most relevant aspects of differential geometry related to pseudo-Riemmannian (Lorentzian) manifolds, which is the basis for Chapter 3 where the field equations of the αR^2 model are discussed in detail. In Chapter 4, the composition of neutron stars, as well as the cooling process and the equations of energy and heat-transport are discussed. The numerical results of stellar structure and the cooling process are presented in Chapters 5 and 6, respectively. The equations, as well as the boundary conditions and the software employed for solving them are introduced. The discussion of the results and the conclusions can be found in the last Chapter. In this work, the $(-,+,+,+)$ metric signature is adopted, as well as Einstein sum convention of repeated indices.

Chapter 2

A Brief Look at Pseudo-Riemannian Manifolds

> "*And yet [...] there are mathematicians of extraordinary genius who doubt the whole universe [...] was created only according to Euclidean geometry [...]*"
>
> *F.Dostoievsky*

Modern differential geometry is at the core of most theories of gravitation, due to its descriptive capability and mathematical elegance: spacetime is represented as a differentiable manifold with a metric tensor which is not always positive defined, a fact that physically translates into the existence of timelike, spacelike or null separation of events. Since Riemann's theorem remains valid for such manifolds, they are usually referred as *pseudo-Riemmanian* or *Lorentzian*, regardless of the signature convention, i.e. the number of positive and negative terms in the diagonal of the metric tensor, in matrix form. The purpose of this chapter is to introduce the most indispensable elements of pseudo-Riemannian geometry for describing torsion-free spacetimes, and give a self-consistent exposition of the concepts and geometric elements which conforms the basis for the $f(R)$ gravity model. In particular, due to the confusions in notations and conventions in the literature, which have a significant impact in quantities such as $\text{sign}(\alpha)$.

In section 1 we review the definitions of manifolds, derivation and integration. In section 2, several results concerning the Ricci tensor are proven. Section 3 presents the static and spherically symmetric metric (SSS metric) along with useful propositions based on it. Here, the Schwarzschild's metric arises as a particular and important case. The equations of the geodesic curve are reviewed in Section 4, while

Section 5 addresses the notions of Lagrangian density, the action and the energy-momentum tensor. We finish with a brief mention of conformal transformations.

Throughout the rest of this work, the $(-,+,+,+)$ metric signature convention is employed.

2.1 Definitions and propositions

An n-dimensional, C^∞ real manifold M is a set which, together with a collection of subsets $\{O_\alpha\}$ satisfy the following properties:
1. $\forall p \in M$ there exist at least one O_α such that $p \in O_\alpha$. The whole collection of substes is designated as a cover of M.
2. $\forall \alpha$, there exists an injective and surjective map $\psi_\alpha : O_\alpha \to U_\alpha$, where $U_\alpha \subset \mathbb{R}^n$ is an open subset. The collection of maps are called charts or coordinate systems. The notion of a differentiable function is given as follows: let M, M' be two manifolds of dimensions n, n', and $\{\psi_\alpha\}$, $\left\{\psi'_\beta\right\}$ their respective coordinate systems. A map $f : M \to M'$ is said C^∞ if for each α, β the composition

$$\psi'_\beta \; o \; f \; o \; \psi_\alpha^{-1} : U_\alpha \subset \mathbb{R}^n \to U'_\beta \subset \mathbb{R}^{n'} \tag{2.1}$$

is C^∞ in the multi-variable calculus sense.
A metric $\mathbf{g}$ on a manifold M is a tensor field of type (0,2) which satisfy the following properties:
1. Symmetry For any two vectors, $\mathbf{g}(A_1,A_2) = \mathbf{g}(A_2, A_1)$,
2. If $\mathbf{g}(A,A_3)= 0$ for all vectors, then $A_3 = 0$.
It is always possible to find an orthonormal basis of vectors such that

$$\mathbf{g}(A_{mu}, A_\mu) = \pm 1 \quad , \quad \mathbf{g}(A_\mu, A_\nu) = 0 \;\; (\mu \neq \nu) \tag{2.2}$$

holds. The number of + and - signs is called the *signature* of the metric. For pure positive ones, the metric is said *Riemannian*, while the presence of a minus sign defines a *Lorentzian metric*.
Given $g_{\mu\nu}$, it is possible to introduce the notion of a proper infinitesimal length or interval,

$$ds^2 = g_{\mu\nu} dx^\mu dx^\nu \ , \tag{2.3}$$

which is *not* always possitive defined. This fact motivates the following definitions: an interval is said *timelike* if $ds^2 < 0$, *spacelike* if $ds^2 > 0$ and *null* if $ds^2 = 0$.
For the rest of this work, the last ones are the only kind of metrics adressed, and the convention $(-,+,+,+,\ldots)$, where the first minus refers to the x^0 coordinate, is adopted. In addition, the pair $(M, g_{\mu\nu})$ conforms a *spacetime*.

At this point it is suitable to introduce the notion of *flatness*: if

$$[g_{\mu\nu}] = [\eta_{\mu\nu}] = \begin{pmatrix} -1 & 0 & 0 & 0 \\ 0 & 1 & 0 & 0 \\ 0 & 0 & 1 & 0 \\ 0 & 0 & 0 & 1 \end{pmatrix} .$$

is the *global* metric tensor for some manifold M, we define such spacetime as flat. On the other hand, if this metric is valid only for some points in M, we refer to these regions as *locally flat*. In principle it is possible to construct regions where the first derivatives of the metric tensor vanish, but the second order do not. This is the basis of the *local - flatness theorem*, which we do not prove but assume as valid for the rest of the book.

2.1.1 Derivation and integration

A *covariant derivative* ∇ is a map which takes differentiable tensor fields of type (k, l) into tensor fields of type $(k, l + 1)$, and satisfies the following properties:
1. Linearity If $\mathbf{A}$ and $\mathbf{B}$ are tensor fields, and $c_1, c_2 \in \mathbb{R}$ fixed numbers,

$$\nabla (c_1\mathbf{A} + c_2\mathbf{B}) = c_1\nabla\mathbf{A} + c_2\nabla\mathbf{B} , \tag{2.4}$$

2. Leibnitz rule:

$$\nabla(\mathbf{AB}) = \nabla\mathbf{A}\ \mathbf{B} + \mathbf{A}\nabla\mathbf{B} , \tag{2.5}$$

3. Commutativity with contraction:

$$\nabla_\mu \left(A^{\ldots\beta\ldots}{}_{\ldots\beta\ldots}\right) = \nabla_\mu A^{\ldots\beta\ldots}{}_{\ldots\beta\ldots} , \tag{2.6}$$

4. Torsion-free: Let f be a scalar function. Thus,

$$\nabla_\alpha\nabla_\beta f = \nabla_\beta\nabla_\alpha f . \tag{2.7}$$

A metric tensor naturally determines a covariant derivative which, in combination with the last property, leads to the Levi-Civitta connection

$$\Gamma^\mu{}_{\alpha\beta} = \frac{1}{2} g^{\mu\nu} \left(\partial_\alpha g_{\beta\nu} + \partial_\beta g_{\alpha\nu} - \partial_\nu g_{\alpha\beta}\right) \tag{2.8}$$

which is symmetric in the lower indices. In addition, the torsion-free property guarantees that

$$\nabla_\mu g_{\alpha\beta} = 0 . \tag{2.9}$$

For vector and dual vector fields, the covariant derivative is written as

$$\nabla_\mu A^\beta = \partial_\mu A^\beta + \Gamma^\beta{}_{\mu\nu} A^\nu , \ \nabla_\mu A_\nu = \partial_\mu A_\nu - \Gamma^\epsilon{}_{\mu\nu} A_\epsilon . \tag{2.10}$$

It is possible to introduce the D'Alembertian operator as

$$\Box = \nabla^\mu \nabla_\mu = \frac{1}{\sqrt{-g}} \left[\frac{\partial}{\partial x^\nu} \left(\sqrt{-g} g^{\mu\nu} \frac{\partial}{\partial x^\mu} \right) \right] = \frac{1}{\sqrt{-g}} \partial_\nu \left[\sqrt{-g} g^{\mu\nu} \partial_\mu \right] . \tag{2.11}$$

Clearly, in flat spacetime this reduces to the well known expression $\Box = \partial_\mu \partial^\mu$. Although the connection is symmetric on the lower indices, in general is not true that $\nabla_\mu \nabla_\nu A_\beta = \nabla_\nu \nabla_\mu A_\beta$. On the other hand, for a differentiable dual vector there exist a tensor field $R^\alpha{}_{\mu\nu\beta}$ such that

$$\nabla_\mu \nabla_\nu A_\beta - \nabla_\nu \nabla_\mu A_\beta = R^\alpha{}_{\mu\nu\beta} A_\alpha \ . \tag{2.12}$$

holds. This is the *Riemann tensor*, and in terms of the Levi-Civitta connection adopts the form

$$R^\alpha{}_{\beta\mu\nu} = \partial_\mu \Gamma^\alpha{}_{\beta\nu} - \partial_\nu \Gamma^\alpha{}_{\beta\mu} + \Gamma^\alpha{}_{\sigma\mu} \Gamma^\sigma{}_{\beta\nu} - \Gamma^\alpha{}_{\sigma\nu} \Gamma^\sigma{}_{\beta\mu} \ . \tag{2.13}$$

It is possible to construct a second rank symmetric tensor from the contraction of the first and third indices,

$$R_{\mu\nu} = R^\alpha{}_{\mu\alpha\nu} \ . \tag{2.14}$$

This is refered as the *Ricci tensor*, and its trace $R = g^{\mu\nu} R_{\mu\nu}$ is usually called the scalar curvature. Finally, from the Bianchi identities for the Riemann tensor it is possible to deduce a divergence free, second rank symmetric tensor, known as Einstein's:

$$G_{\mu\nu} = R_{\mu\nu} - \frac{1}{2} g_{\mu\nu} R \ . \tag{2.15}$$

Integration Let M be an n-dimensional manifold. A differential p-form is a totally anti-symmetric tensor of type $(0, p)$, $\omega_{\alpha_1,\ldots,\alpha_p}$. For simplicity, we shall denote it as $\bar{\omega}$.

Let $U \subset M$ be an open set covered by a single coordinate system ψ. To define the integration of a measurable n-form field $\bar{\alpha}$ over an orientable manifold, we expand both the orientation and the n-form in this coordinate system,

$$\bar{\epsilon} = h \ dx^1 \wedge \ldots \wedge dx^n \ , \quad \bar{\alpha} = a \ dx^1 \wedge \ldots \wedge dx^n \ , \tag{2.16}$$

with a and h functions of $(x^1, \ldots, x^n)$. For $h > 0$, the coordinate system is refered as right-handed and the integration of $\bar{\alpha}$ over U is defined as

$$\int_U \bar{\alpha} := \int_{\psi[U]} a dx^1 \ldots dx^n \ , \tag{2.17}$$

where the integration is the usual Riemann or Lebesgue in $\mathbb{R}^n$. If the coordinate system is left-handed, $h < 0$, a minus sign is added at the front of the expression. For integrations of p-forms, the most important result which is needed here is:

Stokes' theorem: let N be an n-dimensional oriented manifold with boundary ∂N, and $\bar{\alpha}$ an $n-1$-form on M which is C^1. Then

$$\int_{\mathrm{int}(N)} d\bar{\alpha} = \int_{\partial N} \bar{\alpha} \ . \tag{2.18}$$

Having discussed integrations of p-forms, we can now introduce the integration of functions on orientable manifolds through the existence of a volume element $\bar{v}$, which guarantees that

$$\int_M f := \int_M f\bar{v} \tag{2.19}$$

makes sense. For a manifold with a metric $g_{\alpha\beta}$, the natural volume element is

$$\bar{v} = \sqrt{-g} dx^1 \dots dx^n \ . \tag{2.20}$$

where g is the *determinant* of the metric tensor in matrix form.
With the aid of this volume element, it is possible to stablish a "Gauss Law" for integration over manifolds, starting from Stokes' theorem: if V^β is a C^1 vector field,

$$\int_{\mathrm{int}(N)} \nabla_\alpha V^\alpha = \int_{\partial N} n_\alpha V^\alpha \ , \tag{2.21}$$

where n_α is a unit normal vector to ∂N. The measure on the right hand side of this expression can be written as

$$\bar{\sigma} = \sqrt{\gamma} dx^1 \dots dx^{n-1} \ , \tag{2.22}$$

where γ is the determinant of the metric tensor restricted to vectors tangent to ∂N. In the particular case of a spacetime $(M, g_{\alpha\beta})$, it is usual to encounter these kind of integrals where the boundary is related to the time coordinate, rendering γ as the determinant of the spatial part of the metric.

2.2 Useful theorems

Having acquinted the basic notions of derivation and integration over manifolds, it is time to introduce some of the results which are indispensable for the deduction of the equations of motion in the next Chapter. In order to keep a fluid discussion, the proofs can be found in Appendix A, as well as the properties of the *inverse of the metric*, i.e. the (2,0) rank tensor $g^{\mu\nu}$ which satisfies

$$g_{\mu\nu} g^{\nu\alpha} = \delta^\alpha_{\ \mu}. \tag{2.23}$$

for all α, ν, and the *determinant of the metric*, that we found early in this Chapter and which can be written in terms of the 4-dimensional Levi-Civitta symbol as

$$g := \epsilon^{\alpha\beta\gamma\delta} g_{\alpha 0} g_{\beta 1} g_{\gamma 2} g_{\delta 3} \ . \tag{2.24}$$

Proposition 1: Palatini's Identity Let $R_{\mu\nu} = R^{\alpha}{}_{\mu\alpha\nu}$ be the Ricci tensor and ∇_μ the torsion-free covariant derivative. Then

$$\delta R_{\mu\nu} = \nabla_\alpha(\delta\Gamma^{\alpha}{}_{\mu\nu}) - \nabla_\nu(\delta\Gamma^{\gamma}{}_{\mu\gamma}) \tag{2.25}$$

Corollary 1: Palatini's Integral Let $R_{\mu\nu}$ be the Ricci tensor, ∇_μ the torsion-free covariant derivative. If $\delta\Gamma^{\mu}{}_{\alpha\beta}$ is identically zero for all μ, α, β at the boundary of some closed $\Omega \subset M$, then

$$I = \int_\Omega \sqrt{-g} g^{\mu\nu} \delta R_{\mu\nu} d^4x = 0 \tag{2.26}$$

Observation: From the previous proof, the following identity holds

$$g^{\mu\nu}\delta R_{\mu\nu} = \nabla_\sigma W^\sigma \quad . \tag{2.27}$$

In chapter 4, we shall encounter this expression multiplied by a differentiable function. In general, such product does not vanish under integration. It is therefore necessary to write an expression for W^σ in terms of the metric tensor, its inverse and possibly their derivatives. This is the main purpose of the following

Proposition 2: In a locally flat coordinate system, the 4-vector

$$W^\sigma = g^{\mu\nu}\delta\Gamma^{\sigma}{}_{\mu\nu} - g^{\mu\sigma}\delta\Gamma^{\nu}{}_{\mu\nu}$$

can be written as

$$W^\sigma = \partial^\sigma(g_{\mu\nu}\delta g^{\mu\nu}) - \partial^\mu(g_{\mu\nu}\delta g^{\sigma\nu}) \ . \tag{2.28}$$

At our disposal are the necessary elements to prove the following:

Theorem 1: Let A be a scalar and differenciable function, $\Omega \subset M$ a closed set. If $\delta g^{\mu\nu}$, $\delta\Gamma^{\alpha}{}_{\mu\nu}$ are identically zero for all α, μ, ν at $\partial\Omega$, then

$$\int_\Omega d^4x\sqrt{-g}Ag^{\mu\nu}\delta R_{\mu\nu} = \int_\Omega d^4x\sqrt{-g}\delta g^{\mu\nu}\left[g_{\mu\nu}\partial^\sigma\partial_\sigma A - \partial_\mu\partial_\nu A\right] \ . \tag{2.29}$$

Observation: In order to be a tensorial identity, valid for any system of coordinates, the differentials are promoted to its covariant counterparts, that is

$$J = \int_\Omega d^4x\sqrt{-g}\delta g^{\mu\nu}\left[g_{\mu\nu}\Box A - \nabla_\mu\nabla_\nu A\right] \tag{2.30}$$

2.3 Static and spherically symmetric (SSS) metric

Let (ct, r, θ, ϕ) be a 4-dimensional spherical coordinate system.The SSS metric is defined by

$$[g_{\alpha\beta}] = \begin{pmatrix} -e^{2\Phi} & 0 & 0 & 0 \\ 0 & e^{2\Lambda} & 0 & 0 \\ 0 & 0 & r^2 & 0 \\ 0 & 0 & 0 & r^2 \sin^2\theta \end{pmatrix}$$

where Φ and Λ are functions of the radial coordinate only.
By means of direct computation, it is possible to show that the scalar curvature for this metric is

$$R = \frac{2(1-e^{-2\Lambda})}{r^2} - 2e^{-2\Lambda}\left[\frac{2}{r}(\Phi' - \Lambda') + \Phi'' - \Phi'\Lambda' + (\Phi')^2\right] \tag{2.31}$$

A complete list of non-vanishing $\Gamma^{\mu}_{\alpha\beta}$, $G_{\mu\nu}$ elements is provided in Appendix B.
For a radial-dependent and differentiable function A, it is easy to show that:
Proposition 3:

$$\Box A = e^{-2\Lambda}\left[\frac{d^2A}{dr^2} + \left(\frac{2}{r} + \frac{d\Phi}{dr} - \frac{d\Lambda}{dr}\right)\frac{dA}{dr}\right] \tag{2.32}$$

Proof. Since A depends only on r and the off-diagonal elements of the metric tensor are zero,

$$\Box A = \frac{1}{\sqrt{-g}}\left[\frac{\partial}{\partial x^\nu}\left(\sqrt{-g}g^{r\nu}\frac{\partial A}{\partial r}\right)\right] = \frac{1}{\sqrt{-g}}\left[\frac{\partial}{\partial r}\left(\sqrt{-g}g^{rr}\frac{\partial A}{\partial r}\right)\right] .$$

Expanding the right hand side,

$$\Box A = \frac{1}{\sqrt{-g}}\left[\sqrt{-g}g^{rr}\frac{d^2A}{dr^2} + \sqrt{-g}\frac{\partial g^{rr}}{\partial r}\frac{dA}{dr} + \frac{\partial\sqrt{-g}}{\partial r}g^{rr}\frac{dA}{dr}\right] .$$

Clearly,

$$\frac{\partial g^{rr}}{\partial r} = -2\frac{d\Lambda}{dr}e^{-2\Lambda} \quad , \quad \frac{\partial\sqrt{-g}}{\partial r} = \left(\frac{2}{r} + \frac{d\Phi}{dr} + \frac{d\Lambda}{dr}\right)\sqrt{-g} .$$

Thus

$$\Box A = \frac{1}{\sqrt{-g}}\left[\sqrt{-g}e^{-2\Lambda}\frac{d^2A}{dr^2} - 2\sqrt{-g}\frac{d\Lambda}{dr}e^{-2\Lambda}\frac{dA}{dr} + e^{-2\Lambda}\sqrt{-g}\left(\frac{2}{r} + \frac{d\Phi}{dr} + \frac{d\Lambda}{dr}\right)\frac{dA}{dr}\right] .$$

Simplifying terms, we conclude that

$$\Box A = e^{-2\Lambda}\left[\frac{d^2A}{dr^2} + \left(\frac{2}{r} + \frac{d\Phi}{dr} - \frac{d\Lambda}{dr}\right)\frac{dA}{dr}\right] .$$

■

Proposition 4:

$$\nabla_0 \nabla_0 A = -e^{2(\Phi-\Lambda)} \frac{d\Phi}{dr} \frac{dA}{dr} \tag{2.33}$$

$$\nabla_r \nabla_r A = \frac{d^2 A}{dr^2} - \frac{d\Lambda}{dr} \frac{dA}{dr} \tag{2.34}$$

Proof. For a scalar and radial-dependent function, we have

$$\nabla_\mu \nabla_\nu A = \partial_\mu \partial_\nu A - \Gamma^\alpha{}_{\mu\nu} \partial_\alpha A = \partial_\mu \partial_\nu A - \Gamma^r{}_{\mu\nu} \partial_r A \ .$$

For $\mu = \nu = 0$, we must consider that

$$\Gamma^r{}_{00} = e^{2(\Phi-\Lambda)} \frac{d\Phi}{dr} \ ,$$

thus

$$\nabla_0 \nabla_0 A = -e^{2(\Phi-\Lambda)} \frac{d\Phi}{dr} \frac{dA}{dr} \ . \tag{2.35}$$

On the other hand, if $\mu = \nu = r$ we know that

$$\Gamma^r{}_{rr} = \frac{d\Lambda}{dr} \ .$$

After substitution, we conclude that

$$\nabla_r \nabla_r A = \frac{d^2 A}{dr^2} - \frac{d\Lambda}{dr} \frac{dA}{dr} \ .$$

■

2.3.1 Schwarzschild's metric

The particular case

$$\Lambda(r) + \Phi(r) = 0 \quad , \quad e^{2\Phi(r)} = 1 - \frac{2GM}{c^2 r} \tag{2.36}$$

where G is the gravitational constant, c the speed of light in vacuum and M the gravitational mass of a spherical object, is known as Schwarzschild's metric. According to Birkhoff's theorem, if GR is the right theory of gravitation the uniqueness of this metric for describing the exterior of a compact object is guaranteed. This might not be the case if an alternative theory is considered, though. On the other hand, its success on describing spacetime around a NS and the Sun (either in this formal expression or in the weak-field limit) have led to the additional supposition that this metric should be recovered at very long distances from a spherical object under an alternative gravity model.

Some basic properties are:
1. The derivatives of the functions Λ, Φ satisfy

$$\frac{d\Lambda}{dr} = -\frac{d\Phi}{dr} \tag{2.37}$$

2. The scalar curvature is equal to zero.

Proof. In the definition of the scalar curvature, we make the substitutions $\Phi' = -\Lambda'$, $\Phi'' = -\Lambda''$:

$$R = \frac{2}{r^2}(1 - e^{-2\Lambda}) - 2e^{-2\Lambda}\left[2(\Lambda')^2 - \Lambda'' - \frac{4}{r}\Lambda'\right].$$

But

$$\Lambda' = -\frac{1}{2}\left[\frac{1}{1 - \frac{2GM}{c^2 r}}\right]\frac{2GM}{c^2 r^2} = -\frac{GM}{c^2 r^2}e^{2\Lambda}$$

$$\Lambda'' = \frac{2GM}{c^2 r^2}e^{2\Lambda}\left(\frac{1}{r} - \Lambda'\right) .$$

Thus

$$R = \frac{4GM}{c^2 r^3} - 2e^{-2\Lambda}\left[-\frac{2GM}{c^2 r^2}e^{2\Lambda}\left(\Lambda' - \frac{2}{r}\right) + \frac{2GM}{c^2 r^2}\left(\Lambda' - \frac{1}{r}\right)e^{2\Lambda}\right]$$

$$R = \frac{4GM}{c^2 r^3} - \frac{4GM}{c^2 r^2}\left[-\Lambda' + \frac{2}{r} + \Lambda' - \frac{1}{r}\right]$$

$$R = \frac{4GM}{c^2 r^3} - \frac{4GM}{c^2 r^3} = 0$$

■

2.4 Geodesic motion

The combination of integration with the infinitesimal interval is the basis to define the notion of proper distance between two points in a manifold, connected by a curve which is affine parametrized with λ. That is,

$$S = \int ds = \int_{\lambda_a}^{\lambda_b} \sqrt{g_{\alpha\beta}\frac{dx^\alpha}{d\lambda}\frac{dx^\beta}{d\lambda}}\, d\lambda \tag{2.38}$$

Assuming that S is a functional of the metric tensor, it is possible to show, by means of a variational principle, that the coordinates of the curve with extremal length, considering the Levi-Civitta connection, satisfy

$$\frac{d^2 x^\alpha}{d\lambda^2} + \Gamma^\alpha_{\ \mu\nu}\frac{dx^\mu}{d\lambda}\frac{dx^\nu}{d\lambda} = 0 \tag{2.39}$$

These are commonly refered as the equations for the geodesic curve.
For a particle of mass m, it is suitable to re-write these equations in terms of its four-momentum p^μ and its proper time τ,

$$p^\mu = mU^\mu = m\frac{dx^\mu}{d\tau} \ ,$$

where U^μ denotes its four-velocity, $U^\mu U_\mu = -c^2$. Indeed,

$$m\frac{dp^\mu}{d\tau} + \Gamma^\mu{}_{\alpha\beta}p^\alpha p^\beta = 0. \tag{2.40}$$

Regarding massless particles such as photons, which move along null intervals, it is possible to show that the wavenumber 4-vector, by means of a variational principle, obbeys the equations for the geodesic curve, this time in the form

$$\frac{dk^\alpha}{d\lambda} + \Gamma^\alpha{}_{\mu\nu}k^\mu k^\nu = 0 \ , \tag{2.41}$$

where λ cannot be chosen as the proper-time due to the absence of such concept for massless particles.
Either for p^μ or k^μ, we have a set of non-linear differential equations which, in order to be solved, requires the explicit form of the metric functions.
Similar to the classical, non-relativistic mechanics, it would be suitable to find constant quantities along geodesic curves in order to simplify the number of equations to solve. The existence of such numbers for curved manifolds is guaranteed from the following
Theorem 3: If the metric tensor is independent of some fixed coordinate x^σ, i.e. $\partial_\sigma g_{\alpha\beta} = 0$ for all α, β, then p_ϵ is a constant of the motion along a geodesic curve.

Proof. Since $p^\mu = g^{\mu\nu}p_\nu$, in eq. 2.40 we have

$$mg^{\mu\nu}\frac{dp_\nu}{d\tau} = -mp_\nu\frac{dg^{\mu\nu}}{d\tau} - \Gamma^\mu{}_{\alpha\beta}p^\alpha p^\beta.$$

But, from the four-velocity of the particle we see that

$$U^\mu\partial_\mu = \frac{dx^\mu}{d\tau}\frac{\partial}{\partial x^\mu} = \frac{d}{d\tau} \Rightarrow \ p^\mu\partial_\mu = m\frac{d}{d\tau} \ ,$$

thus

$$mg^{\mu\nu}\frac{dp_\nu}{d\tau} = -p_\nu p^\gamma\partial_\gamma g^{\mu\nu} - \Gamma^\mu{}_{\alpha\beta}p^\alpha p^\beta.$$

A contraction with $g_{\mu\epsilon}$ leads to

$$mg_{\mu\epsilon}g^{\mu\nu}\frac{dp_\nu}{d\tau} = -g_{\mu\epsilon}p_\nu p^\gamma\partial_\gamma g^{\mu\nu} - g_{\mu\epsilon}\Gamma^\mu{}_{\alpha\beta}p^\alpha p^\beta$$

$$m\frac{dp_\epsilon}{d\tau} = p^\mu p^\gamma \partial_\gamma g_{\mu\epsilon} - g_{\mu\epsilon}\Gamma^\mu{}_{\alpha\beta}p^\alpha p^\beta \ ,$$
$$g_{\mu\epsilon}\Gamma^\mu{}_{\alpha\beta} = \frac{1}{2}(\partial_\alpha g_{\beta\epsilon} + \partial_\beta g_{\alpha\epsilon} - \partial_\epsilon g_{\alpha\beta}).$$

Back to the full expression,

$$m\frac{dp_\epsilon}{d\tau} = p^\mu p^\gamma \partial_\gamma g_{\mu\epsilon} - \frac{1}{2}(\partial_\alpha g_{\beta\epsilon} + \partial_\beta g_{\alpha\epsilon} - \partial_\epsilon g_{\alpha\beta})p^\alpha p^\beta.$$

Notice that under a contraction with $p^\alpha p^\beta$ the first terms in the parenthesis are the same. Besides, after relabeling indices if follows that

$$m\frac{dp_\epsilon}{d\tau} = p^\mu p^\gamma \partial_\gamma g_{\mu\epsilon} - p^\mu p^\gamma \partial_\gamma g_{\mu\epsilon} + \frac{1}{2}\partial_\epsilon g_{\alpha\beta}p^\alpha p^\beta.$$

Simplifying,

$$m\frac{dp_\epsilon}{d\tau} = \frac{1}{2}p^\alpha p^\beta \partial_\epsilon g_{\alpha\beta}.$$

This expression is valid for all the coordinates, thus we can pick $x^\epsilon = x^\sigma$. By hipothesis, the metric is independent of this coordinate, so

$$m\frac{dp_\sigma}{d\tau} = 0.$$

Therefore, p_σ is a constant quantity along the geodesic curve. ■

While this theorem is suitable for an immediate physical interpretation, it is worth mentioning that a more formal approach consists on defining a Lie derivative, imposing the restriction of being null for the metric tensor, and then deducing that there are some vectors ξ^μ, which guarante that along a geodesic curve, $p^\alpha \xi_\alpha$ are constant quantities. These are the well-known Killing vectors, which satisfy the following equation

$$\nabla_\alpha \xi_\beta + \nabla_\beta \xi_\alpha = 0 \ . \tag{2.42}$$

2.5 On the Lagrangian density and the action

Nowadays, the description of a system or field ϕ through a Lagrangian density $\mathcal{L}$ plays a key role for studying its quantum and gravitational aspects. For the latest, the imposition of a stationary state over the action functional

$$S = \int_\Omega \sqrt{-g}d^4x \ \frac{1}{c}\mathcal{L} \tag{2.43}$$

i.e. $\delta S = 0$, and null variations of the fields at the boundary of Ω, leads to the equations of motion for the fields, also refered as the *Euler - Lagrange equations in curved*

spacetime, which we now proceed to deduce, assuming that $\sqrt{-g}$ is independent of ϕ.

By performing a variation of S and employing integration by parts,

$$\delta S = \int_\Omega d^4x\sqrt{-g}\frac{1}{c}\left[\frac{\delta\mathcal{L}}{\delta\phi}\delta\phi + \frac{\delta\mathcal{L}}{\delta(\partial_\alpha\phi)}\delta(\partial_\alpha\phi)\right] ,$$

$$\delta S = \int_\Omega d^4x\sqrt{-g}\frac{1}{c}\left[\frac{\delta\mathcal{L}}{\delta\phi}\delta\phi + \frac{\delta\mathcal{L}}{\delta(\partial_\alpha\phi)}\partial_\alpha(\delta\phi)\right] ,$$

$$\delta S = \int_\Omega d^4x\sqrt{-g}\frac{1}{c}\left\{\frac{\delta\mathcal{L}}{\delta\phi}\delta\phi + \frac{1}{\sqrt{-g}}\partial_\alpha\left[\sqrt{-g}\frac{\delta\mathcal{L}}{\delta(\partial_\alpha\phi)}\delta\phi\right] - \frac{1}{\sqrt{-g}}\partial_\alpha\left[\sqrt{-g}\frac{\delta\mathcal{L}}{\delta(\partial_\alpha\phi)}\right]\delta\phi\right\} .$$

From the divergence theorem,

$$\int_\Omega d^4x\sqrt{-g}\frac{1}{c}\left\{\frac{1}{\sqrt{-g}}\partial_\alpha\left[\sqrt{-g}\frac{\delta\mathcal{L}}{\delta(\partial_\alpha\phi)}\delta\phi\right]\right\} = \int_{\partial\Omega}\sqrt{\gamma}d^3x\frac{1}{c}\left[\sqrt{-g}\frac{\delta\mathcal{L}}{\delta(\partial_\alpha\phi)}\delta\phi\right]\Big|_{\partial\Omega} n_\alpha = 0 . \tag{2.44}$$

Thus

$$\delta S = \int_\Omega d^4x\sqrt{-g}\frac{1}{c}\delta\phi\left\{\frac{\delta\mathcal{L}}{\delta\phi} - \frac{1}{\sqrt{-g}}\partial_\alpha\left[\sqrt{-g}\frac{\delta\mathcal{L}}{\delta(\partial_\alpha\phi)}\right]\right\} . \tag{2.45}$$

By setting $\delta S = 0$,

$$\frac{1}{\sqrt{-g}}\partial_\alpha\left[\sqrt{-g}\frac{\delta\mathcal{L}}{\delta(\partial_\alpha\phi)}\right] - \frac{\delta\mathcal{L}}{\delta\phi} = 0 . \tag{2.46}$$

Remarkable examples of Lagrangian densities and equations of motion are:
1. Scalar field. Given

$$\mathcal{L}[\phi,\partial_\mu\phi] = -\frac{1}{2}g^{\mu\nu}\partial_\mu\phi\partial_\nu\phi - \frac{1}{2}m^2\phi^2 - V(\phi) \tag{2.47}$$

with $V(\phi)$ a potential, the equations of motion are

$$\left[\Box - m^2\right]\phi = \frac{dV}{d\phi} . \tag{2.48}$$

The case $dV/d\phi = 0$ and $g_{\mu\nu} = \eta_{\mu\nu}$ is known as the *Klein-Gordon* equation, commonly employed for describing fields with zero or integer spin. In this picture, m is usually refered as the *bare* mass, related to the *physical* mass upon renormalization.
2. Electromagnetic field. In the absence of 4-currents,

$$\mathcal{L}_{\text{EM}} = -\frac{1}{4}F_{\mu\nu}F^{\mu\nu} , \tag{2.49}$$

where $F_{\mu\nu} = \partial_\mu A_\nu - \partial_\nu A_\mu$ is the Faraday tensor and A_μ the electromagnetic 4-potential, the equations of motion are

$$\frac{1}{\sqrt{-g}}\partial_\alpha\left[\sqrt{-g}F^{\alpha\beta}\right] = 0 . \tag{2.50}$$

The ϕ-independence restriction over $\sqrt{-g}$ must be removed if equations of motion for $g_{\mu\nu}$ are expected to arise from a variational principle. Indeed, we have:

$$\delta S = \int_\Omega \sqrt{-g} d^4x \delta g^{\mu\nu} \frac{1}{2c} \left[\frac{2}{\sqrt{-g}} \frac{\delta(\sqrt{-g}\mathcal{L})}{\delta g^{\mu\nu}} \right] . \tag{2.51}$$

The term inside the brackets is defined, up to a negative sign, as the energy-momentum tensor

$$T_{\mu\nu} = -\frac{2}{\sqrt{-g}} \frac{\delta(\sqrt{-g}\mathcal{L})}{\delta g^{\mu\nu}} = -2\frac{\delta \mathcal{L}}{\delta g^{\mu\nu}} + \mathcal{L} g_{\mu\nu} , \tag{2.52}$$

which satisfies

$$\nabla_\mu T^{\mu\nu} = 0 . \tag{2.53}$$

We shall come back to Eq. 2.52 in the next chapter, where the Lagrangian density of the energy-matter fields is added to the gravitational one, which is a functional of the metric tensor only, in order to derive the field equations for the $f(R)$ model. However, it is important to mention that Eq. 2.53, still holding in that gravity model, can be interpreted as the *local conservation of energy and momentum* of these matter fields. This role is nicely illustrated as follows [8]: let ξ^β, P^α be vector fields, the former a Killing one and the second defined by $P^\alpha = T^{\alpha\beta}\xi_\beta$. Since $\nabla_\alpha P^\alpha = 0$, we can employ Gauss' Law and interpret the vanishing of the integral as the zero flux of the α component of the energy-momentum over a closed surface as a local conservation law.

The approaches for modeling the Lagrangian density of a perfect fluid can be split in two categories:
1. On shell: The equations of motion are imposed as constrictions for the fields, without invoking a variational principle for them. On the other hand, the Lagrangian density allows the construction of the energy-momentum tensor and adopts a compact form, $\mathcal{L} = P$, with P the pressure [9].
2. Off shell: A Lagrangian density is proposed in order to recover, by means of variational principle, both the equations of motion and the energy-momentum tensor.

We adopt the second approach for two reasons: first, it seems familiar and natural being capable of deducing all the equations of motion from a single Lagrangian density. Second, to explore the consequences of incorporating the equations of motion into the Lagrangian density.

Let j^ν denote the flux particle 4-vector, $j^\nu = nu^\nu$ with $u^\mu u_\mu = -1$, n the number density, s the entropy per particle, α^A Lagrangian coordinates (A=1,2,3) and θ, ϕ, β^A spacetime scalars which guarantees the well-known conservation laws (and thus interpreted as Lagrange multipliers), and $\epsilon(n,s)$ the energy density. The Lagrangian density for the perfect fluid [9], [10] is

$$\mathcal{L}[g_{\alpha\beta}, j^\mu, \theta, \phi, s, \alpha^A, \beta_A] = -\epsilon(n,s) + j^\mu \left(\partial_\mu \phi + s\partial_\mu \theta + \beta_A \partial_\mu \alpha^A \right) . \tag{2.54}$$

We now proceed to deduce the equations of motion for each field, and the energy-momentum tensor. First, by direct substitution in the Euler-Lagrange equations, we obtain

Field	Equation	
ϕ	$\frac{1}{\sqrt{-g}}\partial_\alpha\left[\sqrt{-g}j^\alpha\right]=0$	(2.56)
θ	$\frac{1}{\sqrt{-g}}\partial_\alpha\left[\sqrt{-g}sj^\alpha\right]=0$	(2.57)
s	$-\frac{\partial\epsilon}{\partial s}+j^\mu\partial_\mu\theta=0$	(2.58)
j^μ	$\left(\frac{\epsilon+P}{n}\right)u_\mu+\partial_\mu\phi+s\partial_\mu\theta+\beta_A\partial_\mu\alpha^A=0$	(2.59)

(the first term appears from the chain rule, and the explicit dependence of n with j^μ through the magnitude of this 4-vector),

Field	Equation	
β_A	$j^\mu\partial_\mu\alpha^A=0$	(2.61)
α^A	$\frac{1}{\sqrt{-g}}\partial_\mu\left[\sqrt{-g}j^\mu\beta_A\right]=0.$	(2.62)

Notice that the first pair represents the conservation of the particle and entropy 4-fluxes. Regarding the energy momentum tensor, we must be aware of the following facts:

(a) The partial derivative of the flux 4-vector with respect to the metric tensor components, is

$$\frac{\partial j^\mu}{\partial g^{\alpha\beta}}=\frac{1}{2}g_{\alpha\beta}j^\mu\ . \tag{2.63}$$

Proof. Employing the chain rule,

$$\frac{\partial(\sqrt{-g})}{\partial g^{\alpha\beta}}j^\mu+\sqrt{-g}\frac{\partial j^\mu}{\partial g^{\alpha\beta}}=0\ \ ,$$

$$\frac{\partial j^\mu}{\partial g^{\alpha\beta}}=-\frac{1}{\sqrt{-g}}\frac{\partial(\sqrt{-g})}{\partial g^{\alpha\beta}}\ ,$$

$$\frac{\partial j^\mu}{\partial g^{\alpha\beta}}=\frac{1}{2}g_{\alpha\beta}j^\mu\ .$$

■

(b) The partial derivative of the number density with respect to the components of the metric tensor is

$$\frac{\partial n}{\partial g^{\alpha\beta}}=\frac{n}{2}\left(u_\alpha u_\beta+g_{\alpha\beta}\right)\ . \tag{2.64}$$

Proof. Starting from its definition, the magnitude of the flux 4-vector is

$$g_{\mu\nu} j^\mu j^\nu = n^2 u^\mu u_\mu = -n^2 \ .$$

Performing a variation with respect to $g^{\alpha\beta}$,

$$2n \frac{\partial n}{\partial g^{\alpha\beta}} = -\frac{\partial g_{\mu\nu}}{\partial g^{\alpha\beta}} j^\mu j^\nu - g_{\mu\nu} \frac{\partial \left(j^\mu j^\nu \right)}{\partial g^{\alpha\beta}} \ .$$

But the previous property guarantees that

$$\frac{\partial \left(j^\mu j^\nu \right)}{\partial g^{\alpha\beta}} = \frac{\partial \left(j^\mu \right)}{\partial g^{\alpha\beta}} j^\nu + j^\mu \frac{\partial \left(j^\nu \right)}{\partial g^{\alpha\beta}} = g_{\alpha\beta} j^\mu j^\nu \ .$$

Thus,

$$2n \frac{\partial n}{\partial g^{\alpha\beta}} = -\frac{\partial g_{\mu\nu}}{\partial g^{\alpha\beta}} j^\mu j^\nu - g_{\mu\nu} g_{\alpha\beta} j^\mu j^\nu \ .$$

Employing the identity

$$-\frac{\partial g_{\mu\nu}}{\partial g^{\alpha\beta}} = g_{\mu\alpha} g_{\nu\beta} \ ,$$

the main equation becomes

$$2n \frac{\partial n}{\partial g^{\alpha\beta}} = g_{\mu\alpha} g_{\nu\beta} j^\mu j^\nu - j^\mu j_\mu g_{\alpha\beta} \ ,$$

$$2n \frac{\partial n}{\partial g^{\alpha\beta}} = j_\alpha j_\beta - j^\mu j_\mu g_{\alpha\beta} \ .$$

By introducing the definition of the flux 4-vector, we conclude that

$$\frac{\partial n}{\partial g^{\alpha\beta}} = \frac{n}{2} \left(u_\alpha u_\beta + g_{\alpha\beta} \right) \ .$$

■

(c) The energy and number densities are related with the pressure by

$$P = n \left(\frac{\partial \Pi}{\partial n} \right) - \Pi \ . \tag{2.65}$$

Proof. From the First Law of Thermodynamics, we know that

$$P = -\left(\frac{\partial U}{\partial V} \right)_{s,N} \ , \tag{2.66}$$

where U is the internal energy of the system. Since $U = \Pi V$,

$$P = -\frac{\partial (\Pi V)}{\partial V} = -\Pi - V \frac{\partial \Pi}{\partial V} \ .$$

From chain's rule,

$$P = -\Pi - V\frac{\partial \Pi}{\partial n}\frac{\partial n}{\partial V} = -\Pi + V\frac{\partial \Pi}{\partial n}\left(\frac{N}{V^2}\right) \ .$$

Simplifying,

$$P = -\Pi + n\frac{\partial \Pi}{\partial n} \ .$$

■

(d) From chain's rule,

$$\frac{\delta \epsilon}{\delta g^{\mu\nu}} = \frac{\delta \epsilon}{\delta n}\frac{\delta n}{\delta g^{\mu\nu}} = \left[\bar{m}c^2 + \frac{\partial \Pi}{\partial n}\right]\frac{\delta n}{\delta g^{\mu\nu}} \ . \tag{2.67}$$

Finally, by combining the results of (a), (b), (c) and (d) in eq. 2.52,

$$T_{\mu\nu} = -2\frac{\delta \epsilon}{\delta g^{\mu\nu}} - 2\frac{\delta j^\gamma}{\delta g^{\mu\nu}}\left(\partial_\gamma \phi + s\partial_\gamma \theta + \beta_A \partial_\gamma \alpha^A\right) + \mathcal{L} g_{\mu\nu}, \tag{2.68}$$

$$T_{\mu\nu} = n\left[\bar{m}c^2 + \frac{\partial \Pi}{\partial n}\right](u_\mu u_\nu + g_{\mu\nu}) - g_{\mu\nu} j^\gamma\left(\partial_\gamma \phi + s\partial_\gamma \theta + \beta_A \partial_\gamma \alpha^A\right) + \mathcal{L} g_{\mu\nu} \ , \tag{2.69}$$

$$T_{\mu\nu} = \left[\rho_m c^2 + n\frac{\partial \Pi}{\partial n}\right] u_\mu u_\nu + \left[\rho_m c^2 - \epsilon + n\frac{\partial \Pi}{\partial n}\right] g_{\mu\nu} \ , \tag{2.70}$$

we arrive at the well-known expression for the energy-momentum tensor of the perfect fluid,

$$T_{\mu\nu} = (\epsilon + P)u_\mu u_\nu + P g_{\mu\nu} \ . \tag{2.71}$$

2.6 Conformal transformations

Let Ω be a strictly positive function, M and $\bar{M}$ n-dimensional manifolds endowed with metrics $g_{\mu\nu}$ and $\bar{g}_{\mu\nu}$ respectively. These are said conformally related if

$$\bar{g}_{\mu\nu} = \Omega^2 g_{\mu\nu} \tag{2.72}$$

holds. Causal structure is preserved under such transformations, although in 4 dimensions the Riemann tensor, the connection and the geodesic equations are not. It must be noted that if both manifolds are regarded as pseudo - Riemannian, physical predictions might be completely different in these frames. This point of view is discussed in detail in the next chapter.

Chapter 3

The $f(R)$ Gravity Model

"*In any field, find the strangest thing and then explore it*".

John Wheeler

The indirect evidence for the existence of dark energy and matter, as well as the difficulties on the attempts of quantizing the gravitational field considering only the Hilbert-Einstein action, have led to research on alternative theories of gravitation, which in principle would be capable of explaining one or both aspects.

The first kind of proposals introduce either scalar, vector or tensor fields in addition to $g_{\mu\nu}$. Famous examples are the Brans-Dicke (BD), Tensor-vector-scalar gravity (TeVeS) which is a relativistic expansion of Modified Newtonian Dynamics (MOND), Scalar-tensor-vector gravity (also refered as MOG for Modified Gravity). On the other hand, we have a theory which involves the modification of the Lagrangian density invoking only the metric field tensor, the $f(R)$ model. Its motivation is simple: interpreting the Lagrangian density of GR as the first two terms in a power series which accurately explains low-energy phenomena, then a correct description of gravity should be provided by a function $f(R)$, which must meet the following requirements:

$$\frac{df}{dR} \geq 0 \quad , \quad \frac{d^2 f}{dR^2} \geq 0 \tag{3.1}$$

in order to be physically consistent. The corresponding Lagrangian density is [22]

$$\mathcal{L}_G = \frac{c^4}{16\pi G} \sum_{n=0}^{\infty} a_n R^n = \frac{c^4}{16\pi G} f(R) \ .$$

Since the main interest of this work is neutron stars, objects that belong to the strong-field gravitational regime but have been well explained with GR, only a quadratic term (or a second-order expansion) is added, $f(R) = R + \alpha R^2$. The parameter α must be positive in order to satisfy the above criteria. There exist

additional proposals such as $f(R,T)$ and $f(R,T,\mathcal{L}_m)$ models, where the trace of the energy-momentum tensor and the Lagrangian of matter-energy play a more active role in the description of gravity through couplings of the form R^nT^s, $R^n\mathcal{L}_m^s$, $n,s\in\mathbb{R}$ [11]. It is important to remark that the inclusion of the Lagrangian density of matter requieres an explicit knowledge of its origins, which, as we have seen in the previous chapter, is not a trivial subject. We shall not pursue here these theories, in particular for the polemic around them regarding aspects such as the non-zero divergence of the energy momentum tensor and the exact form of the equations of motion for the fields [12]. The main purpose of this chapter is to analyze the structure of spherical objects obeying the SSS metric and admit an EoS. For an arbitrary $f(R)$ function, in section 1 the field equations are derived. In sections 2 we briefly review the particular case of GR. In section 3 the equations for the quadratic model are deduced in detail, in order to analyze their behaviour at long distances and near the center of the star in Section 4. For completeness in the discussion of the quadratic model, Section 5 is dedicated to the weak-field limit, while Section 6 contains a discussion on the geodesic motion. The final section of this chapter describes the Einstein-Jordan frame issue, and settles the point of view adopted for the rest of this work.

3.1 Field equations

As we have anticipated, the equations of motion for the metric field are deduced by imposing the stationary principle upon the action functional, $\delta S=0$. Since $f(R)$ can be regarded as an integrable function, the propositions of chapter 2 can be employed for this purpose. First we study the variation of the pure gravitational Lagrangian, incorporating the matter-energy content afterwards.

Theorem 3: $f(R)$ field equations in vacuum. Let

$$\mathcal{L}_G=\frac{c^4}{16\pi G}f(R)\ , \tag{3.2}$$

with R the scalar curvature, G the universal constant of gravitation and c the speed of light in vacuum, be the Lagrangian density of gravity. Imposing the stationary principle upon its corresponding action

$$S_G=\int_\Omega d^4x\sqrt{-g}\frac{1}{c}\mathcal{L}_G \tag{3.3}$$

the equations of motion for the metric tensor are [15], [14], [13]

$$\boxed{\frac{df}{dR}G_{\mu\nu}-\frac{1}{2}\left(f-R\frac{df}{dR}\right)g_{\mu\nu}-\left[\nabla_\mu\nabla_\nu-g_{\mu\nu}\Box\right]\frac{df}{dR}=0\ .} \tag{3.4}$$

Proof. The variation of the action with respect to the metric tensor is

$$\delta S_G = \frac{c^3}{16\pi G}\int_\Omega d^4x\delta(\sqrt{-g}f(g^{\mu\nu}R_{\mu\nu}))\ ,$$

$$\delta S_G = \frac{c^3}{16\pi G}\int_\Omega d^4x\left[-\frac{1}{2}\sqrt{-g}g_{\mu\nu}f(g^{\mu\nu}R_{\mu\nu})\delta g^{\mu\nu} + \sqrt{-g}\delta(f(g^{\mu\nu}R_{\mu\nu}))\right]\ .$$

Since

$$\delta(f(R)) = \frac{df}{dR}\delta R = \frac{df}{dR}\left[g^{\mu\nu}\delta R_{\mu\nu} + R_{\mu\nu}\delta g^{\mu\nu}\right]\ ,$$

we have

$$\delta S_G = \frac{c^3}{16\pi G}\int_\Omega d^4x\sqrt{-g}\left\{-\frac{1}{2}g_{\mu\nu}f\delta g^{\mu\nu} + \frac{df}{dR}\left[g^{\mu\nu}\delta R_{\mu\nu} + R_{\mu\nu}\delta g^{\mu\nu}\right]\right\}\ ,$$

$$\delta S_G = \frac{c^3}{16\pi G}\int_\Omega d^4x\sqrt{-g}\left\{\left[\frac{df}{dR}R_{\mu\nu} - \frac{1}{2}g_{\mu\nu}f\right]\delta g^{\mu\nu} + \frac{df}{dR}g^{\mu\nu}\delta R_{\mu\nu}\right\}\ .$$

By hypothesis the variations of the metric at the boundary are null. Moreover, df/dR is a differentiable function with respect to the coordinate system. We can thus employ proposition 2 to the second term in the right hand side, leading to

$$\delta S_G = \frac{c^3}{16\pi G}\int_\Omega d^4x\sqrt{-g}\left\{\left[\frac{df}{dR}R_{\mu\nu} - \frac{1}{2}g_{\mu\nu}f\right]\delta g^{\mu\nu} + \delta g^{\mu\nu}\left[g_{\mu\nu}\Box\frac{df}{dR} - \nabla_\mu\nabla_\nu\frac{df}{dR}\right]\right\}\ ,$$

$$\delta S_G = \frac{c^3}{16\pi G}\int_\Omega d^4x\sqrt{-g}\delta g^{\mu\nu}\left\{\frac{df}{dR}R_{\mu\nu} - \frac{1}{2}g_{\mu\nu}f + \left[g_{\mu\nu}\Box - \nabla_\mu\nabla_\nu\right]\frac{df}{dR}\right\}\ .$$

We now impose $\delta S_G = 0$. In general the variations of the inverse metric tensor are different from zero. This implies that

$$\frac{df}{dR}R_{\mu\nu} - \frac{1}{2}g_{\mu\nu}f + \left[g_{\mu\nu}\Box - \nabla_\mu\nabla_\nu\right]\frac{df}{dR} = 0\ .$$

For further analysis, we can introduce the Einstein tensor by a suitable choice of writting a zero between the first and second term of the left hand side,

$$\frac{df}{dR}\left(R_{\mu\nu} - \frac{1}{2}g_{\mu\nu}R\right) - \frac{1}{2}g_{\mu\nu}\left(f - R\frac{df}{dR}\right) + \left[g_{\mu\nu}\Box - \nabla_\mu\nabla_\nu\right]\frac{df}{dR} = 0$$

$$\frac{df}{dR}G_{\mu\nu} - \frac{1}{2}\left(f - R\frac{df}{dR}\right)g_{\mu\nu} - \left[\nabla_\mu\nabla_\nu - g_{\mu\nu}\Box\right]\frac{df}{dR} = 0\ . \tag{3.5}$$

■

The derivation of the field equations in the presence of matter-energy is straightforward: let $\mathcal{L}_M$ denote the Lagrangian density of matter/energy. The action is

$$S = \int_\Omega d^4x\sqrt{-g}\left[\frac{c^3}{16\pi G}f(R) + \frac{1}{c}\mathcal{L}_M\right] \tag{3.6}$$

Since the variation is a linear operation,

$$\delta S = \int_\Omega d^4x\left[\frac{c^3}{16\pi G}\delta(\sqrt{-g}f(R)) + \delta\left(\sqrt{-g}\frac{1}{c}\mathcal{L}_M\right)\right] \ .$$

The variation of the first term is given by the previous theorem, while the second term corresponds to the definition of the energy-momentum tensor. Thus,

$$\delta S = \int_\Omega d^4x\sqrt{-g}\delta g^{\mu\nu}\left\{\frac{c^3}{16\pi G}\left[\frac{df}{dR}G_{\mu\nu} - \frac{1}{2}\left(f - R\frac{df}{dR}\right)g_{\mu\nu} - (\nabla_\mu\nabla_\nu - g_{\mu\nu}\Box)\frac{df}{dR}\right] - \frac{1}{2c}T_{\mu\nu}\right\} \ .$$

By demanding $\delta S = 0$, we see that

$$\frac{df}{dR}G_{\mu\nu} - \frac{1}{2}\left(f - R\frac{df}{dR}\right)g_{\mu\nu} - [\nabla_\mu\nabla_\nu - g_{\mu\nu}\Box]\frac{df}{dR} = \frac{8\pi G}{c^4}T_{\mu\nu} \ . \tag{3.7}$$

Notice that the field equations in the $f(R)$ model keep a similar structure to general relativity: the geometric and energy terms can be written in opposite sides of the equation,

$$\mathcal{G}_{\mu\nu} = \frac{8\pi G}{c^4}T_{\mu\nu} \ \ , \tag{3.8}$$

with $\mathcal{G}_{\mu\nu}$ reducing to the Einstein tensor in the particular case $f(R) = R$. In addition to this set of equations, we have at our disposal its trace,

$$\boxed{R\frac{df}{dR} - 2f + 3\Box\frac{df}{dR} = \frac{8\pi G}{c^4}T} \ \ , \tag{3.9}$$

which is also a key point for discussing an alternative approach/interpretation of this theory, in terms of a *scalar field*. It must be stressed that this is not an interpretation we pursue in later discussions, but is important to give a little review for theoretical completeness. If $f(R) = R$ is considered, we recover Einstein's field equation,

$$G_{\mu\nu} = \frac{8\pi G}{c^4}T_{\mu\nu} \ . \tag{3.10}$$

On the other hand, if $f(R) = R + \alpha R^2$, we see that the field equations [16], [15], [17] are

$$(1 + 2\alpha R)G_{\mu\nu} + \frac{\alpha R^2}{2}g_{\mu\nu} - 2\alpha[\nabla_\mu\nabla_\nu - g_{\mu\nu}\Box]R = \frac{8\pi G}{c^4}T_{\mu\nu} \ . \tag{3.11}$$

3.1.1 Scalar field approach

The presence of the D'Alembertian operator in the trace equation motivates the following re-arrangement

$$\Box\frac{df}{dR} = \frac{8\pi G}{3c^4}T + \frac{1}{3}\left(2f - R\frac{df}{dR}\right) \ . \tag{3.12}$$

This expression resembles the Klein - Gordon equation for a scalar field [53] $\Psi := \frac{df}{dR}$. For $f(R) = R + \alpha R^2$, this implies $\Psi = 1 + 2\alpha R$, and the right hand side of the trace equation becomes

$$\frac{dV}{d\Psi} = \frac{8\pi G}{3c^4}T + \frac{1}{3}\left[2(R + \alpha R^2) - R(1 + 2\alpha R)\right] \ ,$$

$$\frac{dV}{d\Psi} = \frac{8\pi G}{3c^4}T + \frac{\Psi - 1}{6\alpha} \ . \tag{3.13}$$

The critical points for this "potential" occur when

$$\Psi_c = 1 - \frac{16\pi\alpha G}{c^4}T. \tag{3.14}$$

In the absence of matter, i.e. $T = 0$, there is only one critical point, $\Psi_c = 1$. From the second derivative,

$$\frac{d^2V}{d\Psi^2}\Big|_{\Psi=\Psi_c} = \frac{1}{6\alpha}\Big|_{\Psi=\Psi_c} = \frac{1}{6\alpha} \tag{3.15}$$

we can see that a minimum for $V(\Psi)$ is guaranteed if $\alpha > 0$. This is an additional confirmation that α must be positive for our metric sign convention.
Although the identification has been done in a rather heuristical way, the alternate approach of starting with the Lagrangian density and imposing the extremal principle agrees with the fact that $\Psi = df/dR$. This is promoted as the analogy of the $f(R)$ model with the Brans-Dicke theory of gravity, where an additional scalar field is coupled to the scalar curvature.
For the $f(R) = R + \alpha R^2$ case, where the scalar field has been shown linear in the scalar curvature, it is arguable if this identification is possible, in particular, in the context of the Einstein-Jordan frame debate where the conformal transformation of the metric tensor has consequences over the Lagrangian density and the fields involved.
Indeed: one is free to re-write the Lagrangian density in the following way

$$\mathcal{L}_G = \frac{c^4}{16\pi G}\left[R(1 + \alpha R)\right] = \frac{c^4}{16\pi G}\left[R\left(\frac{\Psi + 1}{2}\right)\right] \tag{3.16}$$

in order to force the similitude with the BD theory and performing a conformal transformation to simplify the equations of motion (going from Jordan to Einstein

frame, as claimed by many sources), or choose a rather unusual way of re-writting the Lagrangian density,

$$\mathcal{L}_G = \frac{c^4}{16\pi G}\left[\frac{\Psi^2 - 1}{4\alpha}\right] \tag{3.17}$$

where the scalar curvature as the central actor has disappeared from the scene, but the metric tensor stands as the only field over which the variational principle must be performed.

The previous identification raises two questions, one of them to be discussed in the final section of this chapter:

1. Is the scalar field analogy physically valid? Indeed, the general case $\Psi = df/dR$ can be deduced from a variational principle over the original Lagrangian density. However, if we plug this expression back, we get an "on-shell" Lagrangian density that formally resembles the BD one and is used to move from Jordan to Einstein frame. However, in order to keep the analogy we are selectively re-writting terms, not the full Lagrangian as we pointed in the lines above.

Finally, transformations and equations of motion over on-shell Lagrangians might imply different equations of motion and completely different physical predictions. This is closely related to the following question:

2. Does the conformal transformation have physical consequences? Regarding the scalar field, a conformal transformation is employed in order to simplify the equations of motion in a further way than a mere re-writing may achieve. However, such transformations alter the equations of motion and are potentially leading to different predictions. In that sense, are we to consider one of the frames as physical and the other not, or simply are we building a completely different theory of gravitation? In the final section of this chapter we adress this question, closely based on the point of view that such transformations are *just a mathematical way of simplifying the equations of motion, but leaving the physical questions unnanswered unless we go back to the original metric and variables.*

3.2 SSS metric in General Relativity

By introducing the SSS metric and the energy-momentum tensor of a perfect fluid and the *mass function*

$$m(r) = \left[\frac{c^2 r}{2G}\left(1 - e^{-2\Lambda(r)}\right)\right] \tag{3.18}$$

it is possible to deduce the following differential equations [5], [6],

$$\frac{dm}{dr} = \frac{4\pi\epsilon}{c^2}r^2 \ , \tag{3.19}$$

$$\frac{d\Phi}{dr} = \frac{1}{r\left(r - \frac{2Gm}{c^2}\right)}\left[\frac{Gm}{c^2} + \frac{4\pi G P r^3}{c^4}\right] \tag{3.20}$$

which, together with the equation for the pressure arising from the radial component of $\nabla_\mu T^{\mu\nu} = 0$,

$$\frac{dP}{dr} = -(P+\epsilon)\frac{d\Phi}{dr} \tag{3.21}$$

are known as the Tolman - Oppenheimer - Volkoff equations. Once provided an EoS, $P = P(\epsilon)$, it is possible to implement a numerical scheme in order to seek for solutions, due to the fact that analytic expressions exist only for simple models such as $\epsilon =$ constant.
In contrast with the model described below, the trace equation is not essential for solving the system. In spite of this, it is worth mentioning that it implies a global relation between the trace of the energy momentum tensor and the scalar curvature,

$$R = -\frac{8\pi G}{c^4}T = \frac{8\pi G}{c^4}(\epsilon - 3P) \tag{3.22}$$

If $\epsilon = P = 0$, the scalar curvature is identically zero and spacetime is described by Schwarszchild's metric, i.e. $\Lambda + \Phi = 0$.

3.3 SSS metric in $f(R) = R + \alpha R^2$

Considering the energy-momentum tensor of a perfect fluid and the static and spherically symmetric metric in eq. 3.11, we can deduce the following set of differential equations, refered as the modified Tolman - Oppenheimer - Volkoff equations [13], [17], [23]:

$$\boxed{\frac{d\Phi}{dr} = \frac{4\pi G P r e^{2\Lambda}}{c^4 A_1} - \frac{1}{4rA_1}\left[A_2 e^{2\Lambda} + 2A_3\right]} \tag{3.23}$$

$$\boxed{\frac{d\Lambda}{dr} = \frac{4\pi G \epsilon r e^{2\Lambda}}{c^4 A_1} + \frac{1}{4rA_1}\left[A_2 e^{2\Lambda} + 2A_3\right] + \frac{\alpha r}{A_1}\frac{d^2R}{dr^2}} \tag{3.24}$$

$$\boxed{\frac{d^2R}{dr^2} = \frac{A_1 A_4 e^{2\Lambda}}{6\alpha A_7} - \frac{1}{rA_7}\left[A_5 + A_6 - \frac{A_2 e^{2\Lambda}}{2}\right]\frac{dR}{dr}}\,, \tag{3.25}$$

where the following functions have been introduced to keep the notation as simple as possible,

$$\boxed{A_1 = 1 + 2\alpha R + \alpha r\frac{dR}{dr}\ ,\ A_2 = \alpha r^2 R^2 - 4\alpha R - 2}\,, \tag{3.26}$$

$$\boxed{A_3 = 1 + 2\alpha R + 4\alpha r\frac{dR}{dr}\ ,\ A_4 = \frac{8\pi G}{c^4}(3P - \epsilon) + R}\,, \tag{3.27}$$

$$\boxed{A_5 = \frac{4\pi G}{c^4}r^2 e^{2\Lambda}(P - \epsilon)\ ,\ A_6 = 1 + 2\alpha R - 2\alpha r\frac{dR}{dr}}\,, \tag{3.28}$$

$$\boxed{A_7 = 1 + 2\alpha R}\ . \tag{3.29}$$

The fifth equation of the system, commonly refered as the hydrostatic equilibrium one,

$$\boxed{\frac{dP}{dr} = -(P+\epsilon)\frac{d\Phi}{dr}}\ , \tag{3.30}$$

is deduced from the zero divergence condition of the energy momentum tensor,

$$\nabla_\alpha T^{\alpha\beta} = 0\ . \tag{3.31}$$

We now proceed to deduce each one of these equations, considering the results of Chapter 2 related to differential operators that explicitly depend on the SSS metric.

3.3.1 First Equation

We proceed to analyze the $\mu = \nu = r$ component,

$$(1+2\alpha R)G_{rr} + \frac{\alpha R^2}{2}g_{rr} + 2\alpha\left[-\nabla_r\nabla_r + g_{rr}\Box\right]R = \frac{8\pi G}{c^4}T_{rr}\ . \tag{3.32}$$

From propositions 3 and 4, we have

$$2\alpha\left[-\nabla_r\nabla_r + g_{rr}\Box\right]R = 2\alpha\left[-\frac{d^2R}{dr^2} + \frac{d\Lambda}{dr}\frac{dR}{dr} + \frac{d^2R}{dr^2} + \left(\frac{2}{r} + \frac{d\Phi}{dr} - \frac{d\Lambda}{dr}\right)\frac{dR}{dr}\right]$$

$$2\alpha\left[-\nabla_r\nabla_r + g_{rr}\Box\right]R = 2\alpha\left(\frac{2}{r} + \frac{d\Phi}{dr}\right)\frac{dR}{dr}. \tag{3.33}$$

By replacing eq. 3.33 in eq. 3.32,

$$(1+2\alpha R)G_{rr} + \frac{\alpha R^2 g_{rr}}{2} + 2\alpha\left(\frac{2}{r} + \frac{d\Phi}{dr}\right)\frac{dR}{dr} = \frac{8\pi G}{c^4}T_{rr}. \tag{3.34}$$

Considering that $g_{rr} = e^{2\Lambda}$, $T_{rr} = Pe^{2\Lambda}$ and

$$G_{rr} = \frac{2}{r}\frac{d\Phi}{dr} + \frac{(1-e^{2\Lambda})}{r^2}\quad ,$$

eq. 3.34 becomes

$$(1+2\alpha R)\left[\frac{2}{r}\frac{d\Phi}{dr} + \frac{(1-e^{2\Lambda})}{r^2}\right] + \frac{\alpha R^2 e^{2\Lambda}}{2} + 2\alpha\left(\frac{2}{r} + \frac{d\Phi}{dr}\right)\frac{dR}{dr} = \frac{8\pi G P e^{2\Lambda}}{c^4}. \tag{3.35}$$

Rearranging terms,

$$\frac{2}{r}\left(1 + 2\alpha R + \alpha r\frac{dR}{dr}\right)\frac{d\Phi}{dr} = e^{2\Lambda}\left(\frac{8\pi G P}{c^4} - \frac{\alpha R^2}{2}\right) - \frac{4\alpha}{r}\frac{dR}{dr} - \frac{(1+2\alpha R)(1-e^{2\Lambda})}{r^2}$$

$$\left(1+2\alpha R+\alpha r\frac{dR}{dr}\right)\frac{d\Phi}{dr}=\frac{4\pi GPre^{2\Lambda}}{c^4}-\frac{1}{4r}\left[2\left(1+2\alpha R+4\alpha r\frac{dR}{dr}\right)+e^{2\Lambda}\left(\alpha r^2R^2-2-4\alpha R\right)\right].$$

By defining

$$A_1=A_1(r)=1+2\alpha R+\alpha r\frac{dR}{dr} \tag{3.36}$$

$$A_2=A_2(r)=\alpha r^2R^2-2-4\alpha R \tag{3.37}$$

$$A_3=A_3(r)=1+2\alpha R+4\alpha r\frac{dR}{dr} \tag{3.38}$$

the first differential equation is

$$\frac{d\Phi}{dr}=\frac{4\pi GPre^{2\Lambda}}{c^4A_1}-\frac{1}{4rA_1}\left[A_2e^{2\Lambda}+2A_3\right]. \tag{3.39}$$

3.3.2 Second Equation

We analyze the $\mu=\nu=0$ component of the field equations,

$$(1+2\alpha R)G_{00}+\frac{\alpha R^2}{2}g_{00}-2\alpha\left[\nabla_0\nabla_0-g_{00}\Box\right]R=\frac{8\pi G}{c^4}T_{00}. \tag{3.40}$$

From proposition 3 and 4,

$$2\alpha\left[-\nabla_0\nabla_0+g_{00}\Box\right]R=2\alpha\left[e^{2(\Phi-\Lambda)}\frac{d\Phi}{dr}\frac{dR}{dr}-e^{2(\Phi-\Lambda)}\frac{d^2R}{dr^2}-e^{2(\Phi-\Lambda)}\left(\frac{2}{r}+\frac{d\Phi}{dr}-\frac{d\Lambda}{dr}\right)\frac{dR}{dr}\right]$$

$$2\alpha\left[-\nabla_0\nabla_0+g_{00}\Box\right]R=-2\alpha e^{2(\Phi-\Lambda)}\left[\frac{d^2R}{dr^2}+\left(\frac{2}{r}-\frac{d\Lambda}{dr}\right)\frac{dR}{dr}\right]. \tag{3.41}$$

By substitution of eq. 3.41 in eq. 3.40,

$$(1+2\alpha R)G_{00}+\frac{\alpha R^2}{2}g_{00}-2\alpha e^{2(\Phi-\Lambda)}\left[\frac{d^2R}{dr^2}+\left(\frac{2}{r}-\frac{d\Lambda}{dr}\right)\frac{dR}{dr}\right]=\frac{8\pi G}{c^4}T_{00}\ . \tag{3.42}$$

Since $T_{00}=\epsilon e^{2\Phi}$, $g_{00}=-e^{2\Phi}$ and

$$G_{00}=e^{2(\Phi-\Lambda)}\left[\frac{2}{r}\frac{d\Lambda}{dr}+\frac{e^{2\Lambda}-1}{r^2}\right]\quad,$$

eq. 3.42 is rewritten as

$$e^{2(\Phi-\Lambda)}(1+2\alpha R)\left(\frac{2}{r}\frac{d\Lambda}{dr}+\frac{e^{2\Lambda}-1}{r^2}\right)-\frac{\alpha R^2e^{2\Phi}}{2}-2\alpha e^{2(\Phi-\Lambda)}\left[\frac{d^2R}{dr^2}+\left(\frac{2}{r}-\frac{d\Lambda}{dr}\right)\frac{dR}{dr}\right]=\frac{8\pi G\epsilon e^{2\Phi}}{c^4}\ . \tag{3.43}$$

Rearranging terms,

$$\frac{2}{r}\left(1+2\alpha R+\alpha r\frac{dR}{dr}\right)\frac{d\Lambda}{dr}=\frac{8\pi G\epsilon e^{2\Lambda}}{c^4}+\frac{e^{2\Lambda}}{r^2}\left[-(1+2\alpha R)+\frac{\alpha r^2R^2}{2}\right]$$
$$+\frac{1}{r^2}\left[(1+2\alpha R)+4\alpha r\frac{dR}{dr}\right]+2\alpha\frac{d^2R}{dr^2}$$

$$\left(1+2\alpha R+\alpha r\frac{dR}{dr}\right)\frac{d\Lambda}{dr}=\frac{4\pi G\epsilon re^{2\Lambda}}{c^4}+\frac{1}{4r}\left[e^{2\Lambda}(\alpha r^2R^2-2-4\alpha R)+2\left(1+2\alpha R+4\alpha r\frac{dR}{dr}\right)\right]$$
$$+\alpha r\frac{d^2R}{dr^2}\ .$$

Introducing the same functions A_1, A_2 and A_3, the second differential equation is

$$\frac{d\Lambda}{dr}=\frac{4\pi G\epsilon re^{2\Lambda}}{c^4A_1}+\frac{1}{4rA_1}\left[A_2e^{2\Lambda}+2A_3\right]+\frac{\alpha r}{A_1}\frac{d^2R}{dr^2}\ . \tag{3.44}$$

3.3.3 Third Equation

From the trace equation,

$$(1+2\alpha R)G+\frac{\alpha R^2}{2}g^{\mu\nu}g_{\mu\nu}-2\alpha\left[g^{\mu\nu}\nabla_\mu\nabla_\nu-g^{\mu\nu}g_{\mu\nu}\Box\right]R=\frac{8\pi G}{c^4}T.$$

Since $g^{\mu\nu}g_{\mu\nu}=4$, $g^{\mu\nu}\nabla_\mu\nabla_\nu=\Box$ and $G=-R$,

$$-(R+2\alpha R^2)+2\alpha R^2-2\alpha\left[\Box-4\Box\right]R=\frac{8\pi G}{c^4}T$$

$$6\alpha\Box R-R=\frac{8\pi G}{c^4}T.$$

Due to $T=3P-\epsilon$ and $\alpha\neq 0$,

$$\Box R-\frac{1}{6\alpha}R=\frac{8\pi G}{6\alpha c^4}(3p-\epsilon).$$

By propositon 3

$$e^{-2\Lambda}\left[\frac{d^2R}{dr^2}+\left(\frac{2}{r}+\frac{d\Phi}{dr}-\frac{d\Lambda}{dr}\right)\frac{dR}{dr}\right]-\frac{1}{6\alpha}R=\frac{8\pi G}{6\alpha c^4}(3P-\epsilon)$$

$$\frac{d^2R}{dr^2}+\left(\frac{2}{r}+\frac{d\Phi}{dr}-\frac{d\Lambda}{dr}\right)\frac{dR}{dr}=\frac{e^{2\Lambda}}{6\alpha}\left[\frac{8\pi G}{c^4}(3P-\epsilon)+R\right]. \tag{3.45}$$

From the equations for Λ and Φ, we see that

$$\frac{2}{r}+\frac{d\Phi}{dr}-\frac{d\Lambda}{dr}=\frac{2}{r}+\frac{4\pi Gre^{2\Lambda}}{c^4A_1}(p-\epsilon)-\frac{1}{2rA_1}\left(A_2e^{2\Lambda}+2A_3\right)-\frac{\alpha r}{A_1}\frac{d^2R}{dr^2}. \tag{3.46}$$

Plugging this result in eq. 3.45 and re-arranging terms,

$$\frac{d^2R}{dr^2}\left[1-\frac{\alpha r}{A_1}\frac{dR}{dr}\right]=\frac{e^{2\Lambda}}{6\alpha}\left[\frac{8\pi G}{c^4}(3p-\epsilon)+R\right]-\frac{dR}{dr}\left[\frac{2}{r}+\frac{4\pi G r e^{2\Lambda}}{c^4A_1}(P-\epsilon)-\frac{1}{2rA_1}(A_2e^{2\Lambda}+2A_3)\right]$$

$$\left(\frac{1+2\alpha R}{A_1}\right)\frac{d^2R}{dr^2}=\frac{e^{2\Lambda}}{6\alpha}\left[\frac{8\pi G}{c^4}(3p-\epsilon)+R\right]-\frac{1}{A_1}\frac{dR}{dr}\left[\frac{4\pi G r e^{2\Lambda}}{c^4}(P-\epsilon)-\frac{A_2e^{2\Lambda}}{2r}+\frac{(2A_1-A_3)}{r}\right].$$

By defining the following functions

$$A_4=\frac{8\pi G}{c^4}(3P-\epsilon)+R \tag{3.47}$$

$$A_5=\frac{4\pi G r^2e^{2\Lambda}}{c^4}(P-\epsilon) \tag{3.48}$$

$$A_6=2A_1-A_3=1+2\alpha R-2\alpha r\frac{dR}{dr} \tag{3.49}$$

$$A_7=1+2\alpha R \tag{3.50}$$

the differential equation for the scalar curvature is

$$\frac{d^2R}{dr^2}=\frac{A_1A_4e^{2\Lambda}}{6\alpha A_7}-\frac{1}{rA_7}\left[A_5+A_6-\frac{A_2e^{2\Lambda}}{2}\right]\frac{dR}{dr}. \tag{3.51}$$

Notice that

$$\frac{d^2R}{dr^2}=f\left(R,\frac{dR}{dr},\epsilon,P,\Lambda\right). \tag{3.52}$$

Therefore, we can substitute eq. 3.51 in eq. 3.44 to keep the condition

$$\frac{d\Lambda}{dr}=f\left(R,\frac{dR}{dr},\epsilon,P,\Lambda\right)\ , \tag{3.53}$$

which is necessary for solving the system of differential equations numerically.

3.3.4 Fourth Equation

From the zero-divergence condition of the energy momentum tensor, we consider the radial equation $\nabla_\beta T^{\beta r}=0$, which in expanded form is

$$\partial_\beta T^{r\beta}+\Gamma^r_{\ \beta\epsilon}T^{\epsilon\beta}+\Gamma^\beta_{\ \beta\epsilon}T^{r\epsilon}=0\ .$$

Since $T^{\mu\nu}$ is diagonal,

$$\partial_\beta T^{r\beta}=\partial_r T^{rr}=\partial_r(pe^{-2\Lambda})=-2Pe^{-2\Lambda}\partial_r\Lambda+e^{-2\Lambda}\partial_r P\ .$$

In addition, we claim that

$$\Gamma^{r}_{\ \beta\epsilon}T^{\epsilon\beta} + \Gamma^{\beta}_{\ \beta\epsilon}T^{r\epsilon} = e^{-2\Lambda}\epsilon\partial_r\Phi + e^{-2\Lambda}P(\partial_r\Phi + 2\partial_r\Lambda) \ .$$

Plugging these expressions in eq. 3.3.4, we see that

$$e^{-2\Lambda}\partial_r p - 2Pe^{-2\Lambda}\partial_r\Lambda + e^{-2\Lambda}\epsilon\partial_r\Phi + e^{-2\Lambda}P(\partial_r\Phi + 2\partial_r\Lambda) = 0 \ ,$$

$$(\epsilon + P)\frac{d\Phi}{dr} = -\frac{dP}{dr} \ . \tag{3.54}$$

3.3.5 $\theta\theta$ and $\phi\phi$ components of field equations

For the SSS metric, we know the following facts:

$$g_{\theta\theta} = r^2, \qquad g_{\phi\phi} = \sin^2\theta g_{\theta\theta} \ , \tag{3.55}$$

$$\Gamma^{r}_{\ \theta\theta} = -re^{-2\Lambda(r)}, \quad \Gamma^{r}_{\ \phi\phi} = \sin^2\theta\Gamma^{r}_{\ \theta\theta}, \tag{3.56}$$

$$G_{\theta\theta} = re^{-2\Lambda(r)}\left[\frac{d\Phi}{dr} + r\left(\frac{d\Phi}{dr}\right)^2 - \frac{d\Lambda}{dr}\left(1 + r\frac{d\Phi}{dr}\right) + r\frac{d^2\Phi}{dr^2}\right] \ , \ G_{\phi\phi} = \sin^2\theta G_{\theta\theta} \ , \tag{3.57}$$

$$T_{\theta\theta} = r^2P \ , \qquad T_{\phi\phi} = \sin^2\theta P \ , \tag{3.58}$$

Moreover: since the curvature scalar is a function of the radial coordinate only,

$$\nabla_\theta\nabla_\theta R = -\Gamma^{r}_{\ \theta\theta}\frac{dR}{dr} = re^{-2\Lambda(r)}\frac{dR}{dr}, \qquad \nabla_\phi\nabla_\phi R = \sin^2\theta\nabla_\theta\nabla_\theta R \ . \tag{3.59}$$

Therefore, the $(\theta\theta)$ and $(\phi\phi)$ components of the field equations are practically the same,

$$(1 + 2\alpha R)G_{\theta\theta} + \frac{\alpha R^2}{2}g_{\theta\theta} - 2\alpha\left[\nabla_\theta\nabla_\theta - g_{\theta\theta}\Box\right]R = \frac{8\pi G}{c^4}T_{\theta\theta} \ . \tag{3.60}$$

Notice that both sides tends to zero as $r \to 0$. Also, it depends on a linear combination of Φ'' and R'', rendering it as a consistent condition which is not relevant for solving the differential system already written.

3.3.6 Supplementary equation: scalar curvature

From chapter 2, we know that R is an scalar arising from contractions of the Riemann and metric tensors, leaving this as a theory-invariant function composed of $g_{\mu\nu}$ and its derivatives. For the SSS case, the expression is

$$\boxed{R(r) = \frac{2(1 - e^{-2\Lambda})}{r^2} - 2e^{-2\Lambda}\left[\frac{2}{r}(\Phi' - \Lambda') + \Phi'' - \Phi'\Lambda' + (\Phi')^2\right]} \tag{3.61}$$

Notice that the scalar curvature can be defined in terms of the first and second derivatives of the metric functions. This makes impractical its substitution in the equation for d^2R/dr^2, suggesting that R should be treated as an independent variable for the solution of the differential equations system, although it stands as a consistency condition, and an important part in obtaining the behaviour of R near the origin of coordinates. This fact is exploited in the next subsection.

3.3.7 Rewriting the metric differential equations

For an easier comparison between general relativity and the quadratic theory, particularily of gravitational mass and the local surface gravity, the differential equations for Λ, Φ are rewritten by considering the mass function and its derivative,

$$m(r) = \frac{c^2 r}{2G}(1 - \exp(-2\Lambda(r))) \ , \quad \frac{d\Lambda}{dr} = \frac{Ge^{2\Lambda}}{c^2 r}\left(\frac{dm}{dr} - \frac{m}{r}\right) \ . \tag{3.62}$$

In both cases, it is possible to separate pressure-dependent terms from the pressure-independent ones.
First equation: Recall that

$$\frac{d\Lambda}{dr} = e^{2\Lambda}\left\{\frac{4\pi G\epsilon r}{c^4 A_1} + \frac{A_2}{4A_1 r} + \frac{\alpha r}{A_1 A_7}\left[\frac{A_1 A_4}{6\alpha} + \frac{A_2}{2r}\frac{dR}{dr} - \frac{A_9}{r}\frac{dR}{dr}\right]\right\} + \frac{A_3}{2A_1 r} - \frac{\alpha A_6}{A_1 A_7}\frac{dR}{dr}.$$

The terms inside the brackets can be written as

$$\{\} = \frac{1}{A_1}\left[\frac{4\pi G\epsilon r}{c^4}\gamma_1 + \gamma_2 + \frac{4\pi G P r}{c^4}\gamma_3\right] \tag{3.63}$$

where the following functions were introduced

$$\gamma_1(r) = 1 - \frac{A_1}{3A_7} + \frac{\alpha r}{A_7}\frac{dR}{dr} \tag{3.64}$$

$$\gamma_2(r) = \frac{A_1 R r}{6A_7} + \frac{A_2}{4r}\left(1 + \frac{2\alpha r}{A_7}\frac{dR}{dr}\right) \tag{3.65}$$

$$\gamma_3(r) = \frac{A_1}{A_7} - \frac{\alpha r}{A_7}\frac{dR}{dr} \tag{3.66}$$

Since

$$\gamma_4(r) = \frac{A_3}{2r} - \frac{\alpha A_6}{A_7}\frac{dR}{dr} \tag{3.67}$$

our differential equation becomes

$$\frac{d\Lambda}{dr} = \frac{e^{2\Lambda}}{A_1}\left[\frac{4\pi G\epsilon r}{c^4}\gamma_1 + \gamma_2 + \frac{4\pi G P r}{c^4}\gamma_3\right] + \frac{\gamma_4}{A_1}. \tag{3.68}$$

Introducing the derivative of the m function,

$$\frac{dm}{dr} = \frac{m}{r} + \frac{c^2 r}{GA_1}\left[\frac{4\pi G\epsilon r}{c^4}\gamma_1 + \gamma_2 + \frac{4\pi GPr}{c^4}\gamma_3\right] + \frac{c^2 r}{G}\left(1 - \frac{2Gm}{c^2 r}\right)\frac{\gamma_4}{A_1}. \tag{3.69}$$

Rearranging terms,

$$\frac{dm}{dr} = \frac{m}{r}\left(1 - \frac{2\gamma_4 r}{A_1}\right) + \frac{c^2 r}{GA_1}\left[\frac{4\pi G\epsilon r}{c^4}\gamma_1 + \frac{4\pi GPr}{c^4}\gamma_3 + \gamma_2 + \gamma_4\right]. \tag{3.70}$$

Second equation This case is far easier. There is no need for additional functions, and the steps are solely algebraic:

$$\frac{d\Phi}{dr} = \frac{e^{2\Lambda}}{A_1 r}\left\{\frac{4\pi GPr^2}{c^4} - \frac{1}{4}\left[\alpha r^2 R^2 + 2(1+2\alpha R)(e^{-2\Lambda} - 1) + 8\alpha r e^{-2\Lambda}\frac{dR}{dr}\right]\right\}.$$

$$\frac{d\Phi}{dr} = \frac{e^{2\Lambda}}{A_1 r}\left\{\frac{4\pi GPr^2}{c^4} + \frac{Gm}{c^2 r}(1+2\alpha R) - \frac{1}{4}\left[\alpha r^2 R^2 + 8\alpha r\frac{dR}{dr}(e^{-2\Lambda} - 1) + 8\alpha r\frac{dR}{dr}\right]\right\} \tag{3.71}$$

$$\frac{d\Phi}{dr} = \frac{e^{2\Lambda}}{A_1 r}\left\{\frac{4\pi GPr^2}{c^4} + \frac{Gm}{c^2 r}(1+2\alpha R) + 4\alpha r\frac{dR}{dr}\frac{Gm}{c^2 r} - \frac{1}{4}\left[\alpha r^2 R^2 + 8\alpha r\frac{dR}{dr}\right]\right\} \tag{3.72}$$

$$\frac{d\Phi}{dr} = \frac{[r - 2Gm/c^2]^{-1}}{A_1}\left\{\frac{4\pi GPr^2}{c^4} + \frac{Gm}{c^2 r}\left(1 + 2\alpha R + 4\alpha r\frac{dR}{dr}\right) - \frac{\alpha r}{4}\left[rR^2 + 8\frac{dR}{dr}\right]\right\}. \tag{3.73}$$

It is easy fo see that eqs 3.70 and 3.73 reduce to its general relativity counterparts when $\alpha \to 0$.

Proof. If $\alpha \to 0$, $A_1, A_3, A_6, A_7 \to 1$ and $A_2 \to -2$. Thus, $\gamma_1 \to 2/3$, $\gamma_2 \to (Rr/6) - (1/2r)$, $\gamma_3 \to 1$, $\gamma_4 \to 1/2r$. As a consequence,

$$\frac{dm}{dr} = \frac{c^2 r}{G}\left[\left(\frac{4\pi Gr}{c^4}\right)\left(\frac{2}{3}\epsilon + P\right) + \frac{Rr}{6}\right]. \tag{3.74}$$

But $R = (8\pi G/c^4)(\epsilon - 3P)$ in general relativity, therefore

$$\frac{dm}{dr} = \frac{c^2 r^2}{G}\left(\frac{4\pi G}{c^4}\right)\left[\frac{2}{3}\epsilon + P + \frac{1}{3}\epsilon - P\right]. \tag{3.75}$$

Finally,

$$\frac{dm}{dr} = \frac{4\pi r^2}{c^2}\epsilon = 4\pi\rho r^2. \tag{3.76}$$

The second equation is immediate: since $\alpha \to 0$, the additional terms inside the square brackets vanish. Thus,

$$\frac{d\Phi}{dr} = \left(r - \frac{2Gm}{c^2}\right)^{-1}\left[\frac{4\pi GPr^2}{c^4} + \frac{Gm}{c^2 r}\right]. \tag{3.77}$$

■

In GR, the mass function is called the *gravitational mass* of the object due to the form of the differential equations which this function satisfy,

$$\frac{dm}{dr} = 4\pi\rho r^2 \ .$$

We can still keep this name, although the differential equation is completely different, due to the fact that the transport equations do not distinguish between theories, that is, only the values of the metric functions are requiered, not their interpretation. Moreover, as we explore in the next section it is possible and desirable to recover a Schwarzschild limit for the metric functions, at a very far away radial distance from the origin of coordinates, justifying the name of gravitational mass.

3.4 Behaviour near the origin and at long distances

Analysis of the metric functions beyond the differentiability hypothesis requires the solution of the set of equations, which is not an analytically immediate tasks. Moreover, it has been shown that a perturbative approach results in small differences with respect to GR [18], [19], [20], in contrast with a non-perturbative one [13], [21]. However, studying the behaviour of the differential equations near and far away from the origin of coordinates might help to extract information about the functions and the boundary conditions that must satisfy in order to describe physical objects such as NSs. We divide this task in two subsections.

3.4.1 Near the origin

Back to the suplementary equation for the scalar curvature, we perform a Taylor expansion over $r = 0$ on the first term,

$$\frac{2}{r^2}\left(1 - e^{-2\Lambda(r)}\right) = \frac{2}{r^2}\left[1 - \exp\left(-2\Lambda(0) - 2\Lambda'(0)r - \Lambda''(0)r^2 - \mathcal{O}(r^3)\right)\right] \ . \quad (3.78)$$

If we desire for this term to remain finite in the limit $r \to 0$, we must demand that

$$\boxed{\Lambda(0) = \Lambda'(0) = 0} \quad (3.79)$$

Next, by combining the differential equations of Φ and Λ we arrive at

$$\Lambda'(r) + \Phi'(r) = \frac{4\pi G r e^{2\Lambda(r)}(P + \epsilon)}{c^2 A_1} + \frac{\alpha r}{A_1}\frac{d^2R}{dr^2} \ . \quad (3.80)$$

Clearly, if $r \to 0$ the condition

$$\boxed{\Phi'(0) = 0} \quad (3.81)$$

is obtained.

Finally, if we move to eq. 3.35, the right hand side is regular at the origin. However, on the left side the problematic term is

$$\frac{4\alpha}{r}\frac{dR}{dr} \ . \tag{3.82}$$

In order to be regular, the condition

$$\boxed{dR/dr|_{r=0} = 0} \tag{3.83}$$

must be met.

The conclusion of the previous arguments is that, in order to attain regularity of the metric functions and the derivative of the cuvature scalar at the origin of coordinates, we must demand

$$\lim_{r\to 0}\Lambda'(r) = \lim_{r\to 0}\Phi'(r) = \lim_{r\to 0}R'(r) = 0. \tag{3.84}$$

Due to the abscence of Φ on the right hand side of the system of differential equations, we are free to choose an arbitrary value of $\Phi(0)$, and re-adjusting it in order to match the boundary conditions discussed in the next part. On the other hand, the pair $(\epsilon(0), P(0))$ are provided by the EoS, giving rise to a family of NS for each of the possible tabulated values.

What about $R(0)$? In GR, there is an immediate relation with the $(\epsilon(0), P(0))$ pair, so we could try to find an analogy in the quadratic model. Employing the previous limits on the trace equation, we see that [14]

$$\boxed{R(0) = \frac{8\pi G}{c^4}(\epsilon(0) - 3P(0)) + 18\alpha R''(0)} \ . \tag{3.85}$$

Clearly, the scalar curvature depends on its GR counterpart. However, an expression for $R''(0)$ is missing if we desire to write R_0 in terms of $(\epsilon(0), P(0))$ only. We can go a little further:

First: in the limit $r \to 0$, the supplementary equation for R tells us that

$$\boxed{R(0) = 6(\Lambda''(0) - \Phi''(0))} \ . \tag{3.86}$$

Second: if we combine the equations for $d\Lambda/dr$, $d\Phi/dr$, we can notice that

$$\Lambda'(r) + \Phi'(r) = \frac{4\pi G r e^{2\Lambda}}{c^4 A_1}(P + \epsilon) + \frac{\alpha r}{A_1}\frac{d^2R}{dr^2} \ . \tag{3.87}$$

By computing its derivative and considering the limit $r \to 0$,

$$\boxed{\Lambda''(0) + \Phi''(0) = \frac{1}{1 + 2\alpha R(0)}\left[\frac{4\pi G}{c^4}(P(0) + \epsilon(0)) + \alpha R''(0)\right]} \ . \tag{3.88}$$

Therefore, eqs. 3.85, 3.86 and 3.88 constitute a system of algebraic equations from which the R_0 value can be computed. Since there are three equations but four variables, at least one parameter remains free.

3.4.2 Away from the origin

A remarkable difference between the quadratic model and GR is the fact that $P = \epsilon = 0$ is not equivalent with a zero curvature. This renders the differential equations of the metric function as completely different from the Schwarzschild's one, and to the emergence of a *gravitational sphere* [23], which is refered as the region outside the star where R goes to zero. We might still ask if there is a possibility of recovering this limit outside the star, at long distances from the surface. Although an exact expression for the metric functions is missing, at this point we can extract important features which must be imposed in order to recover Schwarzschild's solution. First: the scalar curvature must be zero. Second, from the fact that $\Lambda' + \Phi' = 0$, together with eq. 3.87, it follows that $R''(r) = 0$. Combining the first consideration with the general solution of this differential equation, $R(r) = A + Br$, we see that $A = B = 0$. Thus, at very far away distance from the star it is possible to recover Schwarzschild's limit.
We can move a little step ahead from this quick observations. The trace equation, in the case $T = 0$, becomes

$$\frac{d^2R}{dr^2} + \left(\frac{2}{r} + \frac{d\Phi}{dr} - \frac{d\Lambda}{dr}\right)\frac{dR}{dr} = \frac{e^{2\Lambda}R}{6\alpha} \ . \tag{3.89}$$

For large values of r, $2/r$ rapidly converges to zero. The next assumption is regarding $d\Phi/dr$ and $d\Lambda/dr$ as functions that converge to zero at the same rate as $1/r$. A quick look at eqs. 3.70 and 3.73 allows to corroborate this approximation. As a consequence, the trace equation becomes

$$\frac{d^2R}{dr^2} - \frac{e^{2\Lambda}}{6\alpha}R = 0 \ . \tag{3.90}$$

Aside from the trivial solution $R = 0$, we can find exponentials or oscillating functions according to the sign of α. Since Λ' is almost zero, $\exp(2\Lambda)$ becomes a constant and:
Case $\alpha < 0$**:** The most general solution is

$$R(r) = A\sin\left(\sqrt{-\frac{e^{2\Lambda}}{6\alpha}}r\right) + B\cos\left(\sqrt{-\frac{e^{2\Lambda}}{6\alpha}}r\right) . \tag{3.91}$$

An oscillating curvature appears odd, although not unreasonable: even inside relativistic stars this phenomena occurs, and the value of α may be tuned to produce long or short variations of sign(R). The real issue comes at the estimation of the gravitational mass: from the suplementary equation we know that

$$R(r) \propto \frac{2(1 - e^{-2\Lambda})}{r^2} = \frac{4Gm(r)}{c^2r^3} \ . \tag{3.92}$$

By matching both expressions, we see that

$$m(r) \propto r^3 \left[A \sin\left(\sqrt{-\frac{e^{2\Lambda}}{6\alpha}} r \right) + B \cos\left(\sqrt{-\frac{e^{2\Lambda}}{6\alpha}} r \right) \right] . \tag{3.93}$$

This is disastrous: the gravitational mass grows without limits, becoming a position dependent quantity, and the Schwarzschild limit cannot be recovered. Therefore, α must be non-negative *for the metric sign convention under consideration.* Another reason to discard this sign is the failure on recovering Schwarzschild's limit or at least asymptotic flatness.

Case $\alpha > 0$**:** The most general solution is a combination of exponentials:

$$R(r) = A \exp\left(\sqrt{\frac{e^{2\Lambda}}{6\alpha}} r \right) + B \exp\left(-\sqrt{\frac{e^{2\Lambda}}{6\alpha}} r \right) . \tag{3.94}$$

The growing exponential may be disastrous, but the negative one indeed leads to a zero scalar curvature. Moreover: the mass function can be regarded as a convergent function, although the issue of a position-dependent mass still remains. This is corroborated with the differential equation for the Λ function, where the terms involving R and dR/dr allows for a growing/decreasing behaviour. Nevertheless, this quantitative behaviour illustrates the possibility of building compact objects if $\alpha \geq 0$.

It is then clear that the following boundary conditions for the scalar curvature and its derivative lead to the possibility of building compact objects for $\alpha \geq 0$,

$$\boxed{\lim_{r\to\infty} R(r) = \lim_{r\to\infty} \frac{dR(r)}{dr} = 0} . \tag{3.95}$$

Regarding the gravitational mass, we demand consistency with the observations: a constant value must be measured at long distance from the center of the object,

$$\boxed{M_{\text{grav}} = \lim_{r\to\infty} \frac{c^2 r}{2G} \left(1 - \exp(-2\Lambda(r))\right)} . \tag{3.96}$$

The assumptions about Λ', Φ' cannot be kept globally, but might be regarded as asymptotic,

$$\boxed{\lim_{r\to\infty} \frac{d\Phi}{dr} = \lim_{r\to\infty} \frac{d\Lambda}{dr} = 0} . \tag{3.97}$$

This also guarantees that, at long distance from the object, the Schwarzschild's metric $\Lambda(r) + \Phi(r) = 0$ is recovered.

3.5 Weak Field Limit

This regime consists on the approximation of the metric tensor as

$$g_{\mu\nu} = \eta_{\mu\nu} + h_{\mu\nu} \tag{3.98}$$

where $h_{\mu\nu}$ is regarded as a small perturbation upon flat-spacetime, $|h_{\mu\nu}| \ll 1$. The rest of the metric-dependent geometric quantities such as the Levi-Civitta connection, the Riemann and Ricci tensors and the scalar curvature are changed according with this approximation,

$$\Gamma^{(1)\alpha}{}_{\mu\nu} = \frac{1}{2}\eta^{\alpha\epsilon}\left(\partial_\mu h_{\epsilon\nu} + \partial_\nu h_{\epsilon\mu} - \partial_\epsilon h_{\mu\nu}\right) \ , \tag{3.99}$$

$$R^{(1)\alpha}{}_{\beta\mu\nu} = \frac{1}{2}\left[\partial_\beta\partial_\mu h^\alpha{}_\nu + \partial^\alpha\partial_\nu h_{\beta\mu} - \partial_\beta\partial_\nu h^\alpha{}_\mu - \partial^\alpha\partial_\mu h_{\beta\nu}\right] \ , \tag{3.100}$$

$$R^{(1)}{}_{\mu\nu} = \frac{1}{2}\left[\partial_\mu\partial_\alpha h^\alpha{}_\nu + \partial_\nu\partial_\alpha h_\mu{}^\alpha - \partial_\mu\partial_\nu h - \Box h_{\mu\nu}\right] \ , \tag{3.101}$$

$$R^{(1)} = \left[\partial_\alpha\partial_\beta h^{\beta\alpha} - 2\Box h\right] \ , \tag{3.102}$$

where $h = h^\alpha{}_\alpha$. Naturally, the Lagrangian density must also be rewritten to first order:

$$f(R) = R^{(1)} \quad , \quad \frac{df}{dR} = 1 + 2\alpha R^{(1)} \ . \tag{3.103}$$

Consequently, the field equations are

$$-\frac{R^{(1)}}{2}\eta_{\mu\nu} + R^{(1)}_{\mu\nu} - 2\alpha\partial_\mu\partial_\nu R^{(1)} + 2\alpha\eta_{\mu\nu}\Box R^{(1)} = \frac{8\pi G}{c^4}T^{(1)}_{\mu\nu} \ . \tag{3.104}$$

Regarding the trace,

$$\Box R^{(1)} - \frac{1}{6\alpha}R^{(1)} = \frac{8\pi G}{6\alpha c^4}T^{(1)} \ . \tag{3.105}$$

Clearly, this equation resembles the well-known Klein-Gordon equation with a source,

$$\left[\Box - \left(\frac{mc}{\hbar}\right)^2\right]\Phi = \frac{dV}{d\Phi} \ . \tag{3.106}$$

In order to compute $h_{\mu\nu}$, it is suitable to perform a gauge transformation [24], [25] of the form

$$h_{\mu\nu} = \bar{h}_{\mu\nu} - \left(2\alpha R^{(1)} + \frac{\bar{h}}{2}\right)\eta_{\mu\nu} \ , \quad \bar{h}_{\mu\nu} = h_{\mu\nu} - \left(2\alpha R^{(1)} + \frac{h}{2}\right)\eta_{\mu\nu} \ , \tag{3.107}$$

where the second rank tensor $\bar{h}_{\mu\nu}$ is divergence-free,

$$\partial^\mu\bar{h}_{\mu\nu} = 0 \ . \tag{3.108}$$

This is usually refered as the Lorentz - de Donder gauge, and this choice allows to re-write the field and trace equations as

$$\Box \bar{h}_{\mu\nu} = -\frac{16\pi G}{c^4} T^{(1)}_{\mu\nu} \ , \tag{3.109}$$

$$\Box R^{(1)} - \frac{1}{6\alpha} R^{(1)} = \frac{4\pi G}{3\alpha c^4} T^{(1)} \ . \tag{3.110}$$

This set of differential equations can be easily solved with the method of the Green Function [25], [7]: let $\xi^2 > 0$ be a real number. The solution of

$$\left[\Box - \xi^2\right] G(x - x_1) = -\delta(x - x_1) \ , \tag{3.111}$$

with $\delta(x - x_1)$ the 4-dimensional Dirac delta function, is

$$G_\xi(x - x_1) = \int \frac{dk_0}{2\pi} \frac{\exp\left(-ik_0 (x - x_1)^0\right)}{4\pi |\vec{x} - \vec{x}_1|} \begin{cases} \exp\left[i \left(k_0^2 - \xi^2\right)^{1/2} |\vec{x} - \vec{x}_1|\right] & k_0^2 > \xi^2 \\ \exp\left[-\left(\xi^2 - k_0^2\right)^{1/2} |\vec{x} - \vec{x}_1|\right] & k_0^2 < \xi^2 \ . \end{cases}$$

The respective solutions are

$$\bar{h}_{\mu\nu}(x) = \frac{16\pi G}{c^4} \int d^4 x_1 G_0(x - x_1) T^{(1)}_{\mu\nu}(x_1) \ , \tag{3.112}$$

$$R^{(1)}(x) = -\frac{4\pi G}{3\alpha c^4} \int d^4 x_1 G_{\sqrt{1/6\alpha}}(x - x_1) T(x_1) \ . \tag{3.113}$$

In the weak-field limit, only matter-energy density contributes, i.e. $|T_{00}| \gg |T_{\alpha j}|$. An instructive and suitable choice for this component is that of a point-particle, $T_{00} = \epsilon = Mc^2 \delta(\vec{x}_1)$, $T = -\epsilon$. The solutions for the gauge perturbation and the scalar curvature are

$$\bar{h}_{00}(x) = \frac{4GM}{c^2 |\vec{x}|} \ , \quad \bar{h}_{0i} = \bar{h}_{ij} = 0 \ , \tag{3.114}$$

$$R^{(1)}(x) = -\frac{GM}{3\alpha c^2} \frac{\exp\left(-|\vec{x}|/\sqrt{6\alpha}\right)}{|\vec{x}|} \ . \tag{3.115}$$

Direct substitution of these expressions in the $h_{\mu\nu}$ term leads to

$$h_{00} = \frac{2GM}{c^2 |\vec{x}|} \left[1 - \frac{\exp\left(-|\vec{x}|/\sqrt{6\alpha}\right)}{3}\right] \ , \quad h_{ij} = \frac{2GM}{c^2 |\vec{x}|} \left[1 + \frac{\exp\left(-|\vec{x}|/\sqrt{6\alpha}\right)}{3}\right] \delta_{ij} \ . \tag{3.116}$$

If we make the identification $-(1+2U/c^2) = \eta_{00} + h_{00}$, then the *gravitational potential* of a point particle is

$$U(\vec{x}) = -\frac{GM}{|\vec{x}|} \left[1 - \frac{\exp\left(-|\vec{x}|/\sqrt{6\alpha}\right)}{3}\right] \ , \tag{3.117}$$

which correspond to a Newtonian plus a Yukawa-type. Here, $r_a = \sqrt{6\alpha}$ plays the role of the effective range of this interaction. If we set $\alpha \sim \mathcal{O}(10^{12})$ cm^2, $r_a \sim 10^6$ cm and for the Solar System, for example, its contribution becomes irrelevant for the orbits of the planets. Indeed: since the average distance between Mercury and the Sun is $d \sim 5.8 \times 10^{12}$, $\exp(-d/r_a) \approx 0$.

3.6 Geodesics motion of massive particles

Since the covariant derivative of the $f(R)$ field equations is still torsion-free, the equations of the geodesic curve remain valid for this theory. As with the energy transport equations, here we might expect significant deviations for the trajectories of massive or massless particles.

Regarding the SSS metric, the abscence of the time and azimutal coordinates implies that the correspondent 4-momentum components of some particle, p_t, p_ϕ, are constant quantities. We can identify them with the energy and angular momentum measured at infinity, $p_0 = -E^\infty/c$, $p_\phi = L^\infty$. If we combine this fact with the magnitude of its 4-momentum, $p^\mu p_\mu = -mc^2$, and fixing a direction θ, it is possible to deduce the differential equation for the radial coordinate. Indeed, expanding the expression for the magnitude we have

$$-e^{-2\Phi}\frac{E^2}{c^2} + m^2 e^{2\Lambda}\left(\frac{dr}{d\tau}\right)^2 + \frac{L^2}{r^2\sin^2\theta} = -m^2c^2 \ ,$$

$$\left(\frac{dr}{d\tau}\right)^2 = e^{-2(\Phi+\Lambda)}\frac{E^2}{m^2c^2} - e^{-2\Lambda}\left(c^2 + \frac{L^2}{m^2r^2\sin^2\theta}\right) \ . \tag{3.118}$$

We can introduce the energy and angular momentum per unit mass, $\tilde{E} = E^\infty/m$, $\tilde{L} = L^\infty/m$. Thus,

$$\left(\frac{dr}{d\tau}\right)^2 = e^{-2(\Phi+\Lambda)}\frac{\tilde{E}^2}{c^2} - e^{-2\Lambda}\left(c^2 + \frac{\tilde{L}^2}{r^2\sin^2\theta}\right) \ . \tag{3.119}$$

For $\tilde{L} \neq 0$ we can employ chain's rule

$$\frac{dr}{d\tau} = \frac{dr}{d\phi}\frac{d\phi}{d\tau} = \frac{\bar{L}}{r^2\sin^2\theta}\frac{dr}{d\phi} \ , \tag{3.120}$$

to write eq. 3.119 in terms of the azimutal angle ϕ,

$$\frac{\tilde{L}^2}{r^4\sin^4\theta}\left(\frac{dr}{d\theta}\right)^2 = e^{-2\Lambda}\left[\frac{e^{-2\Phi}\tilde{E}^2}{c^2} - c^2 - \frac{\bar{L}^2}{r^2\sin^2\theta}\right] \ , \tag{3.121}$$

$$\frac{dr}{d\phi} = r\sin\theta e^{-\Lambda}\sqrt{\left[\frac{e^{-2\Phi}\tilde{E}^2 - c^4}{c^2\tilde{L}^2}\right]r^2\sin^2\theta - 1} \ . \tag{3.122}$$

An important difference of the quadratic model with GR, regarding geodesic motion, appears in eq. 3.119 where it is not globally true that $\Lambda + \Phi = 0$. Moreover, since an analytic expression for these functions is not avaliable, numerical methods must be employed for solving the differential equations.

3.7 Einstein and Jordan Frame issue

We devote the final part of this chapter to an extensively debated aspect of the modified theories of gravity, including $f(R)$: the invariance of the physical predictions under a particular conformal transformation, connecting the so-called *Einstein and Jordan frames* [53], [27], [26]. In first place, a Lagrangian density is said to be formulated in:
Einstein frame: if the scalar curvature is not multiplied by any other field,

$$\mathcal{L} = \kappa R + \text{additional terms} \ , \tag{3.123}$$

with κ a real constant;
Jordan frame: if the scalar curvature is multiplied by a functional of the additional fields,

$$\mathcal{L} = F[\phi]R + \text{additional terms} \ . \tag{3.124}$$

Over the years it has been shown that, for certain Lagrangian densities related to Brans-Dicke and Scalar-Tensor theories, it is possible to move between frames through a conformal transformation. Moreover, such procedure is desirable in order to simplify the equations of motion of the fields, rendering them easier to handle.
The actual issue of this scheme is the "physical" meaning of conformal invariance: it is sometimes argued that physical predictions *must* be the same, no matter which frame is chosen. While some quantities (for example, gravitational mass and radius of the star) might be conformally invariant, this could be an only incidental due to the following facts:
1. The equations for the geodesic curve are not conformally invariant [7]: the $\Gamma^{\alpha}_{\ \mu\nu}$ connection explicitely depends on the metric. Therefore, a geodesic curve under $g_{\mu\nu}$ is not necesarily geodesic under $\bar{g}_{\mu\nu}$.
2. For certain theories, the positiveness of the energy conditions holds in one of the frames only.
Clearly, not all predictions are conformally invariant. This conclusion has raised the question of which frame must be regarded as physical. However, this only makes sense if we consider that both Lagrangian densities and equations of motion represent the same physical system.
There is another point of view that, although theoretically discouraging, might be more suitable: each Lagrangian density and the correspondent equations of motion represent a different theory of gravitation. The fact that they are conformally related is only a mathematical aspect that helps simplifying the equations and finding

solutions for them. However, if we desire to make physical predictions we must go back to the original frame. If any physical prediction is incompatible with observational constrains, the correspondent theory must be discarded.[27] . This point of view does not exclude the possibility of seeking for a conformally invariant theory of gravity, although such task is beyond the scope of the present work. As a note aside, GR is not conformally invariant, so the possibility of discarding a theory for the same reason does not seem a promising path. Instead (and that is the point of view for the rest of this work), we should choose a more pragmatic approach of confronting theoretical predictions in the original frame, either we solve the equations of motion in this or in the conformal one.

Chapter 4

Thermal Physics in Curved Spacetime: Neutron Stars

"*Three quarks for Muster Mark!*"

James Joyce

In chapter 2 and 3, we have seen that concepts such as local-flatness hold for the quadratic model. Moreover, at the microscopic level it has been shown that the quadratic term in the equations of motion is negligible regardless of the α chosen (and still treating the Lagrangian density as an effective, classialc theory). As a consequence, it is possible to describe internal aspects such as superfluidity (which depends on number densities) or the equation of state (arising from numerical calculations over a Minkowski spacetime), without invoking a gravity model. On the other hand, observed quantities such as luminosity rely on the metric functions under consideration, so it is important to explicitly show that the energy transport equations are valid in the $f(R)$ model.

The structure of this chapter is the following: notation and thermodynamical variables are defined in Section 1. A brief description of the composition and structure of a NS is given in Section 2. The cooling of compact objects constitutes the final section, where the processes involved are explained in detail and the numerical results so far obtained with GR are discussed.

4.1 Generalities

The following list includes all thermodynamical variables which are discussed along the chapter [36]. In order to distinguish between their value at the surface of the star and at long distances, we employ the notation X_r and X^∞ respectively.

$N_b \equiv$ total number of baryons,
$\bar{m} \equiv$ mean baryonic mass (usually the mass of the nucleons),
$M_{\rm b} = \bar{m} N_b \equiv$ baryonic rest-mass.
$n_b \equiv$ number density of baryons,
$\epsilon \equiv$ total energy density,
$\rho = \epsilon c^{-2} \equiv$ mass-energy density,
$P \equiv$ pressure
$\mu \equiv$ chemical potential,
$T \equiv$ temperature,
$S \equiv$ entropy,
$s_b = \frac{S}{N_b} \equiv$ entropy per baryon.
$K \equiv$ thermal conductivity,
$L \equiv$ luminosity.

The *effective temperature* of a star is another way of expressing its luminosity, taking into account its radius. Denoted by T_e, it satisfies the following relation,

$$L = 4\pi\sigma R^2 T_e^4 \ , \tag{4.1}$$

where $\sigma = 5.67 \times 10^{-5}$ erg cm^{-2} s^{-1} K^{-4} is the Stefan-Boltzmann constant, and R is the radius of the star. It must be remarked that the actual temperature of the star (denoted as T_b) can only be constrained from T_e via atmosphere models, which strongly depends in the chemical composition.

For computing total quantities from their correspondent densities, integration is carried at constant time and with the proper spatial volume element,

$$X = \int_\Omega \sqrt{\gamma} d^3x \rho_X \ . \tag{4.2}$$

In the particular case of the SSS metric, $dV = e^{\Lambda(r)} r^2 \sin\theta dr d\theta d\phi$. Additionally, the densities can be assumed as radial functions only. Therefore, $\Omega = [0, R] \times [0, \pi] \times [0, 2\pi]$, where R is a fixed coordinate and

$$X = 4\pi \int_0^R \rho_X(r) e^{\Lambda(r)} r^2 dr \ \ . \tag{4.3}$$

From the fact that information travels along either timelike (for massive particles) or null (for photons) geodesics, where energy is the zero component of its 4-momentum, we can establish the following relation between a quantity X measured at the surface of the NS, i.e., a local value, and its value as measured on the Earth, i.e., "at infinity", denoted by X^∞:

$$(T^\infty, L^\infty) = (e^\Phi T, e^{2\Phi} L) \ . \tag{4.4}$$

The apearence of $e^\Phi \equiv \sqrt{|g_{00}|}$ can be easily explained: since $E = k_B T$ holds in both frames and $E^\infty = e^\Phi E$, then $T^\infty = e^\Phi T$. For the luminosity, we are dealing with

the quotient of the energy and time measured in each frame. Since $t^\infty = e^{-\Phi}\tau$, τ being the local time,

$$L^\infty = \frac{dE^\infty}{dt^\infty} = \frac{e^\Phi dE}{e^{-\Phi}d\tau} = e^{2\Phi}L \ . \tag{4.5}$$

Thus, the luminosity measured at the Earth is

$$L^\infty = 4\pi\sigma(R^\infty)^2(T_e^\infty)^4 \ , \tag{4.6}$$

where we define $R^\infty \equiv e^{-\Phi}R$.

4.2 Composition of a Neutron Star

An *Equation of State* (EoS) is a function which relates several thermodynamic variables, mainly ϵ, P, n and s. Arising from numerical calculations, they are frequently introduced in tabulated form, although some of them have been fit by analytic expressions. They can be classified as *soft* or *stiff* according to their compressibility. In Fig. 4.1 several EoS are included in a P versus ϵ) diagram, where the stiffest region corresponds to $P \geq \epsilon$, while the softest is considered below the relativistic gas EoS.

APR [28] and SLy [29] are models describing nucleon interactions with two and three body potentials including relativistic effects as corrections, while MPA [30] and MS [31], [32] describe nuclear interactions with meson-exchange models and are fully relativistic. Two restrictions for choosing these EoS are compatibility with measured gravitational mass of 2 $M_\odot$ [33], [34], and radius range of [11.5, 13.5] km, infered from NICER and gravitational waves observations, for 1.4 $M_\odot$ stars [3],[49].

Several consequences arise from the choice of an EoS. First, each pair (P, ϵ) can be set as initial conditions for the differential equations of structure, obtaining in this way a family of possible stars. The exact composition and the numerical densities of particles enhance the possibility for some processes to take place, such as the Direct Urca which, as will be seen shortly, has significant consequences over the cooling of NS. An important feature of these families is that, assuming GR is the right theory of gravitation, the shape of the gravitational mass versus radius curves is EoS independent, as can be seen from Fig. 4.2: after a maximum value of M is reached, the curve decreases until a change of concavity takes place. These region is characterized by larger but less massive stars. Finally, when $dM_{\text{grav}}/dr < 0$ holds the branch of the curve corresponds to equilibrium configurations stable under small perturbations while in the part where $dM_{\text{grav}}/dr > 0$ the neutron stars are unstable and prone to gravitational collapse into a black hole [see Chapter 6 of [51]]. The incorporation of the EoS in tensorial language is usually given through the energy-momentum tensor of a perfect fluid,

$$T_{\mu\nu} = (\epsilon + P)u_\mu u_\nu + P g_{\mu\nu} \ , \tag{4.7}$$

where u_μ is the dual vector associated with the 4-velocity normalized to unity, i.e. $u_\mu = U_\mu/c$.

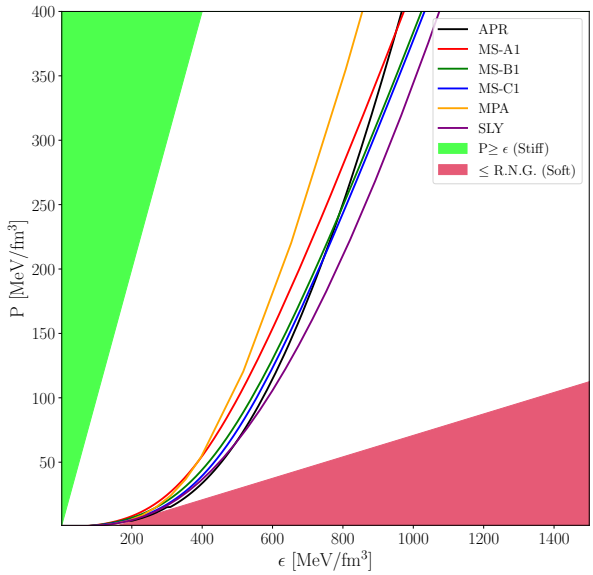

Figure 4.1: Plot of ϵ vs P, both in MeV/fm^3 for the labeled EoS. The region of stiff EoS is coloured in green, while those softer than the relativistic neutron gas (N.R.G.) are enclosed in the crimson region.

The description given below corresponds to the current theoretical point of view on the composition of a neutron star. As a matter of fact the models are more reliable as we move from the center to the surface, in principle from the amount of different EoSs which are observationally acceptable but lack a universal agreement over the composition of the inner parts. Therefore, the discussion begins at the center and ends at the top of the star. For a quick look and as a complement of this section we include Fig. 4.3.
From a theoretical point of view, the interior of a NS can be roughly divided in two parts: the crust and the core. This first-order phase transition between them takes place at $\rho \sim 1.6 \times 10^{14}$ g·cm^{-3}, which is ∼60% of the symmetric nuclear matter density $\rho_{\text{nuc}} \sim 2.8 \times 10^{14}$ g·cm^{-3}. On average, the core occupies 90% of the NS total volume.

While the gravitational mass and stellar radius are well constrained in order of magnitude, the exact composition of the inner core remains a mystery. Several proposals have been made, from pure nuclear matter to deconfined quarks. This uncertainty in the EoS is expected to be reduced in the near future, with the arrival

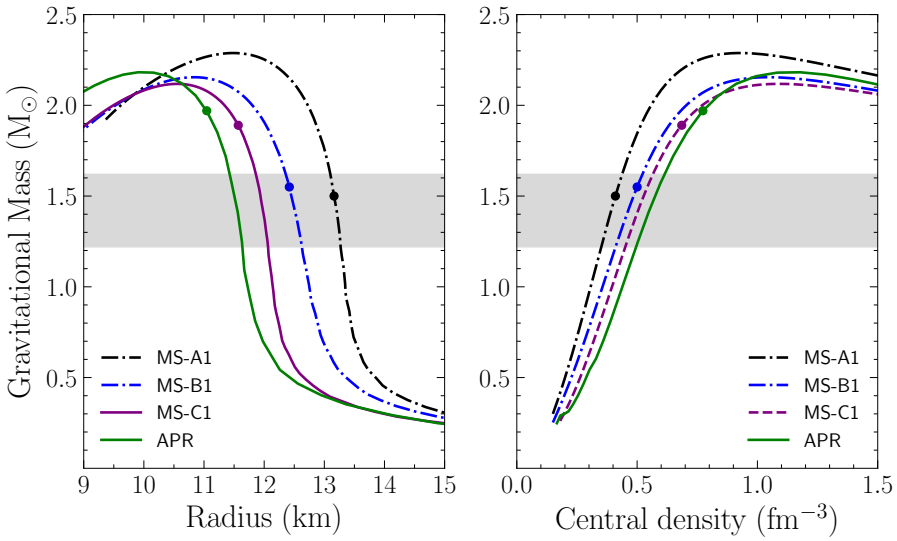

Figure 4.2: (Left) Gravitational mass vs stellar radius diagram, for the labeled EoS and considering GR's equations of structure. (Right) Gravitational mass versus central density. In both panels, the dots indicate the Direct Urca mass-threshold, and the shaded region indicates the mass range for the compact object in SN 1987A. Taken from [32] with permission of the author.

of improved instrumentation capable of measuring gravitational waves arising in tidal deformations or binary systems, for example.

Regarding the outer core, it is likely to find protons and neutrons in a superfluid state, either in the ${}^1S_0$ or ${}^2P_3$ channel depending on their correspondent number densities and the internal temperature. In particular, neutrons are expected in the ${}^2P_3$ state, leading to the presence of vortices. Being charged particles, protons are also expected to be in superconducting state, while the magnetic field can be encountered confined to fluxoids. Due to its high density, neutrino emission is expected to take place in the core, either from β decays processes such as Direct or Modified Urca, as well as the formation of Cooper pairs. These particles are able to carry away a vast amount of energy, thus playing an important role in the cooling of NS. We shall come back to this point in the next section.

Going from the core to the crust, it is possible to find elongated nuclei of increasing Z, A, until the density is low enough to admit a transition from lasagna-spaghetti to spherical shape. At this point, the nuclei form a lattice (usually modeled as a body-centered-cubic one), immersed in a quantum liquid of electrons and free neutrons, very likely in a ${}^1S_0$ superfluid state. This picture is admissible for densities exceeding the neutron drip point, $\rho_{\text{drip}} = 4 - 7 \times 10^{11}$ g·cm^{-3}.

Between the atmosphere and the crust, there is an envelope of not-fully degenerate matter which acts as a thermal insulator between the interior and exterior.

Being several tens of meters thick, this region regulates the amount of heat leaving the star and plays a central role for modeling the relationship between the interior and the effective temperature. In particular, the exact composition of the envelope predominates over the presence of magnetic fields. Additionally, light-elements such as H, He, C or O contributes to increase the luminosity, while heavy-elements as iron tend to reduce it. This is easily explained from scattering theory considering that heat is transported by electrons: the electron-nucleus scattering cross-section is proportional to the charge number number squared, Z^2. Thus, an electron inside a region of light-elements would be scattered less times than inside a heavy-elements one.

Finally, the atmosphere is a thin layer (at most a few tens of centimeters thick) where thermal photons are emitted. As a consequence, this region determines the observed energy distribution of the thermal flux. Modeling the atmosphere is thus of uttermost importance in order to constrain the luminosity/effective temperature.

4.3 Cooling of compact objects

For a neutron star described by the SSS metric, (T, L) can be regarded as time and radial dependent functions only, $T = T(r;t)$ and $L = L(r;t)$. In this case, they obey the following partial differential equations [36], [37]:

$$\frac{e^{-\Lambda-2\Phi}}{4\pi r^2}\frac{\partial}{\partial r}\left(e^{2\Phi}L\right) = -Q_\nu + Q_{\rm h} - \frac{C_V}{e^{\Phi}}\frac{\partial T}{\partial t} \ , \tag{4.8}$$

$$-\frac{L}{4\pi K r^2} = e^{-(\Lambda+\Phi)}\frac{\partial}{\partial r}\left(e^{\Phi}T\right) \ , \tag{4.9}$$

where Q_ν and $Q_{\rm h}$ are the neutrino emissivity and heating source per unit volume, C_V is the heat capacity per unit volume and K the thermal conductivity, all of them also being functions of r and t.

Due to the high densities present in the neutron star interior the equation of state, i.e., the relationship $P = P(\epsilon)$, is independent of the temperature T and, thus, neither T nor L appear in the differential equations for the metric functions in GR or the $f(R)$ model. Thus, it is possible to solve the system of equations 3.23-3.30 independently of 4.8 and 4.9 . Once the structure is given, it remains the same for the whole cooling process. Moreover, these equations 4.8 and 4.9 seem to be indifferent to the gravitation model chosen. In order to prove this assertion, it is useful to review the origin of these equations.

Proof. In Lagrangian coordinates, the change of luminosity with respect to an element of fluid must be equal to the rate of thermonuclear energy generation minus the amount of heat added or removed, per baryon and unit time,

$$\frac{\partial L}{\partial N_b} = q_\nu + q_{\rm h} - \frac{\partial \xi}{\partial t} \ ,$$

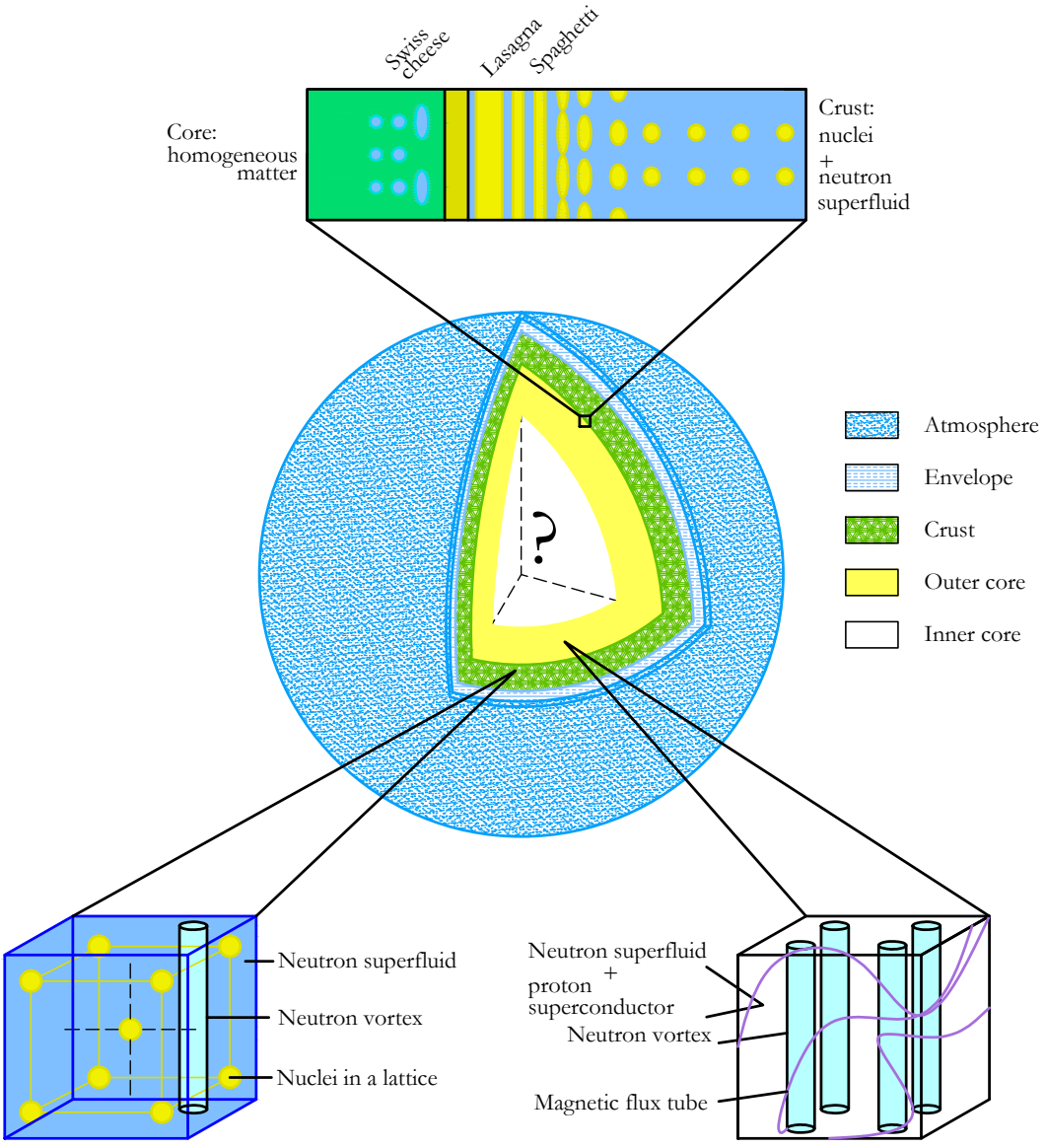

Figure 4.3: Composition of a neutron star. Based on the figure of [44]

where $q_\nu = Q_\nu/n_b$, $q_{\rm h} = Q_{\rm h}/n_b$ are specific rates of neutrino emission and heating per baryon, and $\xi = \epsilon/N_b$. From the definition of specific heat capacity c_V, we have

$$\frac{\partial L}{\partial N_b} = q_\nu + q_{\rm h} - c_V \frac{\partial T}{\partial t} \ .$$

For an observer placed at a very long distance from the surface of the star, we know that measured quantities are are related to the local quantities, i.e., as measured by an observer inside the star and denoted by a sub-indice l, by

$$(L, T, q_i) = (e^{2\Phi} L_l, e^{\Phi} T_l, e^{2\Phi} q_{l,i}) \ . \tag{4.10}$$

Thus,

$$\frac{\partial (e^{2\Phi} L_l)}{\partial N_b} = e^{2\Phi} \left[q_{l,\nu} + q_{l,{\rm h}} \right] - c_V e^{\Phi} \frac{\partial T_l}{\partial t} \ .$$

Applying chain's rule on the left hand side and considering that

$$\frac{\partial r}{\partial N_b} = \frac{1}{4\pi r^2 e^{\Lambda} n_b} \ , \tag{4.11}$$

the differential in terms of the radial coordinate becomes

$$\frac{e^{-(2\Phi+\Lambda)}}{4\pi r^2} \frac{\partial (e^{2\Phi} L_l)}{\partial r} = n_b \left[q_{l,\nu} + q_{l,{\rm h}} \right] - e^{-\Phi} n_b c_V \frac{\partial T_l}{\partial t} \ . \tag{4.12}$$

Therefore, we have recovered 4.8 where, to follow standard notation, sub-indices l to denote local quantities are omitted.

Regarding the second equation, we start from the relation between luminosity and thermal conduction,

$$L = -4\pi r^2 K \frac{\partial T}{\partial r_l} \ , \tag{4.13}$$

where the radial coordinate $r_l \equiv e^{\Lambda} r$ is employed, indicating that the change is measured along the direction of observation. The quantities measured at long distances from the star are again related to local quantities by

$$(L, K, T) = (e^{2\Phi} L_l, e^{\Phi} K_l, e^{\Phi} T_l) \ , \tag{4.14}$$

Thus, the equation becomes

$$L_r = -4\pi r^2 e^{-(\Phi+\Lambda)} K_r \frac{\partial (e^{\Phi} T_r)}{\partial r} \tag{4.15}$$

which gives us eq. 4.9 once the l sub-indices are omitted. ■

To close the discussion, we must emphasize the following points:
1. The critical assumption behind this proof is the existence of an equivalence principle in the gravitation theory under consideration.
2. The differential set of equations for L, T depend on the metric coefficients but are insensitive to the equations of motion that the metric functions satisfy. If both Λ, Φ are very different from their GR counterparts, important deviations could appear in the cooling curves, but as long as these functions remain radial dependent only, the thermal set of equations is still valid.
3. Recently, it has been shown [38], [39] that a causality-consistent expression for heat conduction can be derived. This simply reduces to the second differential equation if the dynamical time-scales of the processes are longer than the explicit causal physics, and for a static space-time. Therefore, it is safe to consider the second equation as viable.

The main goal of the cooling study is to solve these equations, given the appropriate boundary conditions, to obtain T_e^∞ and L^∞ as time functions and compare with NSs observational data in order to constrain their composition, gravitational mass and radius.

While the thickness and composition of the envelope and baryon superfluidity in the core and crust play a major role in the exact behaviour of the cooling curves, there are several common features which extensive theoretical research on the field have revealed, as we now proceed to describe.

In first place, neutrinos and photons are the main responsible for the cooling process, carrying away a significant amount of thermal energy. At earlier times, $\log_{10} t \in [-1, 5]$ neutrino luminosity L_ν is the predominant source, while at later epochs, $t \geq 10^5$, photon luminosity L_γ becomes significant.

4.3.1 Boundary conditions

In order to solve the set of differential equations, we must provide boundary conditions. For the luminosity, it is natural to set $L = 0$ at $r = 0$. At the surface of the star, a natural condition is to simply impose $L = 4\pi\sigma r^2 T^4$, as relationship between the two functions L and T. Since the EoS becomes temperature-dependent at this point, it is convenient to fix a higher value of density, ρ_b usually taken at 10^{10} g cm^{-3}, and find a new boundary condition at this point between the luminosity, L_b and temperature T_b. This layer between ρ_b and the surface is what is called the *envelope*. By solving for the temperature and density/pressure profile within the envelope we obtain the desired relationship between L_b and T_b as follows:

NS envelope

This layer is assumed as time-independent and in thermal equilibrium, and energy sources and losses are negligible. Thus, in 4.8, L becomes constant. And so, the

surface luminosity is equal to L_b. In such a small layer all gravity effects can be also assumed as uniform and the hydrostatic equilibrium simply reduces to

$$\frac{dP}{dr} = -g_s\rho \quad \text{where} \quad g_s \equiv \frac{GM}{R^2}e^{\Lambda} \tag{4.16}$$

The transport equation 4.9 also simplifies to

$$\frac{dT}{dr} = -\frac{e^{\Lambda}}{4\pi K R^2}L \tag{4.17}$$

These two equations are integrated from the photosphere where $T = T_e$ inward until ρ reaches ρ_b giving us T_b at that point [45]. The results of such integrations give the looked for relationship between $L = L_b$ and T_b as the new outer boundary condition. Since L is equivalent to T_e this is often called the "$T_e - T_b$ *relationship*".

Numerical simulations have pointed out the effects of this layer over the cooling process, particulary for the time period $[10^2, 10^5]$ yr where most of the observational data is avaliable. The presence of light-elements might be a result of several unconstrained processes, such as formation during the first hours of the NS's life, the effects of accretion or ejection due to pulsations.

In order to quantify the amount of light-elements (LE), the following adimensional parameter is introduced [46]:

$$\eta = g_{14}^2\frac{\Delta M}{M} \ , \quad g_{14} = \frac{g_s}{1\times 10^{14}\ \frac{\text{cm}}{\text{s}^2}} \ . \tag{4.18}$$

where ΔM denotes the amount of mass of LE, M the gravitational mass of the object and g_s the local surface gravity. It has been shown that T_e^{∞} is significantly larger for increasing values of η. This implies that the surface of NSs are warmer than in the absence of this composition, remaining in this state for at least 10^3 years, after which the cooling process via photon emission takes place.

4.3.2 Superfluidity

In 1959, adressing the problem of superfluidity in finite-size system through the moments of inertia of nuclei, and based on the Bardeen - Cooper - Schrieffer (BCS) superconductivity theory, Migdal was able to predict that the interior of NS should be in a superfluid state [40]. From these results, ten years later Baym justified the speed up of Vela pulsar as solid evidence for the superfluid state in the interior of this object [41]. In recent years, numerical simulations on thermal evolution reveals the importance of superfluidity for explaining most of the observational data. Thus, the presence of such phenomenom inside NS is well stablished.
The mechanism proposed by BCS theory for explaining superconductivity (and later for adressing superfluidity) is the following: near the Fermi surface of a certain

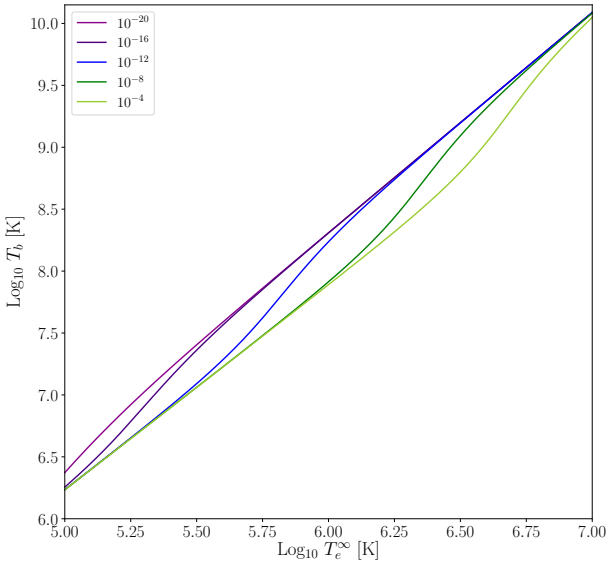

Figure 4.4: Internal temperature T_b versus the effective temperature measured at infinity, for a non-magnetized 1.4 $M_\odot$ NS with several values for the light-elements envelope thickness labelled by their parameter η, see eq. 4.18.

amount of matter, and as a consequence of an atractive interaction, the energy of a two baryon system falls below the Fermi energy, allowing the existence of a bounded stated, the so-called *Cooper pair*. The size of the resulting energy gap Δ depends on the type of interactions included, and in the temperature of the system, which must be less or equal than a certain critical value T_c. Both quantities are simply related by

$$\Delta \approx 1.75 k_b T_c \tag{4.19}$$

where k_b is the boltzmann's constant. This process has no major impact over the EoS chosen due to its proximity with the Fermi surface. On the other hand, for charged baryons such as protons the superfluidity state implies a superconductivity one as well.

Numerical calculations have shown that for low momentum and hence low density, the dominant attraction occurs in the $^1S_0$ spin-orbital state, while at higher momentum/density, the $^3P_2$ triplet state is more likely to happen. These facts translate into $^1S_0$ and $^3P_2$ superfluid neutrons in the inner crust and core respectively, and only $^1S_0$ proton superfluidity due to its low number density.

Due to the energy gap, superfluidity has impact mainly over the heat capacity and neutrino emission of matter. In addition, its presence explains the quantized neutron

vortices and flux tubes of magnetic field.

In Table 4.1, several superfluidity models are briefly described, and in Fig. 4.5 the critical temperature for each one of them is plotted against density.

I refer to Page et al 2014 [69], for an extensive review of superfluidity and superconductivity in neutron stars.

4.3.3 Neutrino Emission Processes

Arising from numerous reactions, neutrinos are capable of carrying away energy, providing an efficient path for cooling of NS with internal temperature $T \geq 10^6$ K. The emission mechanism can be classified into slow and fast, according to the rate at which the matter cools down.

The dominating neutrino emission processes inside NS are enlisted in Table 1. The mosts efficient of them is the Direct Urca (DUrca) cycle/process, which takes place only if the quotient n_p/n_b exceeds 11% , where n_p is the proton and n_b the baryon number densities. This threshold arises from energy and momentum conservation: in triangle's rule:

$$|\vec{p}_{\mathrm{p}}| + |\vec{p}_{\mathrm{e}^-}| \geq |\vec{p}_{\mathrm{n}}| \ . \tag{4.20}$$

where $\vec{p_i}$ is the momentum of the i-th particle, we substitute Fermi's momentum $p_i = (3\pi^2 n_i)^{1/3}\,\hbar$ to set an inequality over number densities,

$$n_{\mathrm{p}}^{1/3} + n_{\mathrm{e}^-}^{1/3} \geq n_{\mathrm{n}}^{1/3} \ . \tag{4.21}$$

If charge neutrality is imposed, $n_{\mathrm{p}} = n_{\mathrm{e}^-}$, we obtain $8n_{\mathrm{p}} \geq n_{\mathrm{n}}$.

Baryon pairing has a dramatic effect on the cooling (cite Page and Applegate 1992) since it strongly suppresses neutrino processes. For example is neutrons are locked into Cooper pairs, a pair has to be broken in order for the neutron to participate in an emission processes and this introduces a Boltzmann-like suppression factor

$$R \sim e^{-\Delta/k_b T} \tag{4.22}$$

in the emissivity Q_ν of the process.

For an extensive review on this subject, I refer to Yakovlev et al, 2001 [48].

Table 4.1: Superfluidity models

$^1S_0$ neutron	
Name	Description
SFB	Renormalization group methods for neutron matter [57].
CCDK	Reid v_4 potential within the method of correlated basis functions [58].
WAP	Particle-hole interaction in the context of Fermi liquid theory, [59].
GC	s-wave part of AV18 interaction and a $\sim \cosh^{-2}(24r/r_0)$ potential [60].
GIPSF1	Quantum Monte Carlo calculations, employing the AV8' and Urbana IX potentials [61],[62].
GIPSF2	Quantum Monte Carlo calculations, employing the AV8' and Urbana IX potentials [61],[62].
GIPSF3	Quantum Monte Carlo calculations, employing the AV8' and Urbana IX potentials [61],[62].
T72	OPEG (Gaussian soft-core mixed with a one-pion-exchange potential) model [72], [73].
Ioffe 1NS	Parametric, analytic model [76], [78],[77].
Ioffe 2NS	Parametric, analytic model [76], [78],[77].
Ioffe 3NS	Parametric, analytic model [76], [78],[77].
$^3P_2$ neutron	
Name	Description
HGRR	Anisotropic pairing chosen to fit scattering data, [63].
AO	Effective OPEG potential, [64].
T72	Restricted version of the OPEG potential, [73].
BCLL92	Nucleon-nucleon interaction modeled with the Argonne v_{14} potential, [65], [66].
CasA	Based on an analytical model. Aimed to explain the rapid cooling of Casssiopeia A NS.[69], [70].
Ioffe 2NT	Parametric, analytic model [76], [78],[77].
$^1S_0$ proton	
Name	Description
CCY_ps	Reid potential within the method of correlated basis functions, [71].
T73	Interactions described by OPEG potential [74].
NS	[75].
BCLL92	Same description than the $^3P_2$ neutron channel. [66].
CCDK	Same description than the $^1S_0$ neutron channel [58].

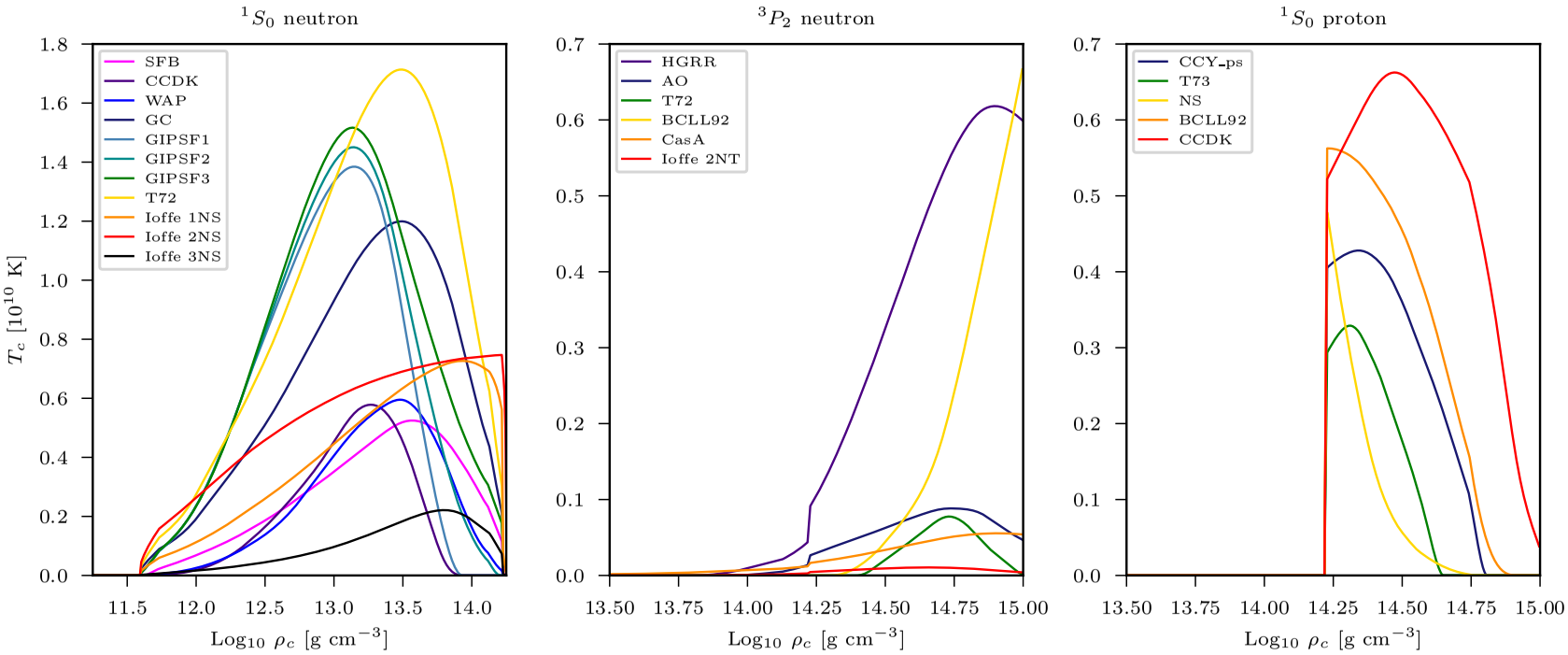

Figure 4.5: Critical temperature for several superfluidity models versus the central density.

Table 4.2: Dominant neutrino emitting processes in NS cores, in the absence of hyperons and quarks.

Name	Process	Emissivity	Rate
Modified Urca cycle (neutron branch)	$\begin{cases} n+n \to n+p+e^- + \bar{\nu}_e \\ n+p+e^- \to n+n+\nu_e \end{cases}$	$2\times10^{21}\ RT_9^8$	Slow
Modified Urca cycle (proton branch)	$\begin{cases} p+n \to p+p+e^- + \bar{\nu}_e \\ p+p+e^- \to p+n+\nu_e \end{cases}$	$\sim 10^{21}\ RT_9^8$	Slow
Bremsstrahlung	$\begin{cases} n+n \to n+n+\nu+\bar{\nu} \\ n+p \to n+p+\nu+\bar{\nu} \\ p+p \to p+p+\nu+\bar{\nu} \end{cases}$	$\sim 10^{19}\ RT_9^8$	Slow
Cooper pair formations	$\begin{cases} n+n \to [nn]+\nu+\bar{\nu} \\ p+p \to [pp]+\nu+\bar{\nu} \end{cases}$	$\begin{cases} \sim 5\times10^{21} RT_9^7 \\ \sim 5\times10^{19} RT_9^7 \end{cases}$	Medium
Direct Urca cycle	$\begin{cases} n \to p+e^- + \bar{\nu}_e \\ p+e^- \to n+\nu_e \end{cases}$	$\sim 10^{27} RT_9^6$	Fast
π^- condensate	$n+\langle\pi^-\rangle \to n+e^- + \bar{\nu}_e$	$\sim 10^{26} RT_9^6$	Fast
K^- condensate	$n+\langle K^-\rangle \to n+e^- + \bar{\nu}_e$	$\sim 10^{25} RT_9^6$	Fast

Chapter 5

Structure of Neutron Stars

> "*What is the answer to life, the universe and everything?*"
>
> *Douglas Adams*

Earlier in this work we stated that the structure of the star cannot be obtained by pure analytic methods, for most of the EoS under consideration. This situation motivates the introduction of numerical methods capable of solving the non-linear set of equations which, as emphasized in Chapter 4, are de-coupled from the energy conservation and heat transport equations. Due to this fortunate fact, the present chapter solely considers the numerical methods and results for the structure of the star.

The first section is devoted to discuss the numerical methods employed: in the first half, the set of equations is re-introduced and the boundary conditions settled, as a consequence of the discussion in § 3.4.1 and 3.4.2. In the second half, we discuss the searching of the right value for the scalar curvature at the center of the star. This part might be regarded as a novelty, since previous literature have not addressed the possibility of an analytic expression for this key value, which is somewhat difficult to fix due to the order-of-magnitude difference with respect to the other quantities. Nevertheless, we expect the arguments and figures to serve as a bridge for future research on similar problems.

In the second and final section of the chapter, the numerical results are described. This part is ordered according to the impact of the elements in the cooling process: in first place, we have the emergence of the *surface gravitational mass* concept, in contrast to the *total* one which is inferred from observations. Having clarified the difference between them, in the next part the typical mass versus radius and versus density are properly introduced. Due to the significant differences between the quadratic model and GR, we intend to answer which model results in a stronger attraction by studying the local surface gravity and the compactness in

the homonyms subsections. Finally, we compare density profiles, thickness of the crust and the proper volume of Direct Urca for stars in both gravity models.

5.1 Numerical Method

5.1.1 System of differential equations

The structure of the star is fully described by five radial functions: Φ, Λ, P, ϵ and R, satisfying the system of equations introduced in Chapter 3. Here, we repeat them for convenience,

$$\frac{d\Phi}{dr} = \frac{1}{A_1}\left\{\frac{4\pi G P r e^{2\Lambda}}{c^4} - \frac{1}{4r}\left[A_2 e^{2\Lambda} + 2A_3\right]\right\} \ , \tag{5.1}$$

$$\frac{d\Lambda}{dr} = \frac{1}{A_1}\left\{\frac{4\pi G \epsilon r e^{2\Lambda}}{c^4} + \frac{1}{4r}\left[A_2 e^{2\Lambda} + 2A_3\right] + \alpha r \frac{d^2R}{dr^2}\right\} \ , \tag{5.2}$$

$$\frac{d^2R}{dr^2} = \frac{1}{A_7}\left\{\frac{A_1 A_4 e^{2\Lambda}}{6\alpha} - \frac{1}{r}\left[A_5 + A_6 - \frac{A_2 e^{2\Lambda}}{2}\right]\frac{dR}{dr}\right\} \ , \tag{5.3}$$

$$\frac{dP}{dr} = -(P+\epsilon)\frac{d\Phi}{dr} \ , \tag{5.4}$$

where

$$A_1 = 1 + 2\alpha R + \alpha r \frac{dR}{dr} \ , \quad A_2 = \alpha r^2 R^2 - 4\alpha R - 2 \ , \tag{5.5}$$

$$A_3 = 1 + 2\alpha R + 4\alpha r \frac{dR}{dr} \ , \quad A_4 = \frac{8\pi G}{c^4}(3P - \epsilon) + R \ , \tag{5.6}$$

$$A_5 = \frac{4\pi G}{c^4} r^2 e^{2\Lambda}(P - \epsilon) \ , \quad A_6 = 1 + 2\alpha R - 2\alpha r \frac{dR}{dr} \ , \tag{5.7}$$

$$A_7 = 1 + 2\alpha R \ , \tag{5.8}$$

are just auxiliary functions, introduced to simplify the notation and the numerical implementation of the system. Regarding ϵ, an Equation of State (EoS) must be provided for introducing the relation between the energy density ϵ and the pressure, thus closing the set.

To solve the system of differential equations, the following boundary conditions are imposed:

1. Surface of the star The radial coordinate r_* where $P(r_*) = 0$ is refered as the surface of the star.

Since the EoS do not cover the range $P \in [0, 10^8]$ (with P in dyn/cm^2), the radial coordinate where $P \approx \mathcal{O}(10^8)$ is defined as the radius of the star. For reference, the central pressure is $\mathcal{O}(10^{35})$ g cm^{-3}.

2. Infinity In order to recover Schwarzschild's metric,

$$\lim_{r\to\infty} R(r) = \lim_{r\to\infty} \frac{dR}{dr} = 0 \tag{5.9}$$

is imposed. Numerically, the point r_g where $|R(r_g)/R_0| = \mathcal{O}(10^{-8})$ is taken as infinity, as elaborated below in § 5.1.2.

3. Origin of coordinates At $r = 0$, either the central pressure P_0 or the central density ϵ_0 can be chosen arbitrarily and the other one is obtained from the EoS. Regularity of the functions at this point demands (see § 3.4.1)

$$\Lambda_0 = 0 \quad , \quad \left.\frac{dR}{dr}\right|_{r=0} = 0 \ . \tag{5.10}$$

Since only $d\Phi/dr$ appears in the system of equations, we are free to choose an arbitrary value for $\Phi(0)$. For simplicity, $\Phi(0) = 0$ was employed at the starting point and, in order to match our metric with Schwarzschild's one at infinity, the integration is performed and then a re-scaling of the Φ function is made: once r_g and the $\Lambda(r_g)$ value are obtained, $\Phi \to \Phi - \Phi(r_g) - \Lambda(r_g)$ so that now $\Phi(r_g) = -\Lambda(r_g)$.

The full system of equations is solved in the range $[0, r_*]$. For $[r_*, \infty)$, only the equations for Φ, Λ and R are solved, considering $\epsilon = P = 0$.

The system is solved numerically, implementing a 4th Order Runge-Kutta method of adaptative stepsize, in FORTRAN 77 language. The subroutines were taken from the "Numerical Recipes" textbook [50], providing good accuracy for the purpose of this work. Regarding the EoS, only four were considered: the classic APR, and the novel MS-A1, MS-B1 and MS-C1. In tabulated form, they were introduced employing a linear interpolation function due to the great amount of available points.

For the parameter α, the following unit is employed:

$$\alpha_0 = \frac{1}{1\times 10^{10}} \left(\frac{GM_\odot}{c^2}\right)^2 = 2.18 \text{ cm}^2 \ . \tag{5.11}$$

where $M_\odot$ is the solar mass. From the rest of this work, we adopt the notation $\alpha X = \alpha_0 \times 10^X$, with $X \in \mathbb{N}$. Due to existent results in the literature [13, 16, 17], which we also confirm here, where it has been shown that for $X \geq 9$ notable deviations from GR start to appear in the mass-radius diagram, we adopt $X = 9, 10, 11, 12$ for studying APR EoS, and only $X = 12$ for analyzing all the EoS. This choice is compatible with observational constrains from the Gravity Probe B experiment [54] and the binary pulsar PSR_J0737-3039, which set $\alpha \leq [5\times 10^{15}, 2.3\times 10^{19}]$ cm^2 [25], [17]. We are aware of the weak-field limit constrain provided by the Eöt-Wash laboratory experiment, $\alpha \leq 10^{-6}$ cm^2, but since the interior of NS stars has been shown completely different in perturbative and non-perturbative approaches [18], [19], [20], [13], [21], significant deviations might still be expected inside NSs.

5.1.2 On the numerical behaviour of the scalar curvature

The treatment of the scalar curvature as an independent variable of the system allows to keep a second-order differential system, but the price to pay is a non-immediate value for this function at origin of coordinates, which must satisfy the desired boundary condition of equation 5.9. Moreover, the vast difference in order of magnitude between the variables stands as the major difficulty reported by previous authors [14, 13, 52]: while P and ϵ lie in the range $10^{35} - 10^{10}$, the scalar curvature and its derivative, in absolute value are found in the range $10^{-11} - 10^{-25}$, in cgs system of units. Besides, the non-linearity of the differential equations gives rise to completely different solutions, even in the case where, for a given value of the central pressure and their associated trial values $R_{0,1}$ and $R_{0,2}$, differ by less than 1%. This

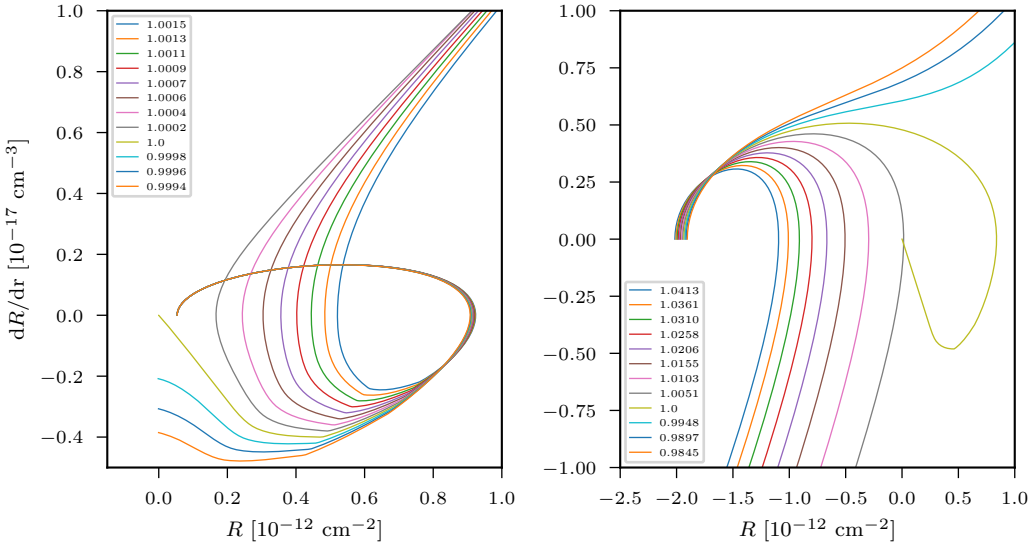

Figure 5.1: Phase space of $R(r)$, considering two different values for the central pressure, $\alpha 9$ and APR EoS. The label 1.0 goes for the curve with the correct value of R_0, while the rest of them are labeled according to the quotient $R_0/R_{0,\text{correct}}$. (Left) $P_1 = 4.9095{\times}10^{35}$ dyn cm^{-2}. (Right) $P_2 = 1.0801{\times}10^{36}$ dyn cm^{-2}.

is clearly illustrated by the phase space of $R(r)$ in Fig. 5.1. Considering APR EoS, $\alpha 9$ and two models with different central pressures it is clear that a small difference in R_0 leads to a completely different behaviour for $R(r)$, which in principle is not surprising due to the non-linearity of the system of equations. This clearly shows that the system of equations we have to solve has the very unfortunate property of having a bifurcation precisely at the value of R_0 we need to find to satisfy the boundary condition of eq. 5.9.

Instead of using the standard technics of changing variable $r \to u = 1/r$ to

solve for the boundary condition eq. 5.9, match it with the surface value $R(r_*)$ for a given initial value R_0 and iterate till a self-consistent solution is obtained we tried searching for a method capable of finding an acceptable value of R_0 which guarantees both $R(r_g) \simeq 0$ and $dR/dr(r_g) \simeq 0$ at a finite value of r_g. In Fig.5.2 we illustrate the scalar curvature and density profiles, considering APR EoS, and different values for the central pressure and αX: on the left column, $P_1 = 4.9095{\times}10^{35}$ dyn cm^{-2} and $\alpha 9$, while on the right we set $P_2 = 1.0801{\times}10^{36}$ dyn cm^{-2} with $\alpha 12$. The label 1.0 in the plot goes for the curve with the "correct" value of R_0, while the rest of them are labeled according to the quotient $R_0/R_{0,\text{correct}}$. We can see that for a small range of variation of R_0 the solution shifts from diverging to $-\infty$ to diverging to $+\infty$. Within this range of R_0 we can find a numerical solution that satisfies $R \simeq dR/dr \simeq 0$ at a finite radius r_g, which we accept as the "correct" solution. The mathematically exact solution cannot be found numerically and if we continue integrating the accepted solution, eventually it starts diverging. In spite of this numerical uncertainty, the density and pressure profiles experiment almost no difference within the small range of variations of R_0 (see the lower panels of this Figure), and thus the structure of the star is accurately calculated by our "correct" solution. As the central panels of Fig.5.2 with logarithmic scale show, $R(r)$ decreases by many orders of magnitude in the range from r_* to r_g.

We close this section illustrating the behaviour of the scalar curvature inside the star. For the same values of the central pressure given above, several αX and APR EoS in Fig.5.3. As $\alpha \gg 1$, the scalar tends to be positive, $\mathcal{O}(10^{-14})$ and tends to be homogeneous in $[0, r_*]$.

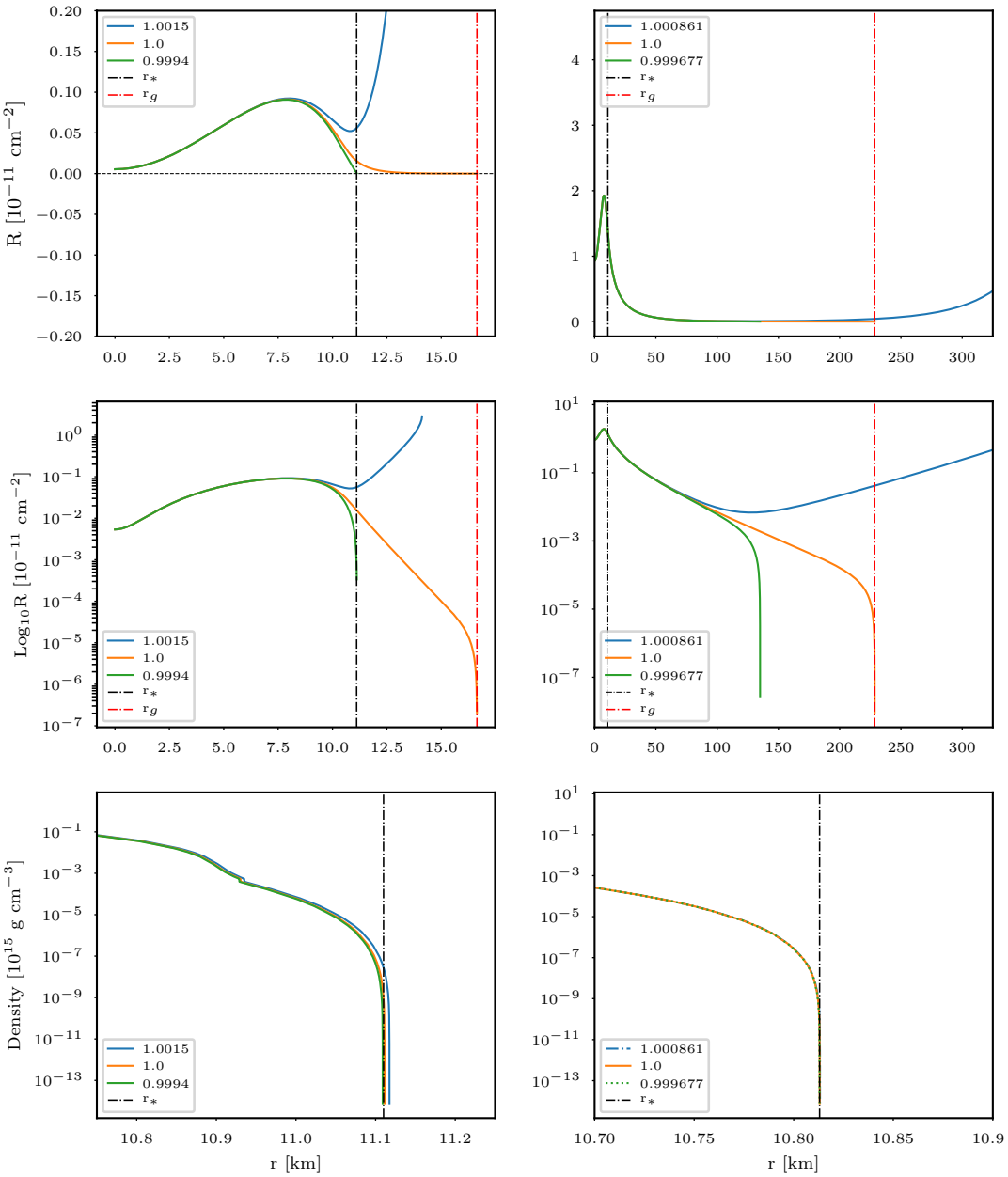

Figure 5.2: Upper panels : Scalar curvature as a function of the radial coordinate. Intermediate plots: scalar curvature in logarithmic scale in order to remark differences near the radii of stars. Lower panels: central density as a function of the radial coordinate. Both stars correspond to APR EoS and: (Left column) $\alpha 9$ and $P_1 = 4.9095{\times}10^{35}$ dyn cm^{-2}; (Right column) $\alpha 12$ and $P_2 = 1.0801{\times}10^{36}$ dyn cm^{-2}. The label 1.0 corresponds to the curve with the correct value of R_0, while the rest of them are labeled according to the quotient $R_0/R_{0,\text{corect}}$.

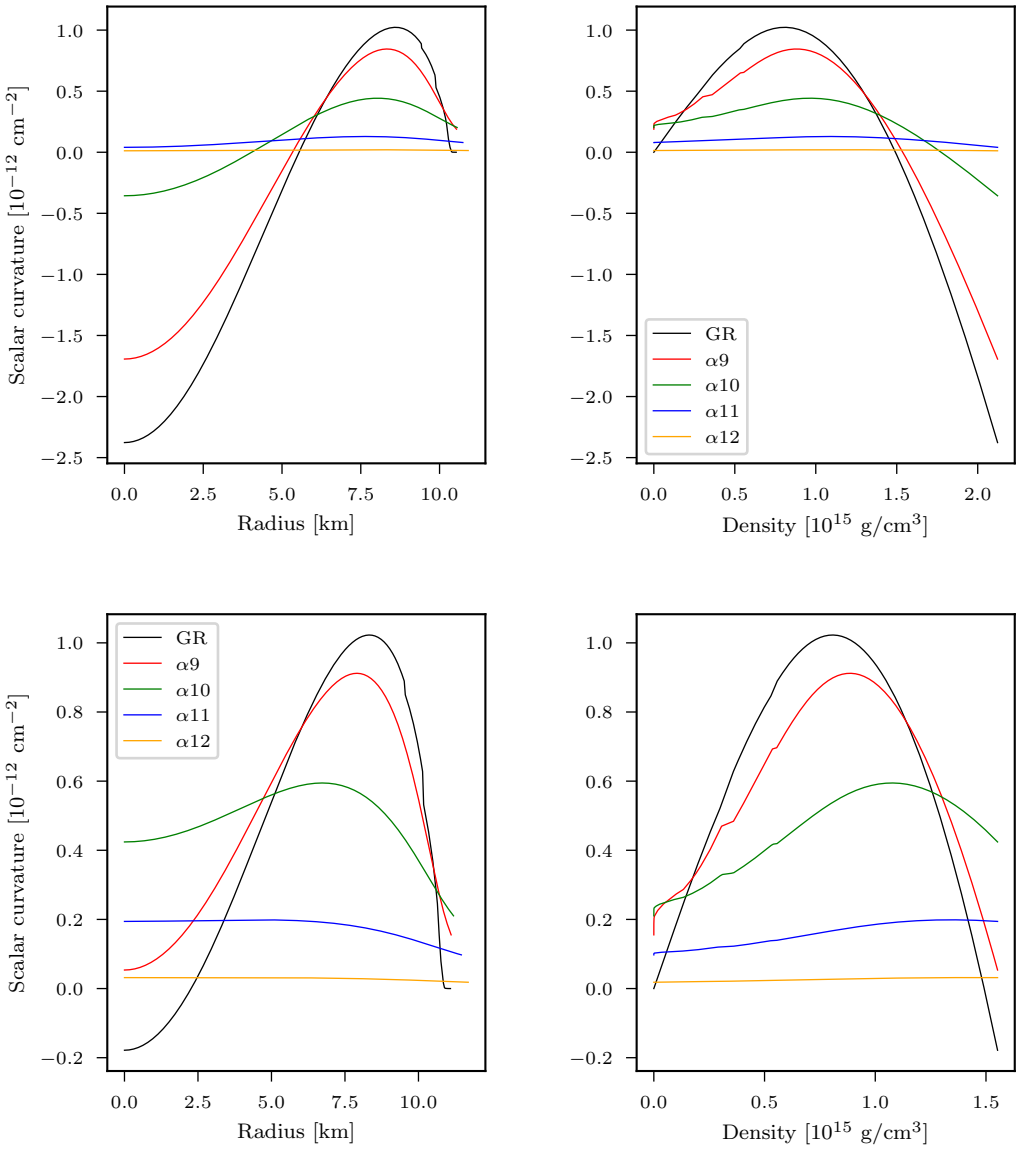

Figure 5.3: Upper panels: Scalar curvature for $P_1 = 1.0103 \times 10^{36}$ dyn cm^{-2} of APR EoS, (Left) as a function of the radius of the star, in km; (Right) as a function of density. The correspondent values for αX are given in the plot. Lower panels: Scalar curvature for $P_2 = 4.9095 \times 10^{35}$ dyn cm^{-2} of APR EoS, (Left) as a function of the radius of the star, in km; (Right) as a function of density. The correspondent values for αX are given in the plot.

5.1.3 Recipe to solve for the scalar curvature

While the TOV equations are independent of the scalar curvature, there is an immediate relation with the energy density and the pressure as we have seen in Chapter 3,

$$R^{\mathrm{GR}}(r) = \frac{8\pi G}{c^4}\left[\epsilon(r) - 3P(r)\right] \ , \ \forall r \in [0, r_*] \ .$$

This facts motivated seeking for a relationship between the value of scalar curvature at $r = 0$, $R(0)$, with the pressure or its general relativistic counterpart, $R^{\mathrm{GR}}(0)$, in order to accelerate the bracketing procedure described in the previous section when calculating a series of neutron star models that cover a broad range of central densities. Although the first trial for a solution

$$R(r=0) = \beta_1 R^{\mathrm{GR}}(r=0) \ , \quad \beta \in \mathbb{R} \tag{5.12}$$

was not successful due to the fact that for any two pair of initial conditions (P_i, P_j) the β_1 parameter is completely different, a relation of this form holds for consecutive initial values R_i, R_{i+1} corresponding with two consecutive values of the central pressure in the EoS table,

$$R_{i+1} = \beta_2 R_i \tag{5.13}$$

where $\beta_2 \in I \subset [0.6, 1.5]$, and I being a subset which depends on the value of α. The resulting function $R(0)$ versus $R^{\mathrm{GR}}(0)$ has a parabolic shape, illustrated in Figures 5.4 and 5.5, which can be almost explained from the results of Chapter 3. Let us recall that the following identities hold at the center of the star:

$$R_0 = R_0^{\mathrm{GR}} + 18\alpha R_0'' \ , \tag{5.14}$$

$$\Lambda_0'' - \Phi_0'' = \frac{1}{6} R_0 \ , \tag{5.15}$$

$$\Lambda_0'' + \Phi_0'' = \frac{1}{1 + 2\alpha R_0}\left[\frac{R_0^{\mathrm{GR}}}{2} + \frac{16\pi G}{c^4} P + \alpha R_0''\right] \ . \tag{5.16}$$

By substracting eq. 5.15 from eq. 5.16 and replacing eq. 5.14, we obtain

$$2\Phi_0'' = \frac{1}{1 + 2\alpha\left(R_0^{\mathrm{GR}} + 18\alpha R_0''\right)}\left[\frac{R_0^{\mathrm{GR}}}{2} + \frac{16\pi G}{c^4} P + \alpha R_0''\right] - \frac{1}{6}\left(R_0^{\mathrm{GR}} + 18\alpha R_0''\right) \ . \tag{5.17}$$

This expression can be inverted in favor of R_0'',

$$R_0'' = \frac{1}{108\alpha^2}\left[-1 - 6\alpha\left(R_0^{\mathrm{GR}} + 6\Phi_0''\right) \pm \sqrt{\frac{1728\alpha\pi G P}{c^4} + 1 + 48\alpha\left(R_0^{\mathrm{GR}} - 3\Phi_0''\right) + 1296\alpha^2\Phi_0''^2}\right] \ . \tag{5.18}$$

By substitution of the solutions in eq. 5.14, we see that

$$R_0 = -\frac{1}{6\alpha} - 6\Phi_0'' \pm \frac{1}{6\alpha}\sqrt{\frac{1728\alpha\pi GP}{c^4} + 1 + 48\alpha\left(R_0^{\mathrm{GR}} - 3\Phi_0''\right) + 1296\alpha^2\Phi_0''^2}\ . \quad (5.19)$$

Since there are four unknown variables and just three equations, at most we expected a relation like this, where R_0 depends on its GR counterpart plus $\Phi''(0)$ which remains as a free parameter, further constrained from the boundary conditions imposed over $R(r)$ and its derivative. A remarkable result, arising from the numerical calculations, is that stable stars can be found in both $\pm$ branches. This is understandable due to the fact that, for a given EoS, sign $\left(R_0^{\mathrm{GR}}\right)$ changes according to the pair (ϵ_0, P_0). The small but important issue with this relation is that we do not know a closed expression for Φ_0''. Therefore, for a set of initial conditions P_0, R_0', Λ_0 we are left with two options: compute the value of Φ_0'' that guarantees the boundary condition, or directly look for R_0 and considering at some point the exact expression to estimate the right value for the next set of conditions.

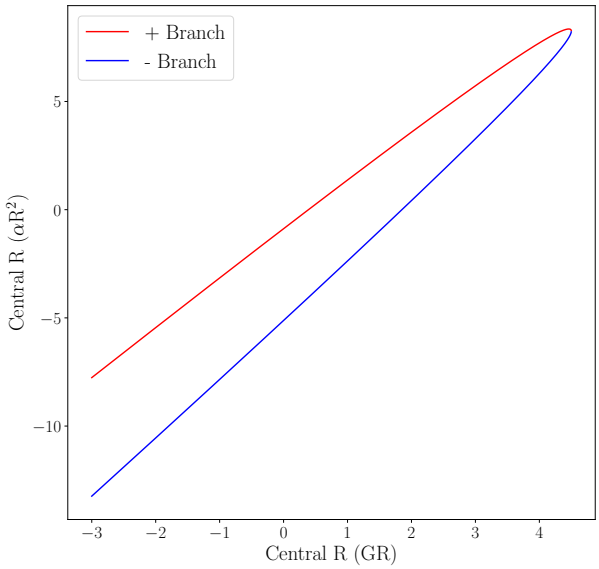

Figure 5.4: Plot of R_0 as a function of R_0^{GR}, considering fictitious values for α and R^{GR}.

The approach taken is more oriented to the second option: provided a correct and initial value R_0 for some pair (P_0, ϵ_0) in the EoS,
Step 1: An interval $I_1 = [aR_0, bR_0]$ is built. $a \approx 0.7$, $b \approx 1.3$, although these values must be adjusted if the value of α approaches to zero.

Step 2: The interval is divided in N equal parts. The numerical separation between them is a fixed $\Delta \ll 1$.
Step 3: For the next pair in the EoS table, (P_0, ϵ_0), the field equations are solved assuming that the initial value for the curvature scalar is $R_{1,j} = aR_0 + j\Delta$. This process stops once a $R_{1,\text{jmax}}$ is found to produce a divergent profile for the scalar curvature, outside the star. The $R_{1,\text{jmax}-1}$ is then stored.
Step 4: Considering a smaller step $\Delta_1 \ll \Delta$, the equations are solved once again, assuming as initial conditions $R_{1,\text{jmax}-1} + \Delta_1, R_{1,\text{jmax}-1} + 2\Delta_1, \ldots$ The process stops once the scalar profile is divergent. A $R^{\text{new}}_{1,\text{jmax}}$ is identified and the $R^{\text{new}_{1,\text{jmax}-1}}$ is stored as R_1.
Step 5: Given R_1, a new interval $I_2 = [0.7R_1, 1.3R_1]$ is built, the pair (P_2, ϵ_0) is introduced and the process begins again from Step 2.

The main advantage of this method is the reliance on the change of sign of R and the numerical precision at hand, instead of fixing a radial value for infinity, which is an important source of error due to the behaviour of the system, where a small change in the initial condition leads to an apparent convergence for 1-10 km outside the star, but which start diverging afterwards, [53]. This feature is illustrated in Fig. 5.2, where for the same values P_1, P_2 of 5.1, APR EoS and $\alpha 9$, $\alpha 12$ respectively, the profile of the scalar curvature drastically changes as we approach the surface of the star, even for small values of the quotient $|R_{0,\text{correct}} + \Delta R_0|/|R_{0,\text{correct}}|$. Not all configurations allow density to reach the lowest regime of 10^{10} g cm^{-3}, but those that do tend to either increase or reduce the radius of the star in less than 1 km. As α increases, r_g extends to 10^2 km and possibly beyond, depending on the numerical precission of the code.

Among the stepbacks of this process we must mention:
1. The first value of the chain must be given. This usually is found by hand, or provided a good shooting method.
2. Dependence in the previous value. Suppose that between $R_{1,j-1} + (N-1)\Delta$ and $R_{1,j-1} + N\Delta$ there exists a value that guarantees a better convergence for both the scalar curvature and its derivative. In that case, the program will not find it due to the size of Δ_1. Moreover: since Δ_1 is smaller than Δ, a poor convergence may occur. Since the initial condition for the next pair (P, ϵ) of the table strictly depends on it, the error could be propagated.
3. Dependence with α. As long as $\alpha \to 0$, the size of the interval and the values of Δ, Δ_1 must be readjusted. This of course has to do with the fact that as $\alpha \to 0$, the central scalar may be negative, or at least two orders of magnitude greater than for the case $\alpha \gg 1$. This can be seen from either Fig.5.2, where the scalar curvature moves from a negative and positive behaviour to a simple positive one, or Fig.5.6 where the scalar curvature inside two NSs becomes smaller ($\mathcal{O}(10^{-11}) \to \mathcal{O}(10^{-14})$ in absolute value) and positive with $\alpha X \to \alpha 12$.
4. Computational time. It strongly depends on the value of α, the number of central values to be found, and the size of the steps Δ, Δ_1. Between 2 and 6 hours

of computation, on a laptop, are needed to guarantee a moderate precision for a family of stars, i.e. for a given EoS and αX fixed.

To close this section, we must emphasize the fact that, provided an accurate value of R_0 that guarantees the vanishing of R at infinity, the second boundary condition

$$\lim_{r\to\infty} \frac{dR}{dr} = 0 \tag{5.20}$$

is automatically met. Numerically,

$$\left.\frac{dR}{dr}\right|_{r=r_g} = \mathcal{O}(10^{-26}) \ . \tag{5.21}$$

Fig. 5.4 illustrates R_0 as a function of R^{GR}, considering fictitious values for α and assuming that $\Phi_0'' \approx R^{\mathrm{GR}}$ in Eq.5.19. The $+$ and $-$ labels denote the sign of the square root considered for R_0. Although this is a rough estimation of the actual curve's shape, there is good agreement with the numerical results, displayed in Fig. 5.5,where independently of the EoS and αX the parabolic shape holds. As αX moves to zero the scalar curvature approaches its GR counterpart.

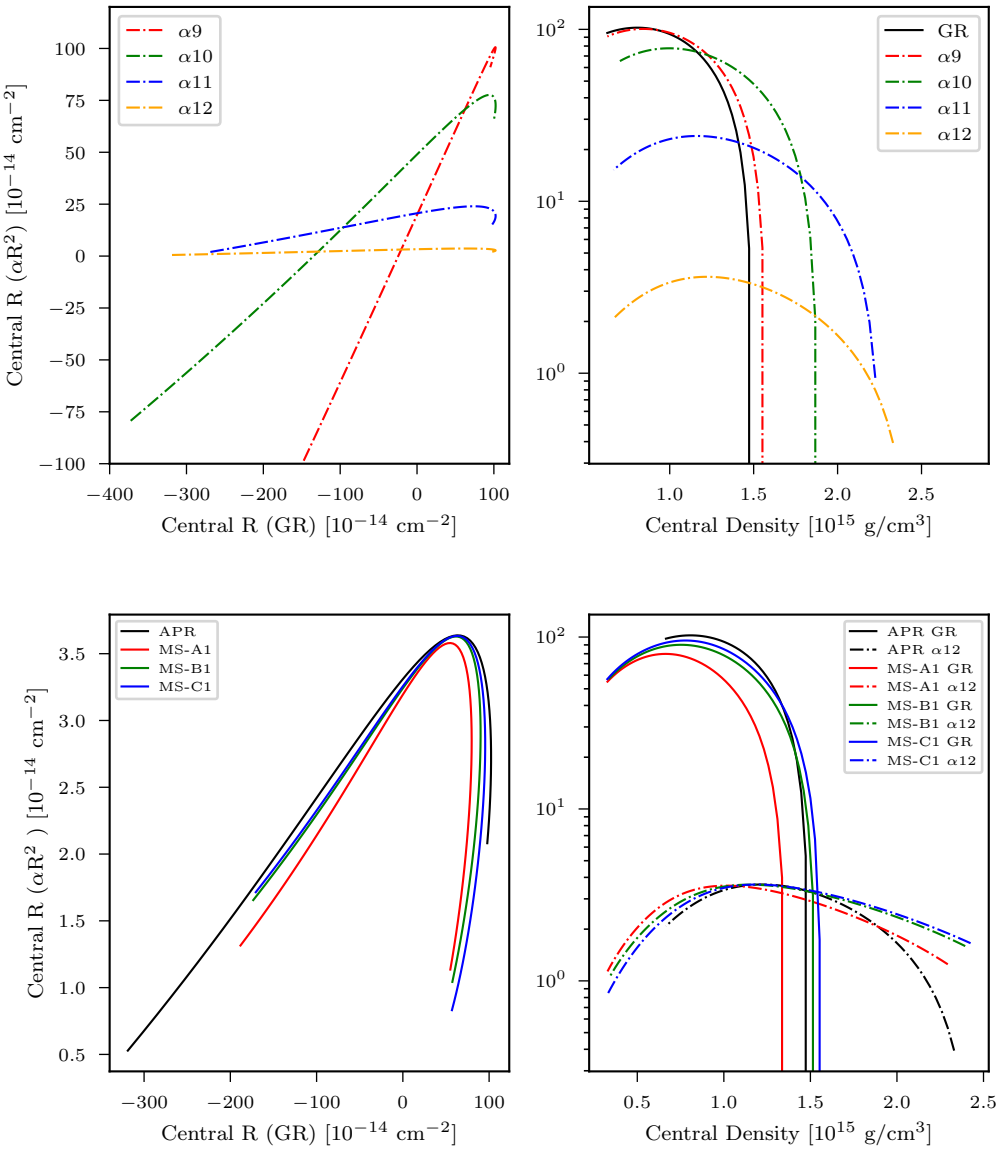

Figure 5.5: (Upper left) R_0 as a function of $R_0^{\rm GR}$, considering the APR EoS and several values for α. (Upper right) R_0 as a function of the central density. Same EoS and α values as the left panel. (Lower left) R_0 as a function of $R_0^{\rm GR}$, considering $\alpha 12$ and several EoS. (Lower right) R_0 as a function of the central density. Same value for α and EoS.

5.2 Results

5.2.1 Gravitational Mass

If we assume that

$$m(r) = \frac{c^2 r}{2G}\left(1 - e^{-2\Lambda}\right)$$

is the actual gravitational mass of the system, we face an interesting phenomenon: a constant value is not reached at the surface of the star, $r = r_*$ where $P \to 0$, but at the point where the scalar curvature is zero. Mathematically the latter only happens at $r = \infty$ but in our numerical scheme it is reached at a finite radius r_g, see below eq. 5.9. Thus, in the interval $[r_*, r_g]$, m is an increasing, positive function, while for $[r_g, \infty)$, it becomes a positive constant. This value is regarded as the *total gravitational mass* of the star

$$M_{\rm grav} \equiv \lim_{r\to\infty} m(r) \cong m(r = r_g) \tag{5.22}$$

We will later need the value of $m(r)$ at the stellar surface and hence define the *surface gravitational mass*

$$M_{\rm surf} \equiv m(r = r_*)\ . \tag{5.23}$$

Of utility is also the third concept of the *baryonic mass* (see § 4.1)

$$M_{\rm bar}\ \equiv \overline{m} N_b \quad \text{with} \quad N_b \equiv \int_0^{r_*} n_b(r)\, e^{\Lambda(r)}\, 4\pi r^2\, dr\ , \tag{5.24}$$

N_b being the total baryon number of the star.

In the interval $[r_{\rm grav}, \infty)$, the metric tensor can be matched to Schwarzschild's and the notion of flat space at infinity is recovered. In addition, the interval $[r_*, r_{\rm grav}]$ has been referred as a *gravitational sphere* in the literature [23], due to the fact that the "extra" mass, going from $M_{\rm surf}$ to $M_{\rm grav}$, does not depend on baryonic matter.

The left panel of Fig.5.6 illustrates a consequence of this fact: for $\alpha 12$, and regardless of the EoS chosen, the baryonic content of the most massive star is always larger than in GR, as well as its total gravitational mass. Under the stability criterion for NSs (see §4.2), the quadratic model predicts stable and more massive stars than GR, although the exact value remains EoS-dependent. However, once both theories agree in some value for $M_{\rm bar}$, $M^{\rm GR}_{\rm grav} > M^{\alpha R^2}_{\rm grav}$, i.e., GR stars are heavier than their R^2 counterparts. Recalling from the previous section that r_g increases with αX, the right panel of 5.6 suggests that the non-vanishing scalar significantly contributes for the increasing in the total gravitational mass. This might suggest a similar effect to the *spontaneous scalarization* occurring in BD-NSs, where the gravitational binding energy is quite different from its GR counterpart.

As $\alpha \to 0$, $r_{\rm grav} \to r_*$, the difference between surface and total gravitational mass dissappears, as can be seen from Fig. 5.8: on the left plot, the gap between

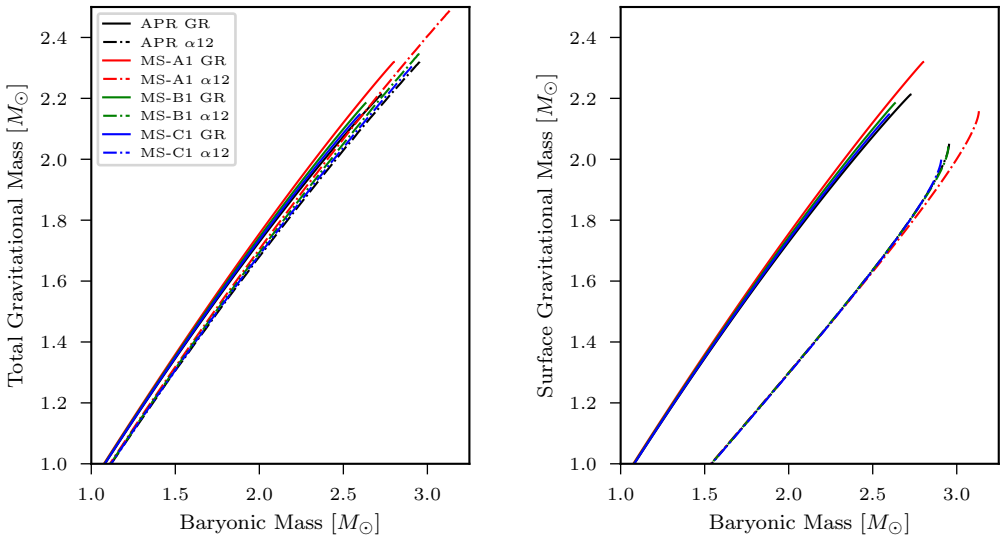

Figure 5.6: Total (left panel) and surface (right panel) gravitational mass as a function of baryonic mass for several EoS, considering $\alpha 12$ and compared to GR predictions.

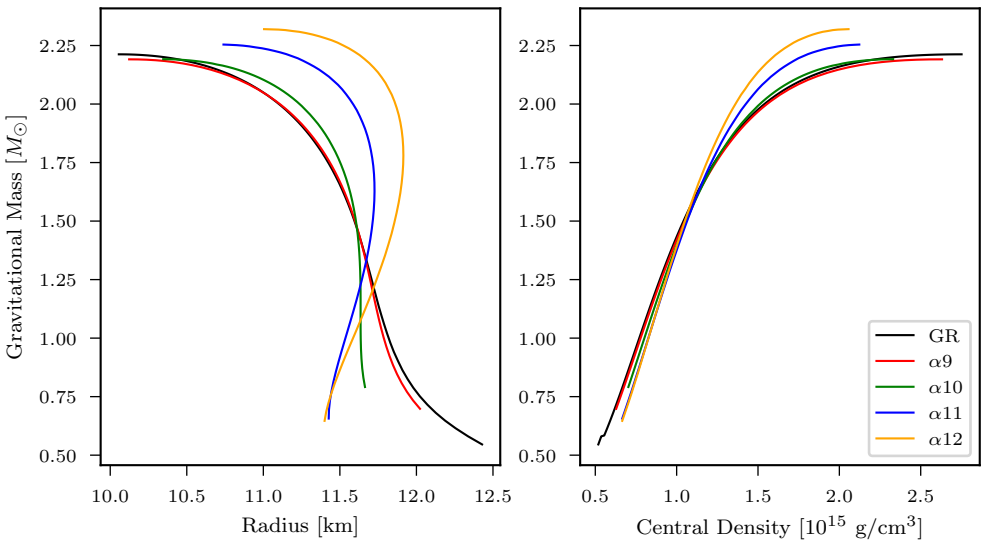

Figure 5.7: (Left) Total gravitational mass as a function of the radius of the star, for several values of α and APR EoS. (Right) Total gravitational mass as a function of the central density, for the same EoS.

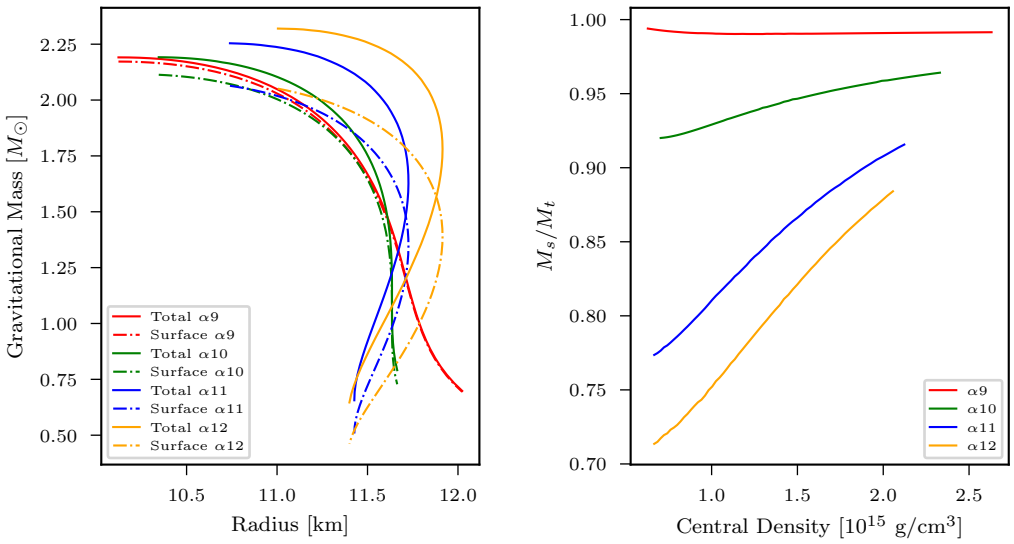

Figure 5.8: (Left) Total and surface gravitational mass as a function of the radius of the star for APR EoS and several values of α. (Right) Ratio of surface to total gravitational mass as a function of the central density. Same EoS than left panel.

surface and total gravitational mass decreases from $\Delta M \approx 0.25 M_\odot$ to almost zero. On the right, a plot of the ratio $\left|\frac{M_{\rm surf}}{M_{\rm grav}}\right|$ versus the central density shows that the contribution of the gravitational sphere diminishes as ρ_c grows up, for $\alpha X > \alpha 9$. On the other hand, the exact size of the gap between surface and gravitational mass is EoS dependent, as we can see from Fig.5.9. Nevertheless, these results are in perfect agreement with the theoretical discussion of chapter 3, where independently of sign[α], the mass was found an increasing function of the radius. The crucial difference, however, is that for $\alpha > 0$ the gravitational mass reaches a finite constant value, in contrast with the other sign where it grows indefinitely [23].

Fig. 5.7 and the lower panels of 5.9 illustrate the total gravitational mass versus radius and versus central density relations, for several αX and several EoS respectively. As $\alpha X > \alpha 9$, the central density for the maximum mass increases, producing stable stars for values which are regarded as unstable in GR. In addition, the maximum value for the gravitational mass is increased with bigger values of αX, independently of the EoS chosen, but its central density is lower than its general relativity counterpart. Under $1.4 M_\odot$, the quadratic model produces smaller stars than GR. The positive slope of these curves roughly resembles the behaviour of the MIT bag model for quark stars. However, the turning point around $0.5 M_\odot$ guarantees the existence of low-mass neutron stars of large radius.

Between $\alpha 9 - \alpha 10$, there is a transition for the sign of dM/dr from negative to

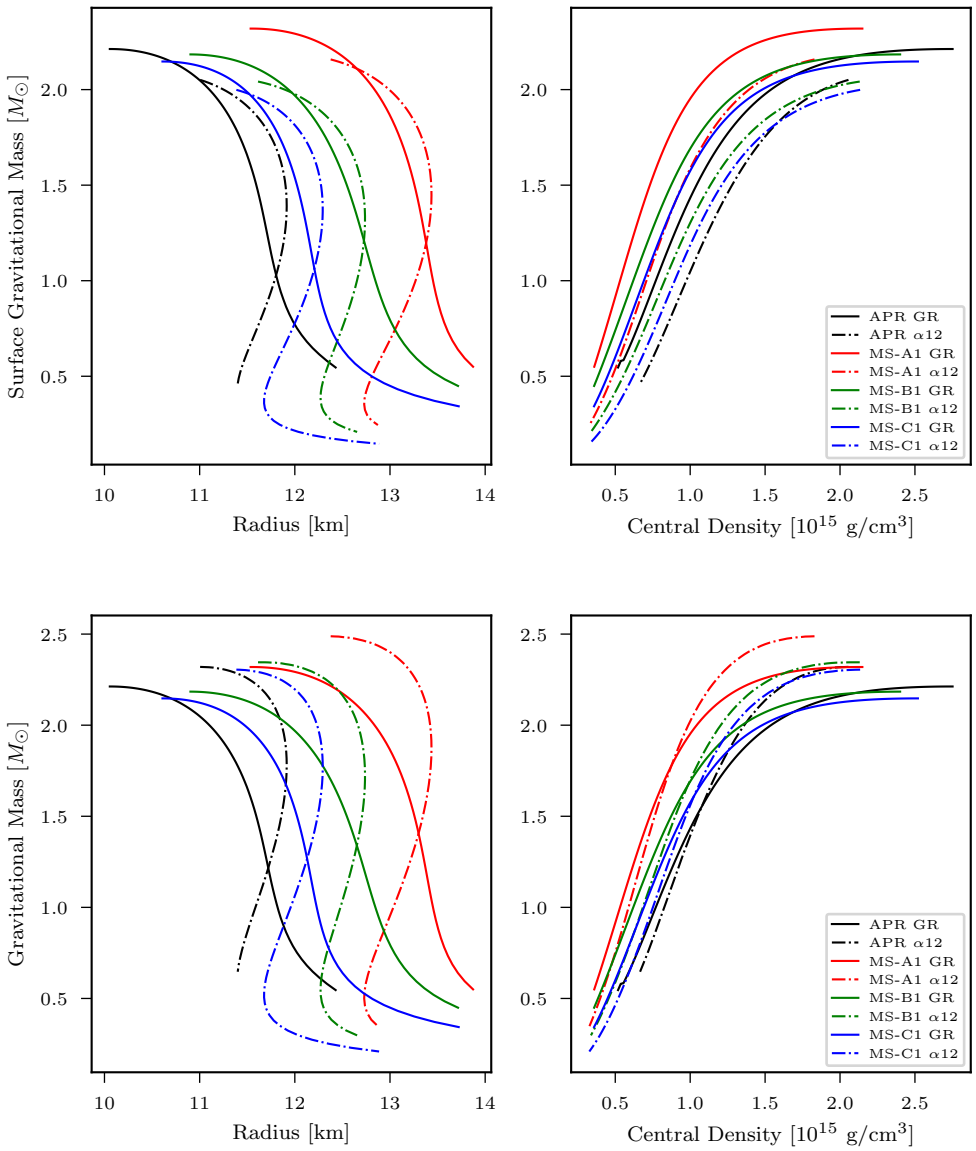

Figure 5.9: (Upper left) Surface gravitational mass as a function of the radius of the star, for several EoS, $\alpha 12$. (Upper right) Surface gravitational mass as a function of the central density. Same value for α and EoS. (Lower left) Total gravitational mass as a function of the radius of the star, for several EoS, $\alpha 12$. (Lower right) Total gravitational mass as a function of the central density. Same value for α and EoS.

positive and back. Going back to Fig.5.8, we can see that this interval corresponds to M_s/M_t moving from ≈ 1 for every central density, to ≈ 0.90 for lower values of ρ_c.

Since the total gravitational mass $M_{\rm grav}$ defined in eq. 5.22 is the observable one, we shall simply address it as *the gravitational mass* of the star for all the `NSCool` models and discussion of further results. It must be noted, nevertheless, that the software recognizes the *surface gravitational mass* for the local surface gravity and the full computation process because it is the last element in the tabulated profile. This distinction might become important for additional aspects such as orbits of particles, accretion disks and the addition of a magnetic field, subjects that are, however, beyond the purpose of the present thesis.

Finally, the results so far introduced suggest that the "gravitational strength" of the αR^2 model might be softer than GR's. The following sections aim to settle this.

5.2.2 Local surface gravity

Since the equations of motion for the metric fields include scalar curvature terms, it is not immediate at first sight if it is possible to employ the same expression for local surface gravity than in GR,

$$g_s^{\rm GR} = -c^2 \lim_{\substack{P\to 0\\ r\to r_*}} \left[\frac{1}{P+\epsilon}\frac{dP}{dl}\right] = \frac{GM}{r_*^2\sqrt{1-\frac{2GM}{c^2 r_*}}} \ . \tag{5.25}$$

However, with the profiles of the star at hand it is possible to show that the local surface gravity expression remains the same, *considering the surface gravitational mass instead of the total one*. To prove this assertion, we move back to the differential equation for Φ:

$$\frac{d\Phi}{dr} = \frac{[r-2Gm/c^2]^{-1}}{1+2\alpha R+\alpha\frac{dR}{dr}}\left\{\frac{4\pi G P r^2}{c^4}+\frac{Gm}{c^2 r}\left(1+2\alpha R+4\alpha r\frac{dR}{dr}\right)-\frac{\alpha r}{4}\left[rR^2+8\frac{dR}{dr}\right]\right\} . \tag{5.26}$$

There is nothing new with the limits $P\to 0$, $r\to r_*$. However, the numerical profile (obtained from the solution of the full system of equations) of every star indicates $R\approx\mathcal{O}(10^{-14})$ cm^{-2} and $-\frac{dR}{dr}\approx\mathcal{O}(10^{-20})$ cm^{-3} in the limit $r\to r_*$. To support the claims $\alpha R\approx\mathcal{O}(10^{-3})$, we refer to Fig.5.6. Thus,

$$\frac{d\Phi}{dr}\to\frac{1}{r_*\left[1-\frac{2Gm}{r_*}\right]}\left\{\frac{Gm}{c^2 r_*}-2\alpha r_*\frac{dR}{dr}\left[1-\frac{2Gm}{c^2 r_*}\right]\right\} ,$$

$$\frac{d\Phi}{dr}\to\frac{Gm}{c^2 r_*^2\left[1-\frac{2Gm}{r_*}\right]}-2\alpha\frac{dR}{dr}.$$

Since $\alpha\in[0,10^{12}]$ cm^2, the second term is numerically irrelevant. Therefore,

$$g_s = -c^2\lim_{\substack{P\to 0\\ r\to r_*}}\left[\frac{1}{P+\epsilon}\frac{dP}{dl}\right] = c^2\sqrt{1-\frac{2GM_{\rm surf}}{c^2 r_*}}\frac{GM_{\rm surf}}{c^2 r_*^2\left[1-\frac{2GM_{\rm surf}}{c^2 r_*}\right]} , \tag{5.27}$$

simplifying,

$$g_s = \frac{GM_{\rm surf}}{r_*^2\sqrt{1-\frac{2GM_{\rm surf}}{c^2 r_*}}} . \tag{5.28}$$

In Fig.5.10, the local surface gravity is shown as a function of the total gravitational mass (left panels) and central density (right panels). In all cases, GR's surface gravity is greater than R^2's one. The gap between them decreases with density and with αX. This suggests that the additional term in the Lagrangian density serves as a repulsive one, softening the gravitational attraction as long as $\alpha\gg 1$.

We close this subsection emphasizing that the numerical invariance of the local surface gravity expression guarantees the usage of `NSCool` code without changing

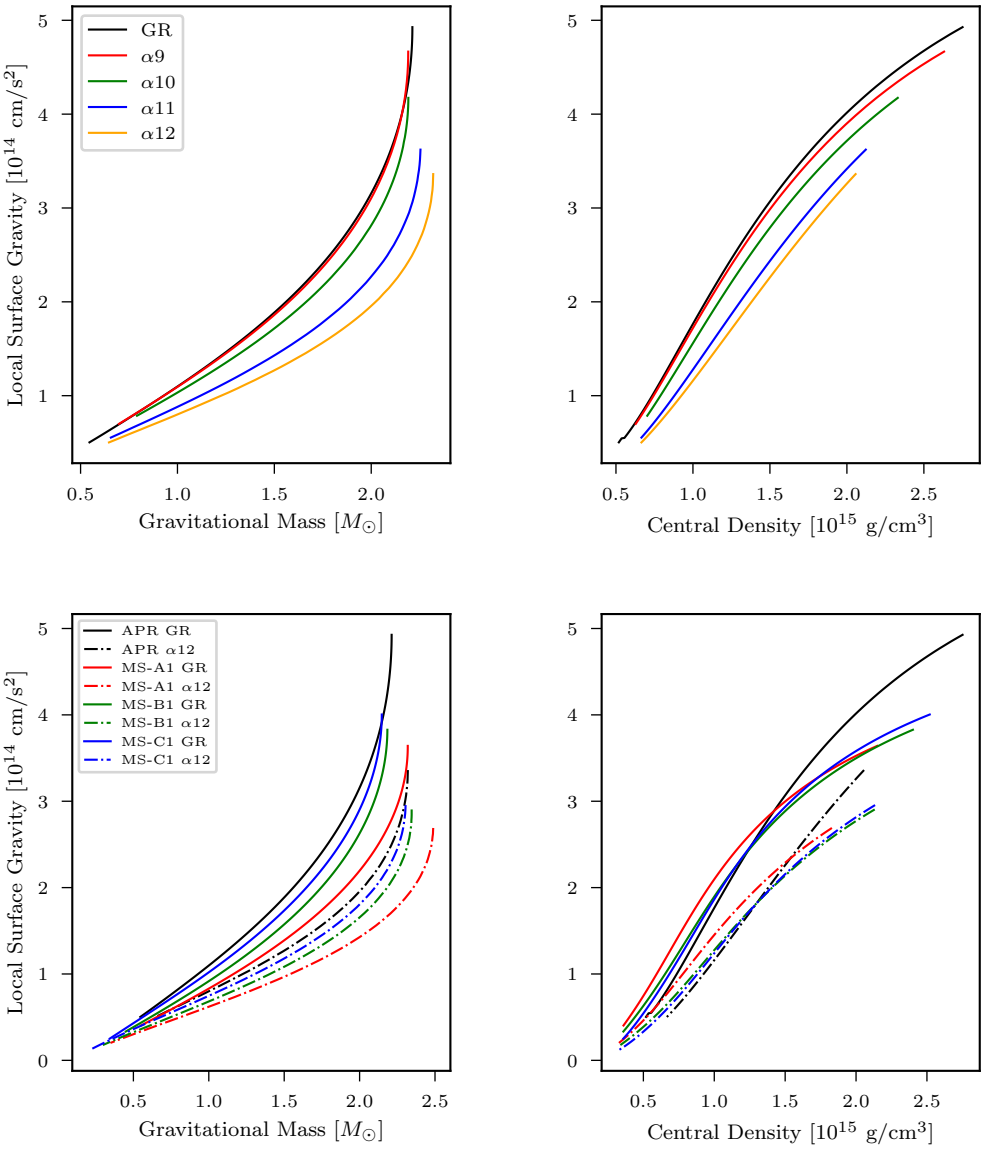

Figure 5.10: (Upper left) Local surface gravity as a function of gravitational mass, considering APR EoS and different values for α. (Upper right) Local surface gravity as a function of central density, with the same EoS and α values as the left panel. Black curves corresponds to GR. (Lower left) Local surface gravity as a function of gravitational mass for several EoS and $\alpha 12$. (Lower right) Local surface gravity as a function of central density, same EoS and value for α. Black curves corresponds to GR.

its structure. Recall, from §4.3.1, that in order to study the envelope and the atmosphere, the approximation $dP \approx -g_s \rho dr$ is employed [45]. On the other hand, since the program uses the value of the gravitational mass at the surface of the star for this expression, we must be aware that the *surface gravitational mass* is the actual value employed, not the total one.

5.2.3 Compactness and redshift

In General Relativity, the "strength" of the gravitational field for a spherical object, described through Schwarzschild's metric, is measured according to the value of the following adimensional parameter,

$$\xi_1 = \frac{GM_{\rm grav}}{c^2 r_*} \tag{5.29}$$

called the *compactness* of the star. In Chapter 3 we found that the weak-field limit is still proportional to this parameter, in spite of the Yukawa term. Additionally, it explicitly appears in the Schwarzschild's metric, which is the limit at infinity for the quadratic model. Hence, it is a good starting point for studying the strength of the gravitational field [80]. Since we now have two different masses we can distinguish between ξ_1 [Total] when M is taken as the (total) gravitational mass $M_{\rm grav}$ in eq. 5.29, and ξ_1 [Surface] when M is taken as the surface gravitational mass $M_{\rm surf}$.

As shown in Fig.5.11, as α becomes larger the stars appear to be more compact in the high density regime if we compare against central density (right panels), while they seem less compact against baryonic mass. There is a crossing point between both models around 1×10^{15} g cm^{-3}. In principle, this is a reflection of the mass-radii diagram, where a transition also takes place. On the other hand, we can be sure that for compactness this is a gravitational sphere effect: in Fig.5.12 it is clear that, by taking into account the surface mass instead of the total one, the compactness of the stars is always smaller in the quadratic model, in agreement with the results for the local surface gravity. Therefore, an increasing in the compactness is a consequence of measuring the mass and radii of stars at very long distances from its surface, being the gravitational sphere the additional "source" of mass.

Of more practical relevance is the surface redshift factor of the models, i.e., $\sqrt{g_{00}} = \exp[\Phi(r = r_+)]$, since this will directly alter observable quantities as the star's thermal luminosity and effective black-body temperature as measured by an observer at infinity. We can see in the right panels of Fig.5.13 a small decrement as $\alpha \to \alpha 12$ in the high density regime. This gap reduces to almost zero around 1×10^{15} g cm^{-3} for all the EoS. The transition between curves around 2 $M_\odot$ (baryonic matter), which translates into ~ 1.7 $M_\odot$ of gravitational mass, might imply that even high mass stars in the quadratic model exhibit a lower temperature than its GR counterparts.

Combining the results from the previous section with the above observations, we conclude that the quadratic model, considering matter content only, induces a weaker gravitational field than GR. The long distance effects, such as increasing gravitational mass, might be regarded as an effect of the quadratic term in the lagrangian, which is almost indistinguishable from GR due to the imposition of Schwarzschild's solution at infinity. The surface gravity is significantly reduced compared to the GR prediction while the surface red-shift factor is very close to the GR prediction.

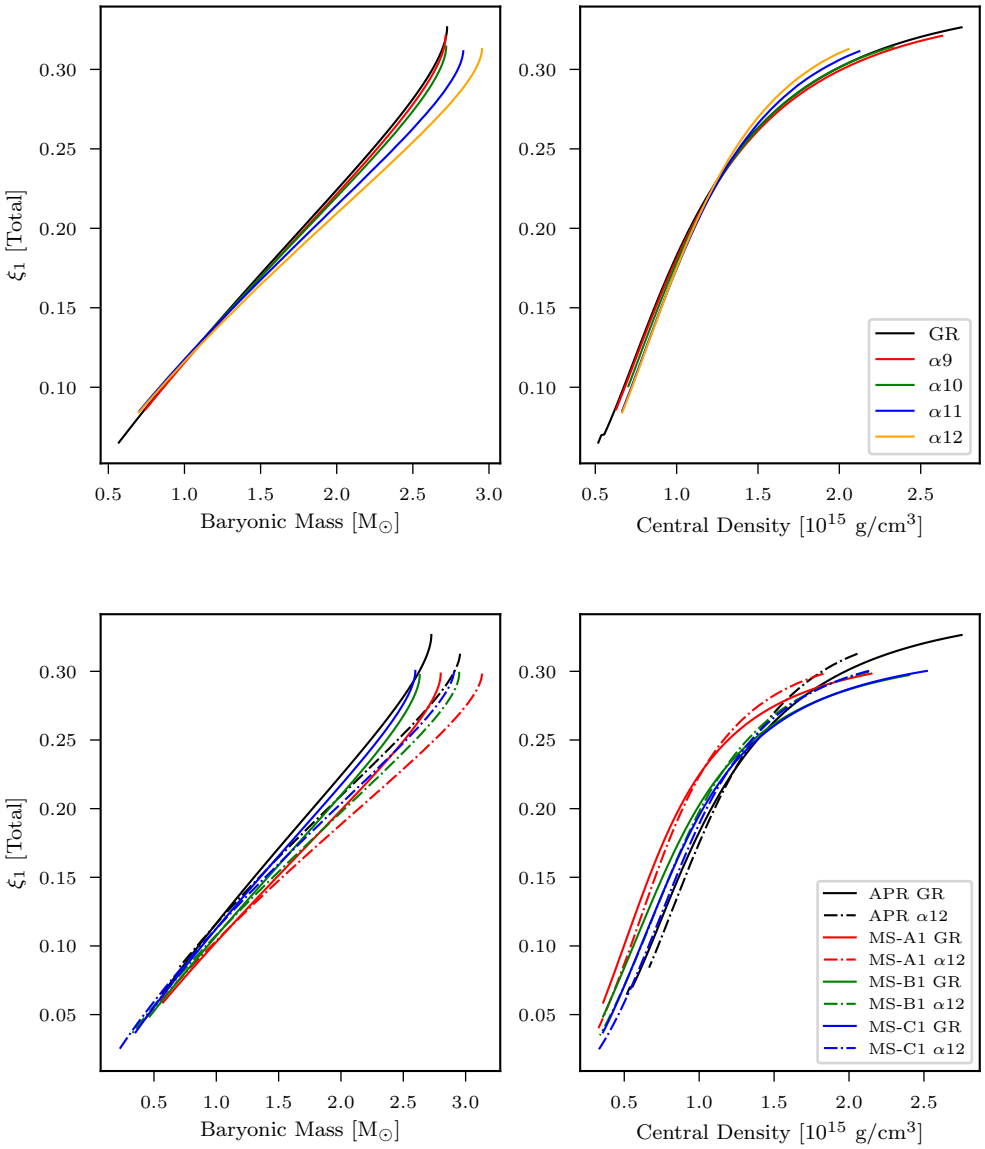

Figure 5.11: (Upper left) Compactness as a function of baryonic mass of the stars, considering APR EoS and several values of α. (Upper right) Compactness as a function of central density. Same EoS and values for α. Black curves corresponds to GR. (Lower left) Compactness as a function of baryonic mass of the stars, for several EoS and α12. (Lower right) Compactness as a function of central density. Same EoS and α12. Black curves corresponds to GR.

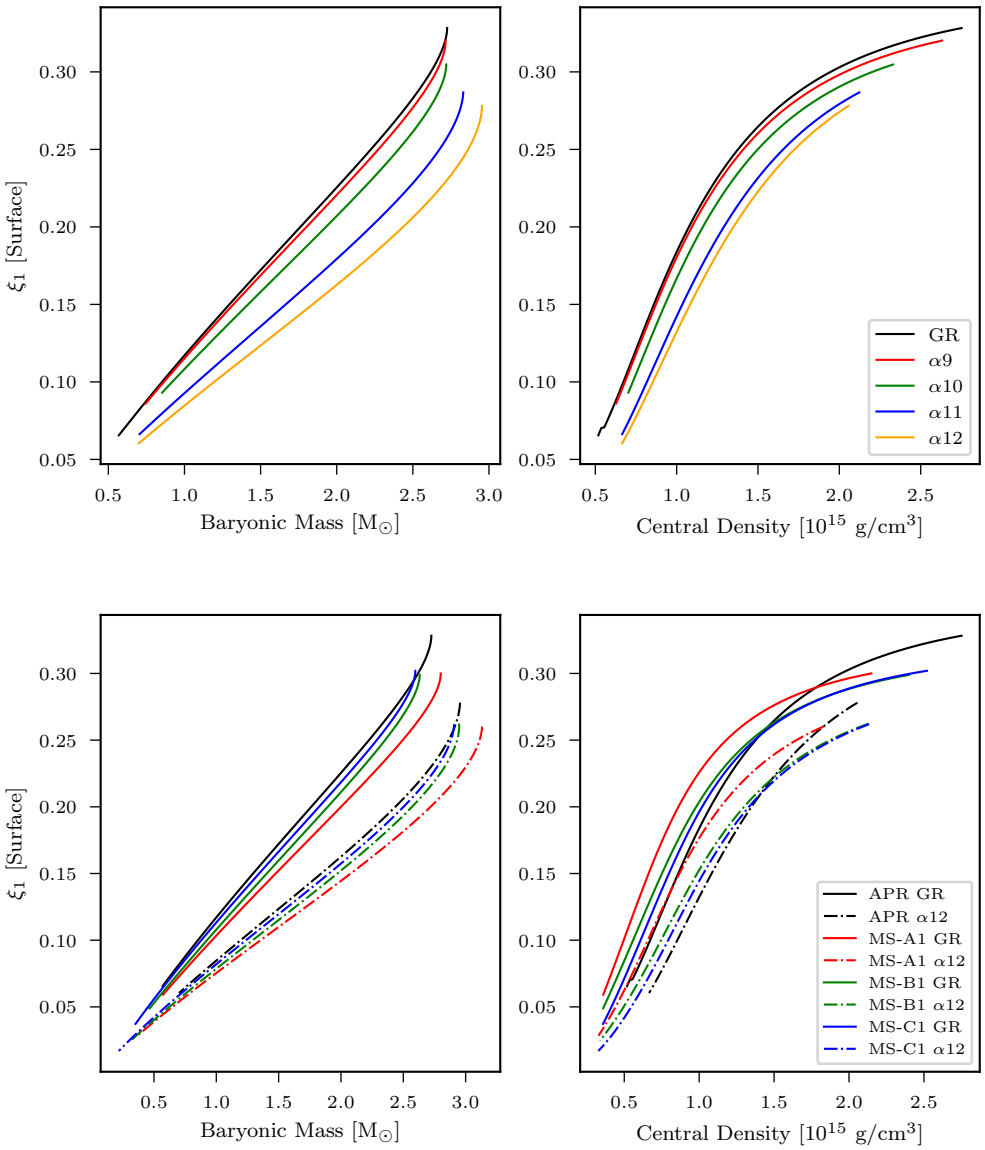

Figure 5.12: (Upper left) Compactness as a function of baryonic mass of the stars, considering APR EoS and several values of α. (Upper right) Compactness as a function of central density. Same EoS and values for α. Black curves corresponds to GR. (Lower left) Compactness as a function of baryonic mass of the stars, for several EoS and $\alpha 12$. (Lower right) Compactness as a function of central density. Same EoS and $\alpha 12$. Black curves corresponds to GR. These panels consider $M_{\rm surf,grav}$ in ξ_1.

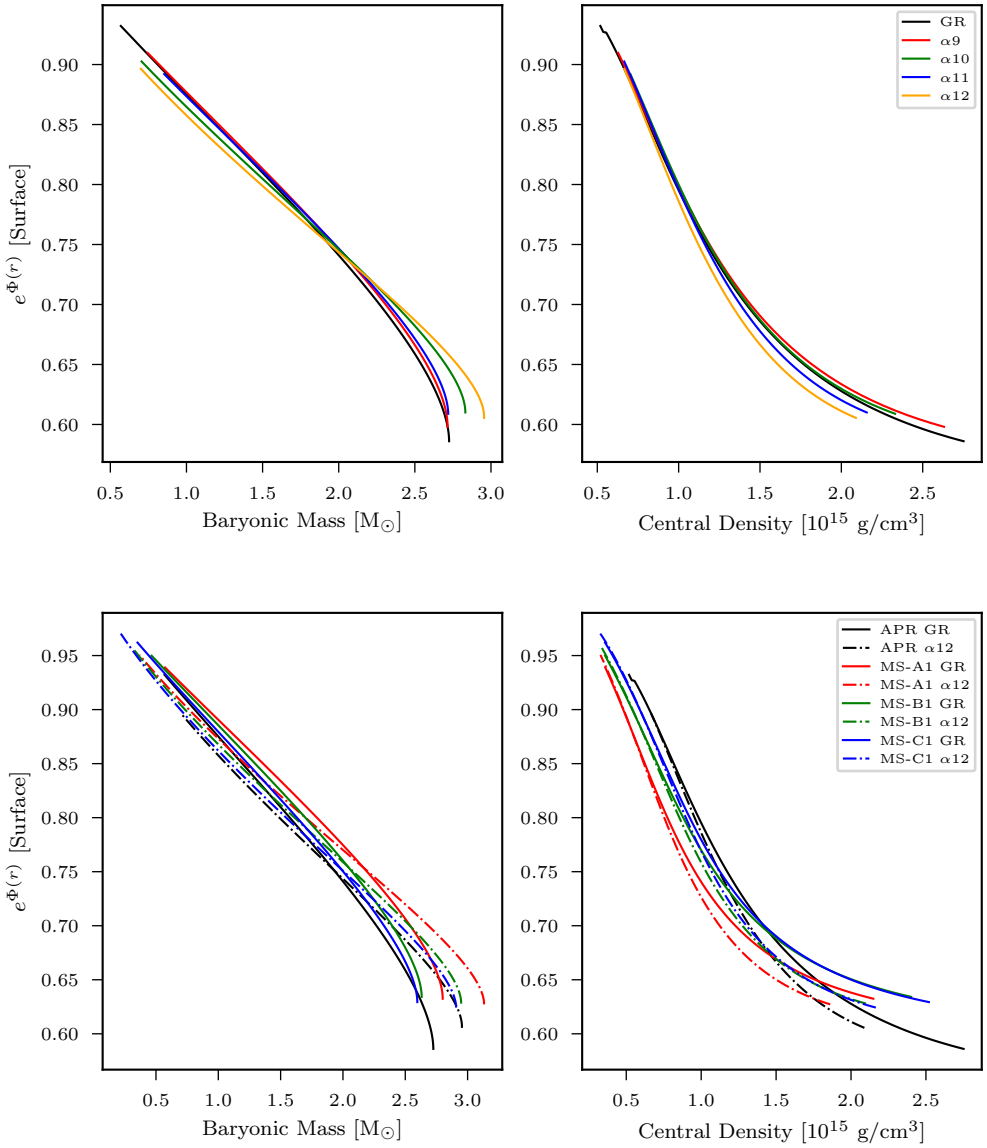

Figure 5.13: (Upper left) Redshift as a function of baryonic mass of the stars, considering APR EoS and several values of α. (Upper right) Redshift as a function of central density. Same EoS and values for α. Black curves corresponds to GR. (Lower left) Redshift as a function of baryonic mass of the stars, for several EoS and $\alpha 12$. (Lower right) Redshift as a function of central density. Same EoS and $\alpha 12$. Black curves corresponds to GR. These panels consider $M_{\rm surf,grav}$ in ξ_1.

5.2.4 Density profiles and crust thickness

We have already seen that the quadratic model is capable of producing neutron star more massive but with lower central densities that GR. This also has consequences over the crust: in Fig.5.14, both density and pressure profiles are given, for two different central values from APR EoS, $P_1 = 1.0103 \times 10^{36}$ dyn cm^{-2} and $P_2 = 4.9095 \times 10^{35}$ dyn cm^{-2}, considering also several values for αX. Regardless of these facts, we can notice that both pressure and density drop to zero at a larger radius in the quadratic model than in GR, as long as $\alpha X \gg 1$.

A non-immediate fact from these figures, however, is that the crust thickness is the same for stars of equal central density, as can be seen in the right panels of Fig.5.15. Let us recall that this thickness is defined as the difference of radial coordinates r_*, $r_{\rm cc}$, with the latest defined by the crust-core transition density $\rho_{\rm cc} = 1.4 \times 10^{14}$ g·cm^{-3}.

On the left hand side of Fig.5.15 the differences appear because the gravitational mass is not the same for a fixed ρ_c and/or several αX values. While the exact thickness is EoS dependent, the tendency of growing ΔR with decreasing ρ_c is a common feature for all EoS employed.

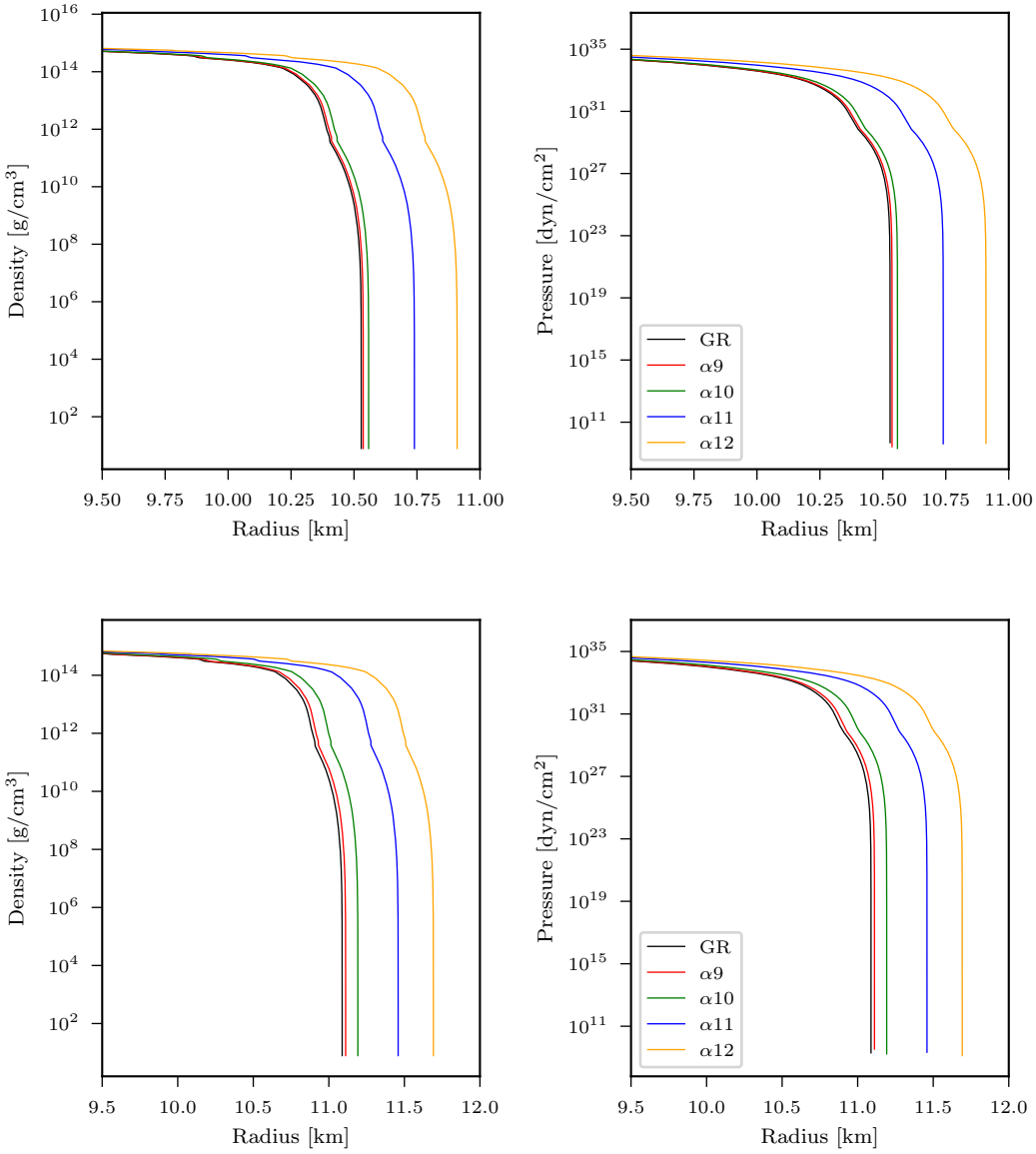

Figure 5.14: (Upper panels) Density and pressure as functions of the radial coordiante (in km), for $P_1 = 1.0103 \times 10^{36}$ dyn cm^{-2} of APR EoS. The values of α are indicated in the plot. (Lower panels) Density and pressure as functions of the radial coordinate (in km), this time for $P_2 = 4.9095 \times 10^{35}$ dyn cm^{-2} of APR EoS. The values of α are depicted in the plot.

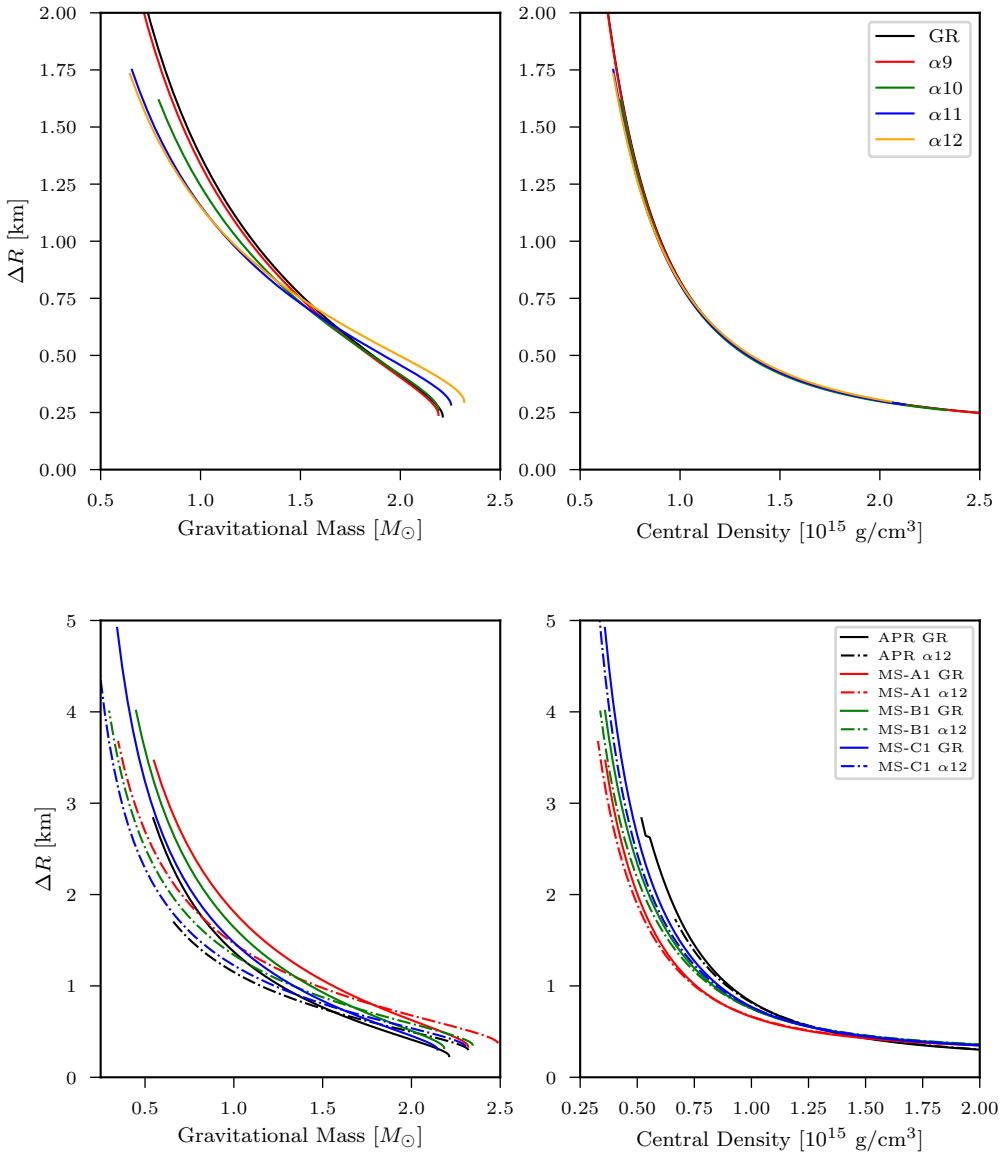

Figure 5.15: (Upper left) Crust thickness as a function of gravitational mass. (Upper right) Crust thickness as a function of central density. Both panels correspond to APR EoS and several values for α. (Lower left) Crust thickness as a function of gravitational mass for different EoS and $\alpha 12$. (Lower right) Crust thickness as a function of central density. Same EoS and value for α.

5.2.5 DUrca proper volume

Let $[0, r_{\rm DU}]$ ($r_{\rm DU} < r_*$), be the radial interval where the DUrca process occur, i.e. where the number density of protons, neutrons and electrons satisfy

$$n_{\rm p}^{1/3} + n_{\rm e^-}^{1/3} \geq n_{\rm n}^{1/3} \ . \tag{5.30}$$

The main interest in studying the proper volume of this region

$$V_{\rm DUrca} = \int_0^{r_{\rm DU}} 4\pi r^2 e^{\Lambda(r)} n(r) dr \ , \tag{5.31}$$

lies in the facts discussed in Chapter 4: this process accelerates the cooling of the stars, so a bigger region implies a faster cooling. Fig. 5.16 illustrates the behaviour for several EoS and several values of αX with APR EoS, respectively.

For APR and MS-C1, α12-model implies slightly shorter volumes than general relativity, while for soft EoS such as MS-A1 and MS-B1 the most massive star proper DUrca volume is larger. On the other hand, a comparison between the volume and the central density illustrates an EoS independent behaviour, where the volume is larger for α12-model but the central density of the most massive star is lower. The limit $\alpha \to 0$ tends to increase the proper volume and the central density. The central density at which the Direct Urca becomes allowed is determined by the particle densities and is thus independent of the gravity model, however, the gravitational mass of the star in which this happens is dependent of gravity as seen by comparing the right versus left panels of Fig. 5.16. This suggests the existence of massive neutron stars (around $2{\rm M}_\odot$) whose thermal evolution is comparatively slower than their relativistic counterparts.

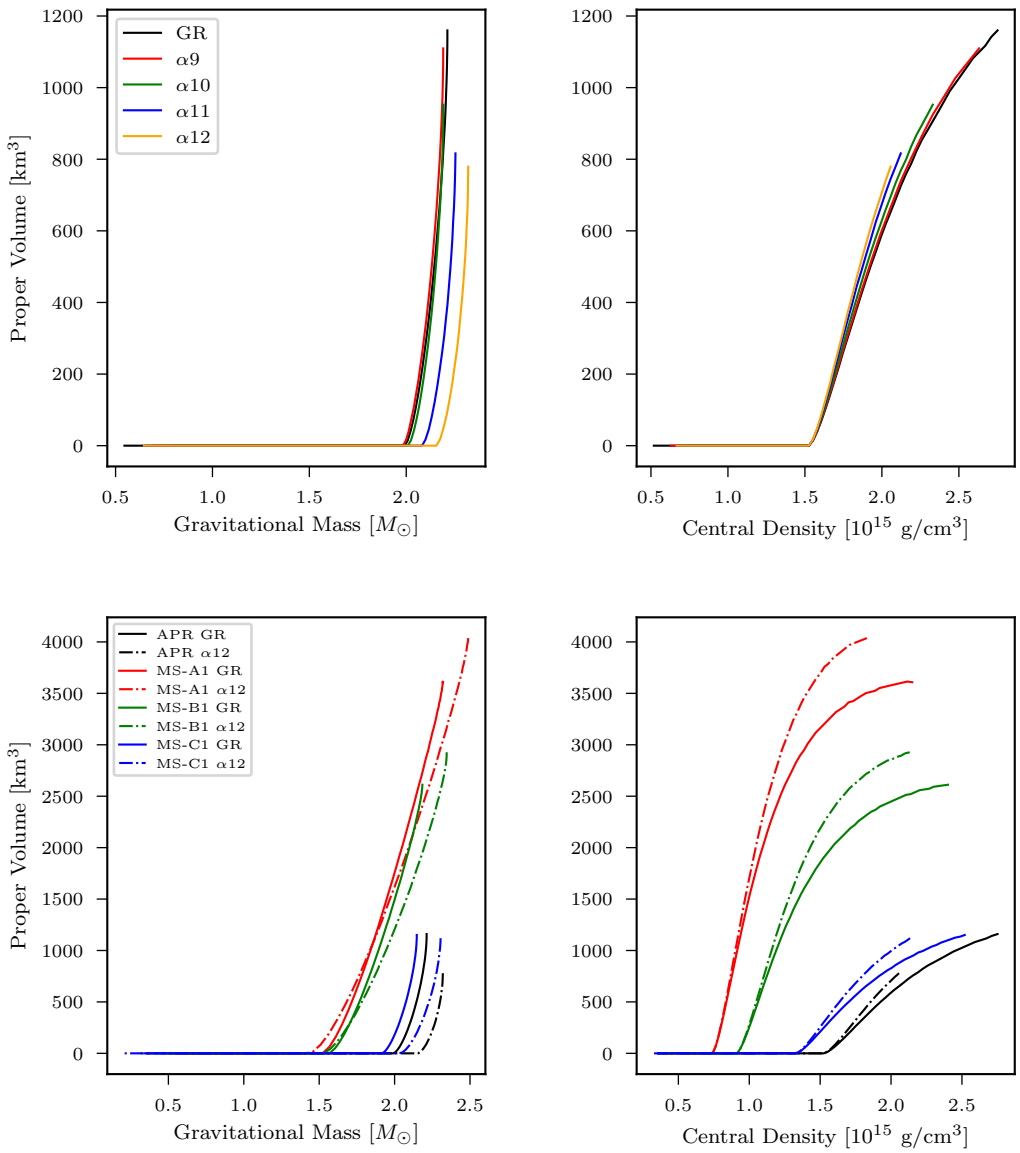

Figure 5.16: (Upper left) Proper volume of DUrca process as a function of gravitational mass, considering APR EoS and several α values. (Upper right) Proper volume as a function of central density. Same EoS and α values. (Lower left) Proper volume of DUrca process as a function of gravitational mass for different EoS and $\alpha 12$. (Lower right) Proper volume as a function of central density. Same EoS and value for α.

Chapter 6

Thermal Evolution of Neutron Stars

"*Symmetry, as wide or as narrow as you may define its meaning, is one idea by which man through the ages has tried to comprehend and create order, beauty and perfection*".

Hermann Weyl

Following the scheme of the previous chapter, here we divide in two parts the numerical study of the cooling process. In section 1 we re-write the differential equations which the temperature and luminosity satisfy, as well as their the boundary conditions. Then we review the most important aspects of the code employed to solve them, `NSCool` [56], [32]. Although this code is originally intended for studying GR neutron stars, the arguments in § 4.3, 5.2.2 are sufficient to justify its application for NSs in the quadratic model. In this section we also detail the purpose and the setup of the experiments performed. The results are reported in the last section of the Chapter.

The study we performed here is an extension within the αR^2 scheme of modified gravity of classical neutron star cooling studies realized within GR and amply described, e.g., in [37], [42], [43] and [69].

6.1 Numerical Method

Once the structure of the star is known, we consider $\Phi(r), \Lambda(r)$ as known functions which can be combined with the energy and transport differential equations,

$$\frac{e^{-\Lambda-2\Phi}}{4\pi r^2}\frac{\partial}{\partial r}\left(e^{2\Phi}L\right) = -Q_\nu + Q_h - \frac{C_V}{e^\Phi}\frac{\partial T}{\partial t} \ ,$$

$$e^{-\Lambda-\Phi}\frac{\partial}{\partial r}\left(e^{\Phi}T\right) = -\frac{L}{4\pi K r^2} \ ,$$

in order to determinate the luminosity and temperature of the star as radial and time functions.

These equations are better handled in terms of the baryon number N as Lagrangian coordinate with $dN = 4\pi r^2 e^\Lambda n dr$ and using the redshifted functions $\widetilde{T}(r;t) = e^{\Phi(r)}T(r;t)$, $\widetilde{L}(r;t) = e^{2\Phi(r)}L(r;t)$, $\widetilde{Q}(r;t) = e^{2\Phi(r)}Q(r;t)$ for both $Q = Q_\nu$ and Q_h, and $\widetilde{K}(r;t) = e^{\Phi(r)}K(r;t)$. (Notice that C_V is not red-shifted, i.e., $\widetilde{C}_V = C_V$.) The system of equations to solve becomes

$$\boxed{\frac{\partial \widetilde{L}}{\partial N} = \left[-\frac{\widetilde{Q}_\nu + \widetilde{Q}_{\rm h}}{n_B}\right] - \frac{C_V}{n_B}\frac{\partial \widetilde{T}}{\partial t}} \tag{6.1}$$

$$\boxed{\frac{\partial \widetilde{T}}{\partial N} = -\frac{\widetilde{L}}{(4\pi r^2)^2 \widetilde{K} n_B}} \tag{6.2}$$

In order to solve this system, two boundary conditions must be provided. These follow from the discussion in § 4.3.1: at the center of the star,

$$\boxed{L(r=0) = 0 \quad \Leftrightarrow \quad \widetilde{L}(r=0) = 0} \tag{6.3}$$

and at the surface, which is implemented at the position r_b with density $\rho_b = 10^{10}$ g cm^{-3} as, with $\widetilde{L}_b \equiv \widetilde{L}(r_b)$ and $\widetilde{T}_b \equiv \widetilde{T}(r_b)$,

$$\boxed{\widetilde{L}_b = e^{2\Phi(r_b)}\, 4\pi r_b^2 \sigma_{SB}\left[T_e(\widetilde{T}_b)\right]^4} \tag{6.4}$$

through an envelope model that provides us with a "$T_e - T_b$" relationship $T_e = T_e(\widetilde{T}_b)$ (see Fig. 4.4).

6.1.1 NSCool

Originally written in FORTRAN 77 language, this 1-D code[56] employs a Heyney scheme (which is based on the multi-dimensional Newton-Raphson method) to solve the system of equations. This scheme has the advantage of reducing computation

time due to the fast convergence of the iterations, which is said to have been achieved if the numerical errors are $\widetilde{O}(10^{-10})$.

The structure of the code can be split in two main parts: the initialization, and the solution of the equations. In the first one, the user must provide two files as input, the *Master file* and the *Profile of the star*. We now proceed to explain their contents:

1. Master file (.in extension): Includes the names and locations of the files which describe the composition of the star under consideration. An example is given in Fig. 6.1: the first section includes the assigned name of the model (for simplicity, this includes the EoS and the value of the gravitational mass), as well as the EoS and the Crust model. On the second part the size of the grid, heat conduction, superfluidity and superconductivity files are specified. Finally, the location and names for the output files are provided.

```
  'NEW'
BASIC MODEL FILES:
  'EOS/Crust/Crust_EOS_Cat_HZD-NV.dat'
  'EOS/v14/APR_EOS_Cat.dat'
  'TOV/Profile/Prof_APR_Cat_1.40.dat'
OTHER MODEL FILES:
  'I_Files/I_Struct_1.5e14-4.3e11-1e10_fine_S3-1.0e15.dat'
  'I_Files/I_Bound_Acc-08.dat'
  'I_Files/I_Pairing_SFB-0-0.dat'
  'I_Files/I_Neutrino_1.dat'
  'I_Files/I_Conduct/I_Conduct_41_T-0-00-00.0-0.00.dat'
  'I_Files/I_Heat_0.dat'
  'I_Files/I_Bfield_0.dat'
  'I_Files/I_Accretion_0.dat'
  'I_Files/I_Fudge_aTD=0.0.dat'
OUTPUT FILES:
  'Models/Pruebas/'
  'I.dat'
  'APR_Cat_1.40.dat'


Cool_APR_Cat_1.40.in
```

Figure 6.1: An example of a Master file.

2. Profile of the star (.dat extension): Includes the structure of the star in tabulated form. This file is obtained from the numerical solutions for the structure equations of the previous chapter. An example is illustrated in Fig. 6.2: on the first line, the numbers represents (from left to right): the blank/text lines that the program must skip in the file to reach the actual profile of the star, the total number of data rows, and the location of the symmetric nuclear density. On the second line, a name for the profile is is asigned. The last line of text indicates the variable described by each column. From left to right: the number of the line (steps), the radius of the star (in m), the baryon number, density, pressure (the three of them in

c.g.s units), the enclosed gravitational mass (solar units), $\Phi(r)$ (adimensional) and the enclosed baryonic mass, in solar units.

6 152 51

| APR_EOS_Cat_1.4.dat

step	radius (m)	baryon# (#/fm3)	density (g/cm3)	pressure (dyn/cm2)	encl. mass (sol. mass)	phi	encl. bar. mass (sol. mass)
0	0.000000	5.447307E-01	9.925265E+14	1.45523E+35	0.000000000E+00	-4.709204E-01	0.000000000E+00
1	10.000000	5.447304E-01	9.925259E+14	1.45523E+35	2.090237440E-09	-4.709201E-01	1.921243342E-09
2	11.666665	5.447303E-01	9.925257E+14	1.45523E+35	3.319217942E-09	-4.709200E-01	3.050861941E-09
3	13.611106	5.447302E-01	9.925254E+14	1.45523E+35	5.270791549E-09	-4.709199E-01	4.844652980E-09
4	15.879620	5.447300E-01	9.925250E+14	1.45523E+35	8.369814021E-09	-4.709198E-01	7.693123556E-09
5	18.526217	5.447298E-01	9.925245E+14	1.45523E+35	1.329093799E-08	-4.709196E-01	1.221638251E-08
6	21.613911	5.447294E-01	9.925238E+14	1.45522E+35	2.110548127E-08	-4.709193E-01	1.939913546E-08
7	25.216214	5.447290E-01	9.925229E+14	1.45522E+35	3.351464482E-08	-4.709189E-01	3.080504925E-08
8	29.418893	5.447284E-01	9.925216E+14	1.45521E+35	5.321984668E-08	-4.709184E-01	4.891714904E-08
9	34.322005	5.447276E-01	9.925199E+14	1.45521E+35	8.451078236E-08	-4.709176E-01	7.767834381E-08
10	40.042280	5.447265E-01	9.925175E+14	1.45519E+35	1.341992077E-07	-4.709167E-01	1.233497341E-07
11	46.715900	5.447249E-01	9.925143E+14	1.45518E+35	2.131016755E-07	-4.709153E-01	1.958735150E-07
12	54.501734	5.447229E-01	9.925099E+14	1.45516E+35	3.383939027E-07	-4.709135E-01	3.110370899E-07
13	63.585121	5.447200E-01	9.925039E+14	1.45514E+35	5.373490621E-07	-4.709110E-01	4.939093328E-07
14	74.182266	5.447162E-01	9.924958E+14	1.45510E+35	8.532732863E-07	-4.709076E-01	7.842966600E-07
15	86.545382	5.447110E-01	9.924847E+14	1.45505E+35	1.354929369E-06	-4.709031E-01	1.245405805E-06
16	100.968668	5.447039E-01	9.924697E+14	1.45499E+35	2.151497671E-06	-4.708968E-01	1.977597250E-06
17	117.795279	5.446942E-01	9.924492E+14	1.45490E+35	3.416325752E-06	-4.708883E-01	3.140219259E-06
18	137.425443	5.446810E-01	9.924213E+14	1.45478E+35	5.424625168E-06	-4.708767E-01	4.986266748E-06
19	160.325901	5.446631E-01	9.923833E+14	1.45462E+35	8.613296462E-06	-4.708610E-01	7.917390697E-06
20	187.040878	5.446387E-01	9.923316E+14	1.45439E+35	1.367585096E-05	-4.708396E-01	1.257119146E-05
21	218.204821	5.446056E-01	9.922613E+14	1.45409E+35	2.171297441E-05	-4.708104E-01	1.995970857E-05
22	254.557149	5.445604E-01	9.921656E+14	1.45368E+35	3.447125229E-05	-4.707707E-01	3.168905924E-05
23	296.959299	5.444989E-01	9.920354E+14	1.45312E+35	5.472147043E-05	-4.707167E-01	5.030761569E-05

Figure 6.2: Example of a Star profile.

From the structure of the equations to solve, eq. 6.1 and 6.2, the only change from GR is the modified values of the metric, i.e., e^{Φ} and e^{Λ}, which `NSCool` obtain when reading the star profile file. The boundary condition of eq. 6.3 is trivial while eq. 6.4 needs a "$T_e - T_b$" relationship which depends on the surface gravity: this was discussed in § 5.2.2 where it was shown that g_s is correctly calculated simply using $M_{\rm surf}$. Besides these small trivial adjustments no further adaptation is needed and `NSCool` automatically gives us the evolution of a neutron star in αR^2 modified gravity.

Details of the numerical methods employed in `NSCool` and how to use it can be found in the NSCool home page. Recently the code has been adapted as a Python package, allowing the user to run the simulations, store and display the results in a single Jupyter Notebook. This also has the advantage of simplifying the process of setting additional parameters for the numerical experiments, such as the thickness of the envelope η and the superfluidity models.

6.1.2 Experiments

Having discussed the structure of the code and concluding that no modifications are needed, we proceed to introduce the purpose and the setup for each numerical experiment.

The models were chosen according to the same criteria as the previous Chapter:
1. APR EoS, and αX variable, with $X = 9, 10, 11, 12$.

2. APR, MS-A1, MS-B1 and MS-C1 EoS, with $\alpha 12$ fixed.

Due to current constrains over the gravitational mass, together with the DUrca mass threshold exposed in the previous chapter, we only consider those profiles capable of producing NSs whose total gravitational mass lie in the interval [1.3, 2.2] $M_\odot$. In order to simplify the exposition, we adopt the following notation for the superfluidity models:

$$\mathrm{SF} = ({}^1S_0\,\mathrm{n}, {}^3P_2\,\mathrm{n}, {}^1S_0\,\mathrm{p})\ , \tag{6.5}$$

where n denotes neutron and p proton. For the list of employed superfluidity models, see Table 4.1.

Experiment 1: Simple models

From the results of the previous chapter, where the shape of the structure functions (I.e., $P(r)$, $\rho(r)$, $\Phi(r)$ and $\Lambda(r)$) is almost the same, we might expect a similar behaviour for the cooling curves, although not completely equal: since T_e is proportional to the local surface gravity, quadratic NSs are likely to be colder. Additionally, since the DUrca mass-threshold is different in both gravity models, we might expect massive stars cooling at a lower rate. Superfluidity should be neglected for the moment, due to its impact over the late stages of thermal evolution and because its appearance does not depend on the gravity model chosen.

Purpose: To analize the effects of the αR^2 model over the cooling process of "basic" NS: no superfluidity, no light-elements envelope.

Numerical Setup: The thickness of the light-elements envelope is fixed to $\eta = 10^{-20}$. Superfluidity is not allowed in any channel.

Experiment 2: Presence of light elements in the envelope

While T_e might be, for NSs in the quadratic model, lower than their GR counterparts, modifying the composition of the envelope is still responsible for increasing T_e during the whole cooling process. Although this effect takes place either superfluidity is present or not, it is convenient to follow the continuity of the previous experiment. That is, for the moment we neglect baryon pairing and focus on modifying the value of η.

Purpose: To analize the impact of changing the composition of the envelope over the cooling curves in the quadratic model, neglecting the presence of superfluidity.

Numerical Setup: We choose 1.4 and 2 $M_\odot$ stars for both sub-experiments, i.e. αX variable and fixed. For η, we consider $10^{-15}, 10^{-10}, 10^{-5}$. No superfluidity is allowed in any channel.

Experiment 3: Superfluidity models

Having observed the consequences of changing η, the EoS and α, we can now proceed to study the impact of superfluidity over the cooling curves. While a similar behaviour to GR is expected, we must pay attention to the small or huge changes that each superfluidity model induces over T_e.

From the numerical results, at least three models for each channel are selected for the setup of the remaining experiments. Moreover, at this point we expect to have gathered enough information to settle whether the quadratic model does or does not have impact over the *Minimal Cooling scenario* [55], where observations favourish a scenario of no DUrca process inside the star, and a gravitational mass in the range [1.4, 2] $M_{\odot}$.

Purpose: Analize the consequences of choosing several superfluidity models over cooling curves. From the numerical results, we choose at least 3 models for each channel, which are employed in late experiments.

Numerical Setup: The thickness of the light-elements envelope is fixed to $\eta = 10^{-15}$. Both variable and fixed α sub-experiment are performed considering a 1.4 $M_{\odot}$ star. To adress individual effects of each superfluidity channel, we adopt the following ordering: SF=(X,0,0), SF=(0,Y,0) and SF=(0,0,Z), where (X,Y,Z) denote the superfluidity model chosen from 4.1.

Experiment 4: Combined Effects

Purpose: Combine the selected superfluidity models with several EoS and η.

Numerical Setup: We consider SF=(0, CasA, T73) and SF=(0,CasA, CCDK) models, for both APR and MS-A1 EoS. Regarding MS-C1 and MS-B1, we consider SF=(0,CasA,CCDK) and SF=(0,Ioffe 2NT, CCDK). The mass range is [1.4, 2] $M_{\odot}$, and for η we choose $10^{-20}, 10^{-16}$, $10^{-12}, 10^{-8}$, 10^{-4}.

6.2 Observational Data

At our disposal we have the effective temperature and the age of 19 NSs, which are plotted in a $\mathrm{Log}_{10}T_e^{\infty}$ versus Log_{10} t plane in Fig. 6.3 and taken from the work [79]. All these stars are isolated ones and we, unfortunately, have no observational information about their masses.

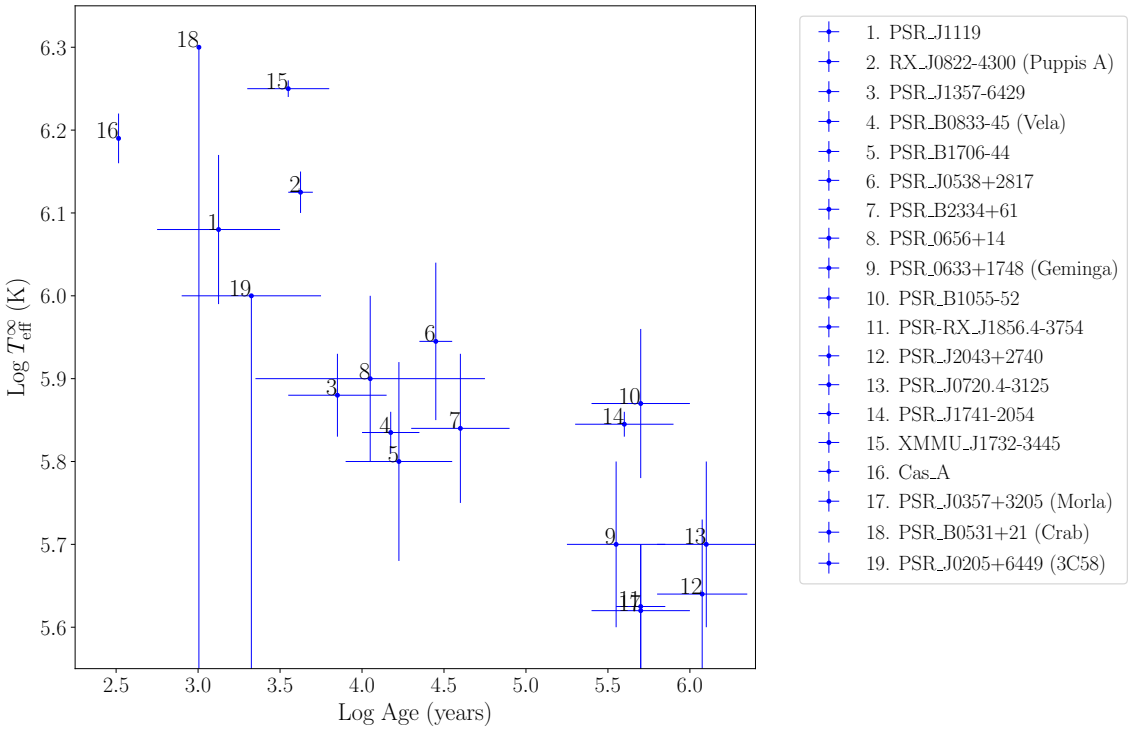

Figure 6.3: Observational data corresponding to 19 NSs, whose names are given in the companion box.

6.3 Results

We now proceed to describe the outcomes of the proposed experiments. For a clearer presentation, each one of them is placed in a particular subsection.

6.3.1 Experiment 1: Simple models

Our purpose here is to analize the effects of the αR^2 model over the cooling process of "basic" NS: no superfluidity, no light-elements envelope.

The results for varying $X = 9, 10, 11, 12$ are given in Fig.6.4. For $\alpha 9$ the cooling curves are practically the same as GR. From $\alpha 10$ to $\alpha 12$, the stars progressively become cooler, save for the 2 $M_\odot$ star which cools slowly in αR^2 gravity. The dramatic change in the cooling of the 2 $M_\odot$ star is simply due to the fact that in GR and $\alpha 9$ the star has the Direct Urca process acting in its innermost core while once α is increased the central density of a 2 $M_\odot$ star is progessively reduced and becomes lower than the threshold density for the Direct Urca as is clearly exhibited in the lower left panel of Fig. 5.16. On the other side, the progressive lowering of T_e^∞ with increasing α is a result of the decrease of the surface gravity g_s, see Fig. 5.10, which changes the $T_e - T_b$ relationship: a lower g_s implies a thicker envelope which is more effective in insulating the surface from the hot interior and results in a reduction of T_e.

Results with varying the EoS are displayed in Fig. 6.5. The EoS MS-C1 is quite similar to APR and the cooling also similar. Both have a threshold mass for the Direct Urca below 2.0 $M_\odot$ in GR but above 2.0 $M_\odot$ in $\alpha 12$ as seen in Fig. 5.16. In GR, for APR only the 2.0 $M_\odot$ is above threshold and cools rapidly while for MS-C1 both 1.9 and 2.0 $M_\odot$ models cool rapidly. MS-A1 and MS-B1, however, have much lower critical densities for the Direct Urca (see, e.g., Fig. 4.2) resulting in critical masses just below 1.5 $M_\odot$ both in GR and in $\alpha 12$ so that only the 1.4 $M_\odot$ stars cool slowly.

Data are plotted for completeness and will be compared with our models in the last experiment 4. It is obvious that these simple cooling models fare pretty badly when compared with data.

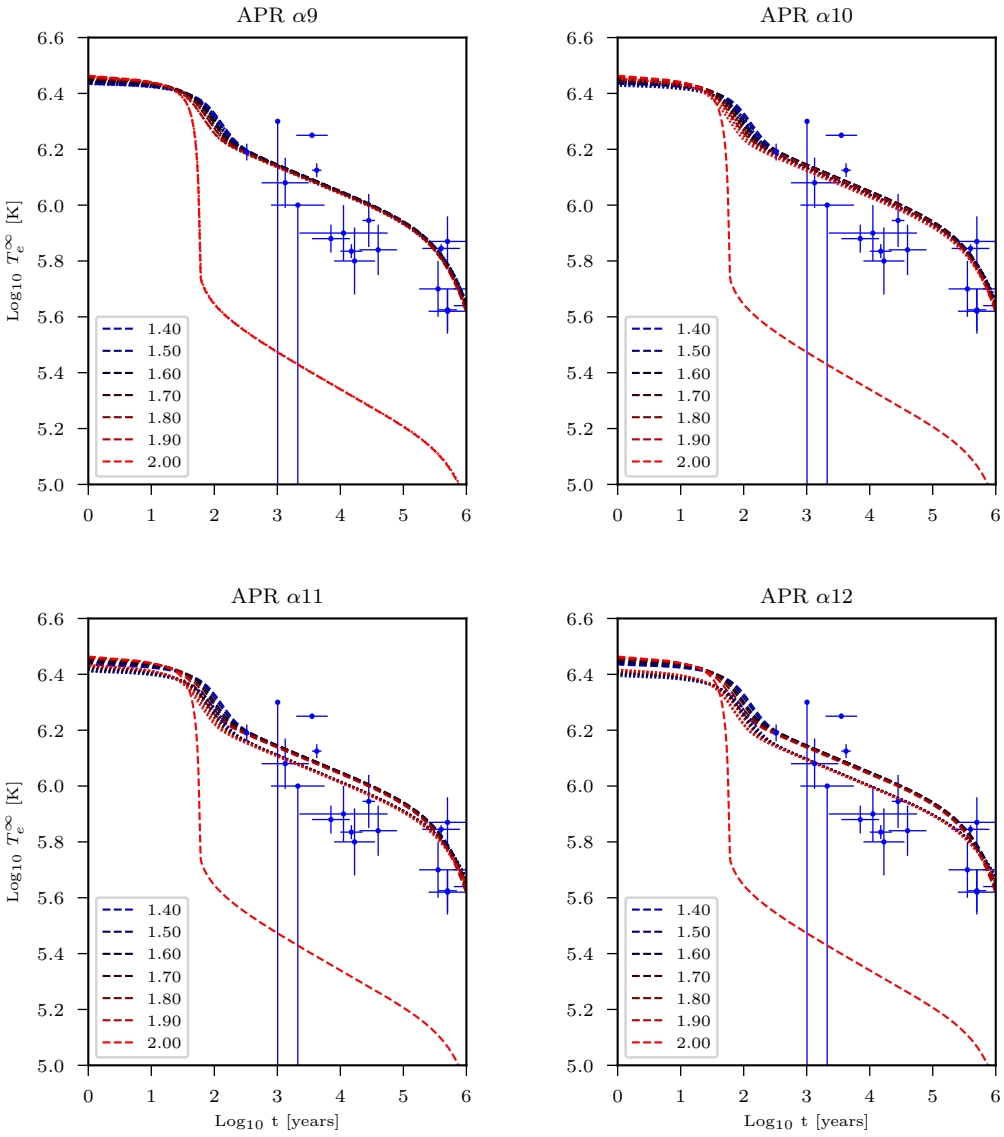

Figure 6.4: Cooling curves for the APR EoS. The dashed lines correspond to the GR models while the dotted lines to the αR^2 models with the αX value as labelled at the top of each panel. Notice that in the $\alpha 9$ panel the two 2.0 $M_\odot$ curves, for GR and $\alpha 9$ gravity, are on top of each other while in the other three cases the αX curve is pushed up and becomes very similar to the lower mass models and only the GR one is cooling rapidly. The gravitational masses of the models, either GR of αR^2, are indicated.

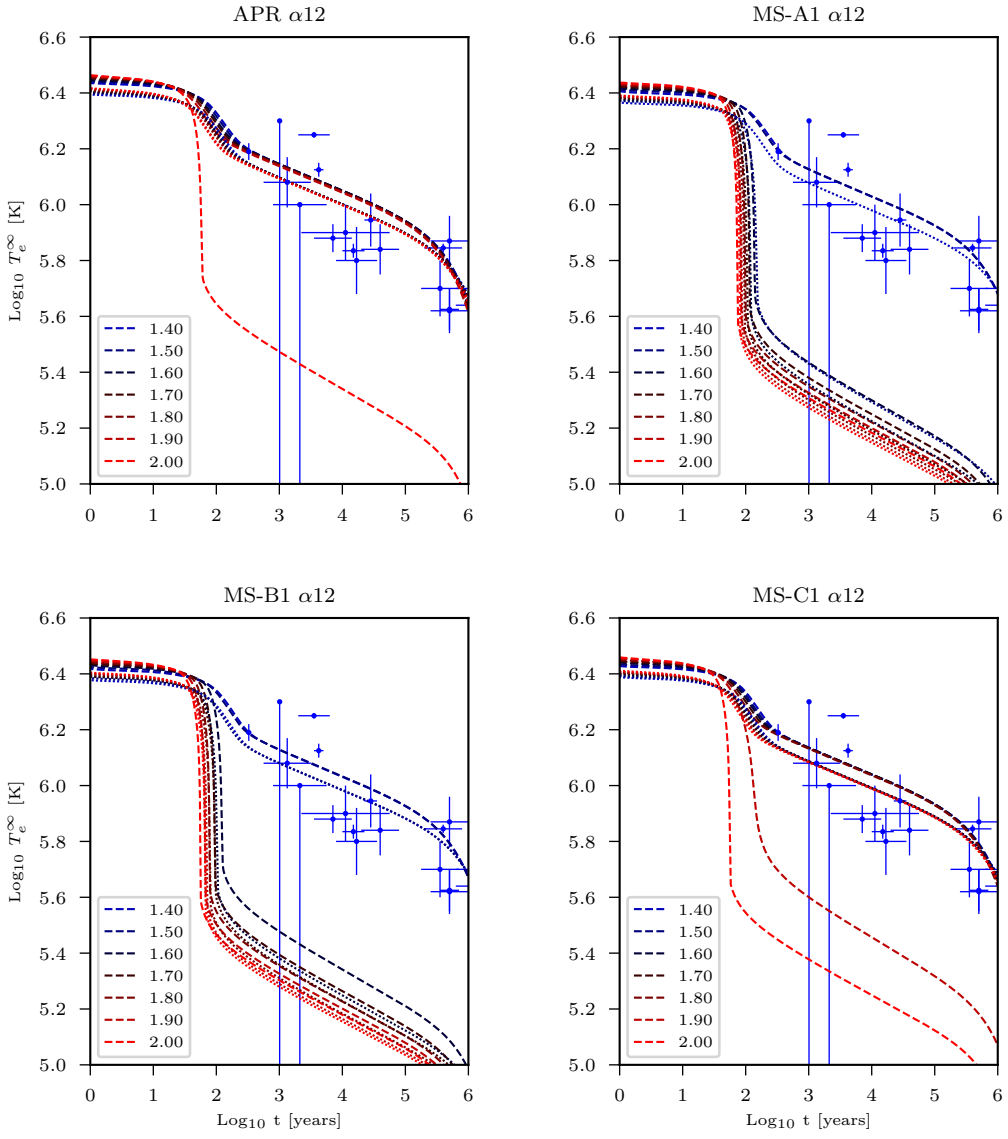

Figure 6.5: Cooling curves for the EoS indicated at the top of each panel. Dashed lines correspond to GR models, while the dotted ones to $\alpha 12$.

6.3.2 Experiment 2: Presence of light elements in the envelope

As mentioned in § 4.3.1, the presence of light elements in the upper layers of the star (the envelope) results in an increase of the surface temperature, T_e. The magnitude of this increase grows with η and is moreover T-dependent as illustrated in Fig. 4.4. In short, the higher T_b (i.e., the internal temperature at the base of the envelope at $\rho_b = 10^{10}$ g cm^{-3}) the higher η needs to be to have an effect and after some threshold the effect saturates and further increase of η has no effect.

Fig. 6.6 illustrates the results for APR and $X = 9, 10, 11, 12$. The green and blue lines correspond to a 2 and a 1.4 $M_\odot$ star respectively. Again, the results of $\alpha 9$ are practically indistinguishable with GR. Regarding the effects of the light elements in the envelope, if we consider the 1.4 $M_\odot$ stars we clearly see that increasing η result in an increase of T_e. In the case of the 2.0 $M_\odot$ stars the effect of increasing η reaches its maximum already at relatively small η and values of 10^{-10} and 10^{-5} give identical results (the saturation effect). This behaviour with respect to η can be seen in all other panels. When $\alpha \gg \alpha 9$ the 2.0 $M_\odot$ star in αR^2 gravity cools slowly, as seen in the previous sub-section, and becomes similar to the 1.4 $M_\odot$ case. Globally we see that increasing α leads to a small decrease of T_e, due to the decrease of g_s as seen in the previous sub-section, but increasing η raises T_e much more significantly, in both 1.4 $M_\odot$ and 2.0 $M_\odot$ stars.

A comparison between Figs. 6.6 and 6.7 allows to conclude that the observations raised in the previous sub-section remain valid here. The effect of light elements and its competition with the change in gravity theory is qualitatively similar for all EoS and only differs in details.

Obviously, the presence of light elements in the superficial layers does not alter the overall cooling controlled by neutrino emission in the deep interior, e.g., the difference between high and low mass stars which do or do not have a Direct Urca process acting. However, the hottest models appear compatible with the hottest observed stars as # 2, 15, and 18. Nevertheless, overall agreement with data is not yet very impressive.

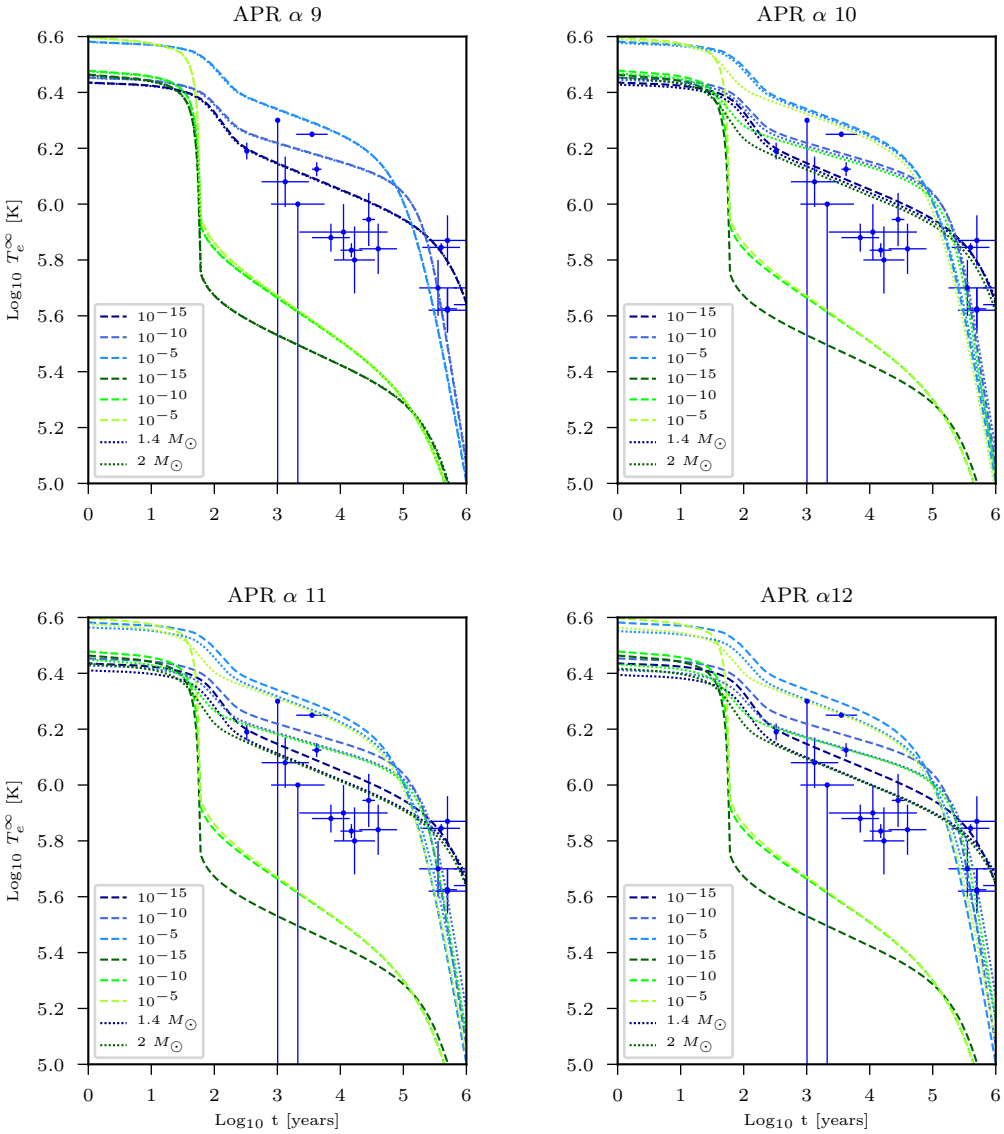

Figure 6.6: Cooling curves for 1.4 $M_\odot$ (in blue scale) and 2 $M_\odot$ (green scale), for three values of η, 10^{-15}, 10^{-10}, and 10^{-5}, as indicated. APR EoS and the correspondent αX on the top of each panel. The dashed lines correspond to the GR models, the dotted lines to the quadratic ones.

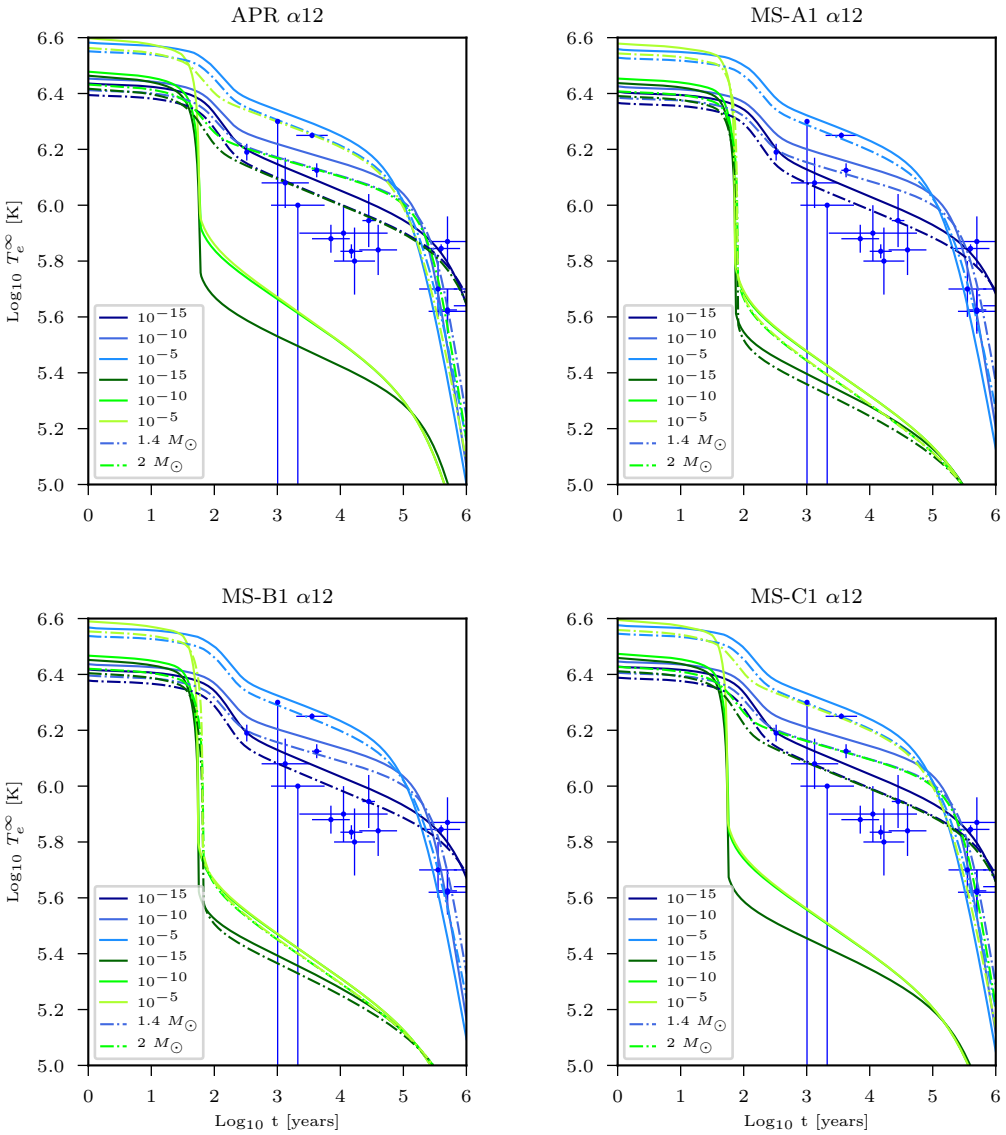

Figure 6.7: Cooling curves for 1.4 $M_\odot$ (in blue scale) and 2 $M_\odot$ (green scale), for the indicated values of η, $\alpha 12$ and the EoS indicated at the top of each panel. The continuous lines correspond to the GR models, the dashdotted lines to the quadratic ones.

6.3.3 Experiment 3: Superfluidity models

From Fig. 4.2, it is clear that the DUrca process is suppressed for all EoS if $M_{\rm grav} \leq 1.4\ M_\odot$ and from Fig. 6.5 one sees that such rapidly cooling models are much colder that any observed star. Thus, a NS of gravitational mass $1.4\ M_\odot$ is a natural choice for studying pure superfluidity effects in relationship with compatibility with the data. It turns out that the three expected types of pairing, $^1S_0$ in the crust and $^3P_2$ in the core for neutrons and $^1S_0$ in the core for protons, have distinctive effects and we will consider them separately.

$^1S_0$ **neutrons.** This channel of superfluidity occurs in the low density region, the crust, and its effect is felt only at early times. For this reason we first focus on the first few centuries of evolution in Fig. 6.8 and 6.9. In all cases, the main effect of superfluidity in this context is to suppress the specific heat of the neutrons and this changes the time at which the first drop in T_e is occurring, in the age range from about 10 to 100 years. The different models for $^1S_0$ differ in their critical temperatures T_c (see Fig. 4.5) resulting in different amount of superfluid neutrons at a given moment and thus, different heat capacity. With respect to gravity effects, as seen previously, increasing values of α (Fig. 6.8) imply lower gravity g_s that result in decreasing values of T_e, almost like an exact vertical translation of the models.

Fig. 6.9 show, moreover, that the different EoSs considered have almost identical behavior both in GR and in αR^2. The slight differences in the cooling times between different EoSs are due to the slight differences in the radius of the stars: larger radii imply thicker crusts and longer times for this temperature drop to occur. However, at $1.4\ M_\odot$ stars built within GR of within αR^2 have practically the same crust thickness (see Fig. 5.15) and so their cooling curves are vertical translations of each other.

The Fig. 6.10 and 6.11 display the same models but on longer times and show that at the ages where data exist models with different neutrons $^1S_0$ superfluidity in the crust follow exactly the same trajectories. However, the possible recent identification of the neutron star remnant produced in the supernova SN 1987A, with a present age of 33 yrs, opens the possibility to probe this early regime as described in [32].

$^3P_2$ **neutrons.** In clear contrast with the former channel, the effects of each model in the cooling curves is more complicated and not just a simple translation. The early cooling, first few decades, is controlled by crust physics (and strongly affected by the $^1S_0$ superfluidity as described above) but after this it is driven by neutrino emission from the core up to ages $\sim 10^5$ yrs, the *neutrino cooling era*, and after this by photon emission from the surface, the *photon cooling era*. During the neutrino cooling era the neutrino luminosity is an integral over the whole core and this grant total depends on many details as the exact central density, the whole density profile, as well as the profile of both metric functions $\Phi(r)$ and $\Lambda(r)$. All these physical properties change when changing the EoS and/or the gravity model. On top of this,

the effect of neutron $^3P_2$ superfluidity is multiple: it suppresses the neutron specific heat and the neutrino emission from all processes in which these neutrons participate (the modified Urca and the n-n and n-p bremsstrahlung processes, see Table 4.2) but it also triggers powerful neutrino emission from the continuous formation of the Cooper pairs during the phase transition. Depending on the precise value of T_c, the latter effect can be dominant and lead to accelerated cooling. During this neutrino cooling era the temperature reached by a 1.4 $M_\odot$ star in the presence of neutron $^3P_2$ superfluidity can be significantly lower than in its absence: compare the overall look of Fig. 6.12 and 6.13 versus Fig. 6.10 and 6.11.

With respect to gravity effects we see that, in the age range between 10^2 to 10^5 yrs, αR^2 models are always colder that GR ones in the $\alpha 12$ case but not in the other cases with smaller α. So in the $\alpha 12$ case gravity effects seem to dominate but not for smaller values of α. We are in the presence of the simultaneous occurrence of several effect of comparable magnitude but acting in different directions and it is not clear which one dominates, except for gravity at large values of α. However, at later times, above 10^5 yrs, GR and αR^2 models give almost identical results.

Comparing with data, we see that some $^3P_2$ neutron superfluidity models result is cold enough neutron stars models at ages between 10^3 to 10^5 yrs that are roughly compatible with most of the coldest observed neutron stars as the data points #3 to #8. This is the essence of the so-called *Minimal Cooling Paradigm* of [55] which attempted to explain all data without the presence of some "exotic" form of matter implying that any observed neutron star too cold to be explained within this paradigm is a serious candidate for an "exotic" object. Within the set of data we consider and within GR gravity only the star #4, the Vela pulsar, is below all theoretical predictions (upper left panel of Fig. 6.12). **However, within extended models of gravity as, e.g., αR^2 with $\alpha \sim 10^{12}$ cm^2, predicted T_e during the neutrino cooling era are lower than in GR and all observed cold neutron stars are now compatible with the** *Minimal Cooling Paradigm* **and this conclusion is independent of the assumed EoS (see 6.13).** We still have two hot stars, #2 and #15, that are much above all predictions of the present "Experiment 3".

$^1S_0$ **protons.** The effects of proton superconductivity are similar to the ones of neutron superfluidity but with two important differences. First the protons are much less abundant than the neutrons so their effect is proportionally smaller. Secondly, the neutrino emission from the formation of Cooper pairs is much less efficient in the case of spherically symmetric pairs in the $^1S_0$ channel than in the case of asymmetric pairs in the $^3P_2$ channel. This is clearly seen by comparing the range of predicted T_e during the neutrino cooling era (10^2 - 10^5 yrs) when considering neutron $^3P_2$ superfluidity, upper left panel of Fig. 6.12, versus proton $^1S_0$ superconductivity. The effect of modified gravity in this case is as expected from our previous experiments: a lowering of the cooling curves when α is increased, as clearly seen in Fig. 6.14. In Fig. 6.15 we see that the effects of proton $^1S_0$ superconductivity are EoS dependent:

an immediate consequence of each EoS implying different proton fractions in the inner core.

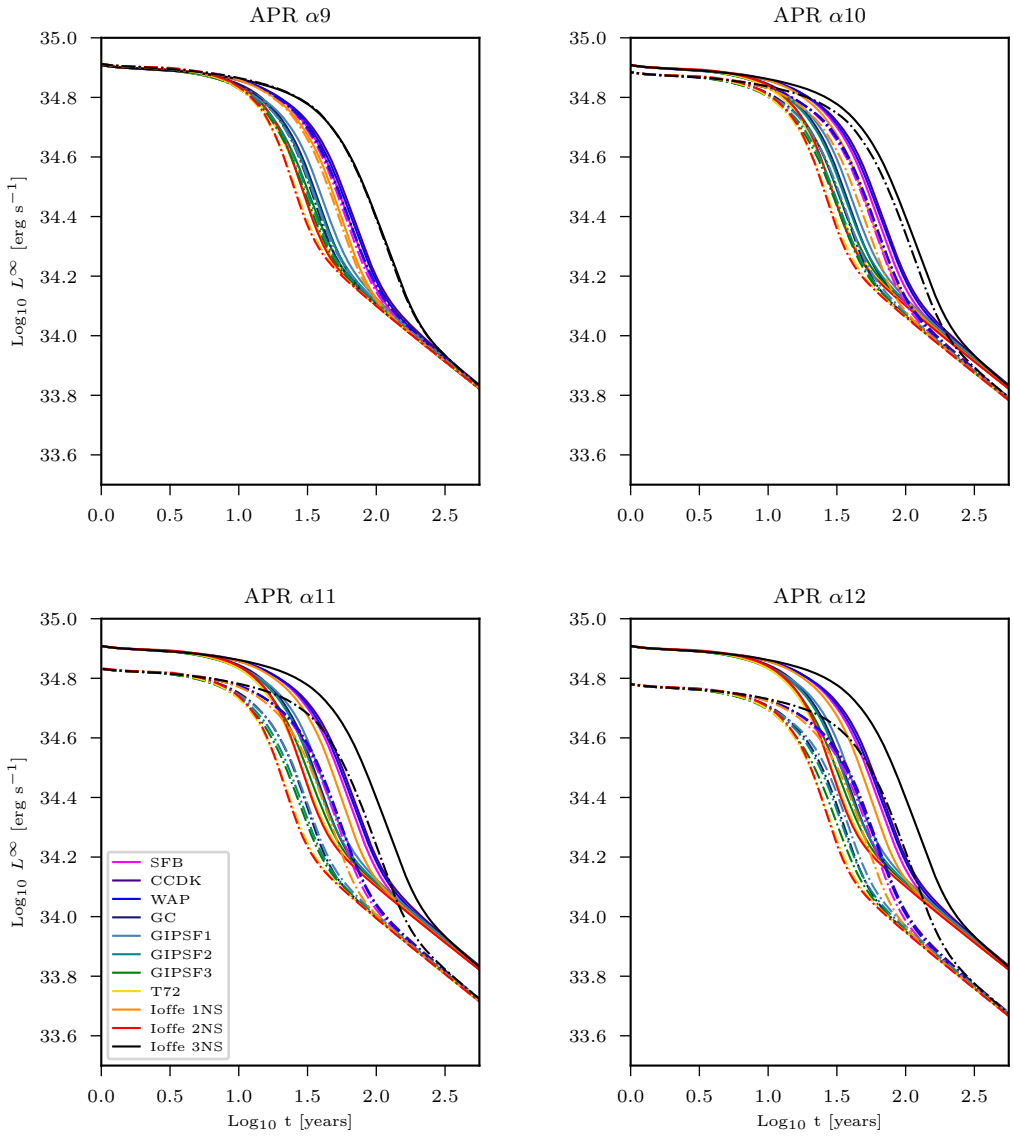

Figure 6.8: Log_{10} of Luminosity versus Log_{10} of time for a 1.4 $M_{\odot}$ - APR EoS NS, with different models of $^1S_0$ neutron superfluidity. The continuous lines correspond to GR while the dashdotted to the αX indicated at the top of the panel.

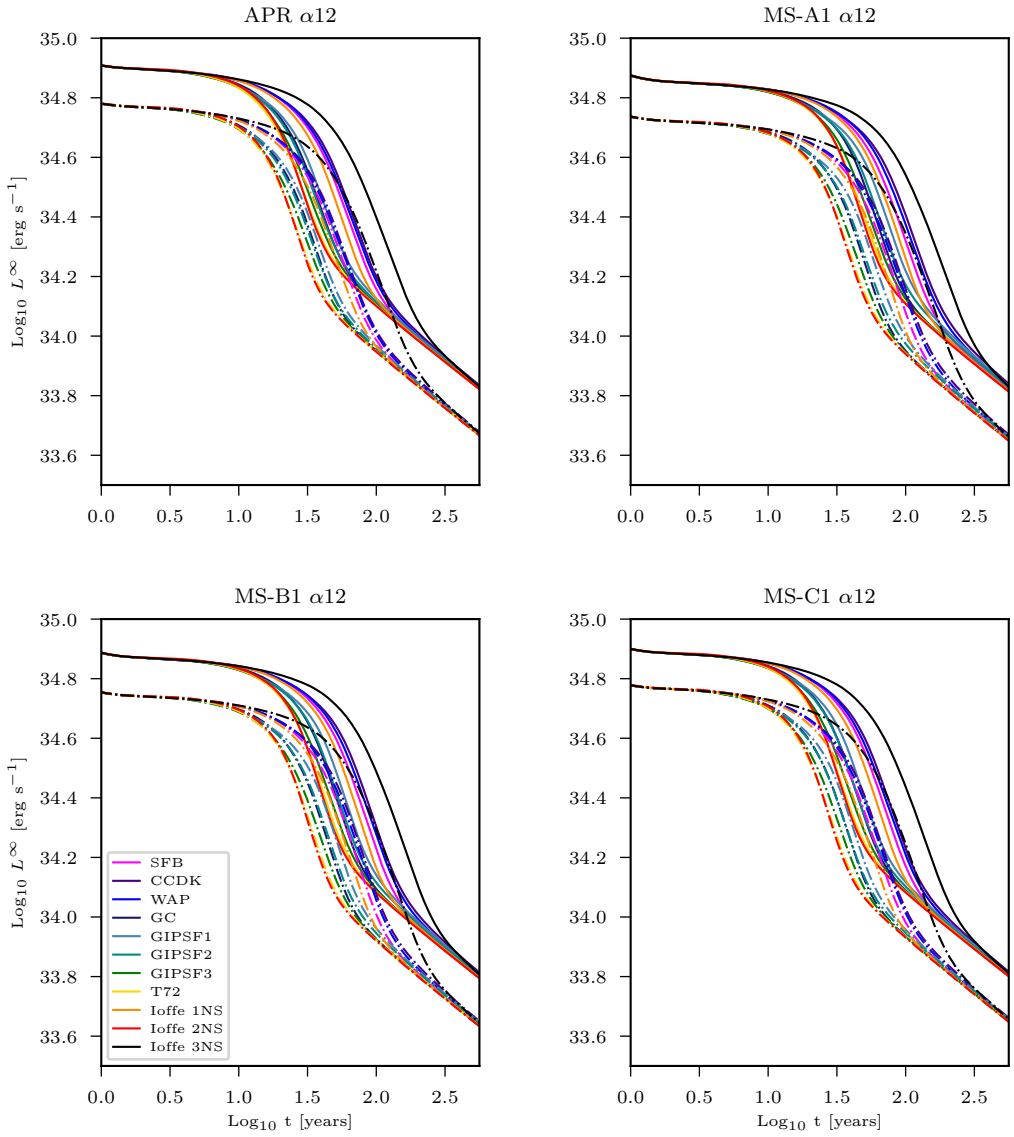

Figure 6.9: Same physical quantities than the previous Figure, this time for $\alpha 12$ and the indicated EoS.

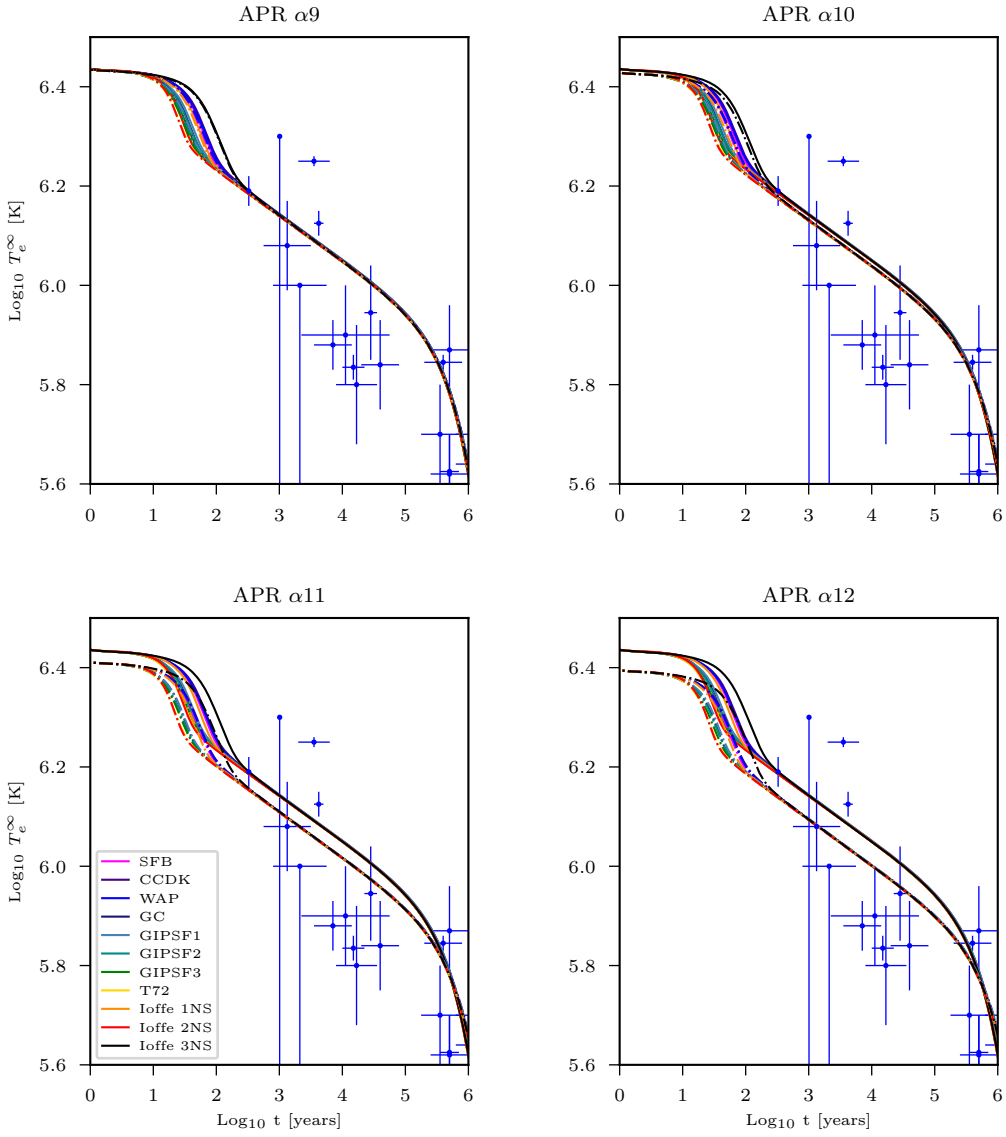

Figure 6.10: Cooling curves for the labeled $^1S_0$ neutron superfluidity models. Continuous curves: GR. Dashdotted: αX indicated at the top of each panel.

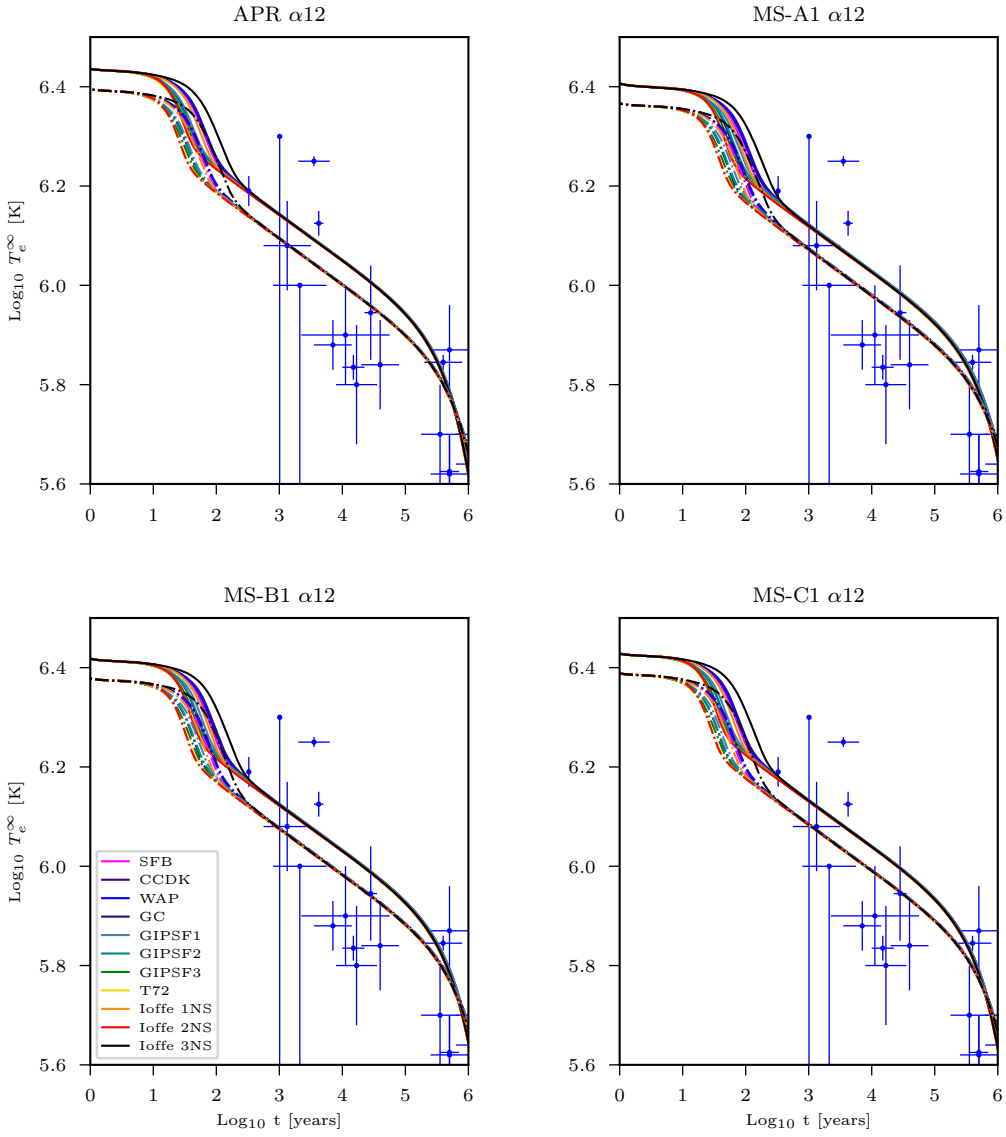

Figure 6.11: Cooling curves for the labeled $^1S_0$ neutron superfluidity models, and the EoS at the top of the panels. Continuous lines: GR. Dashdotted: α12.

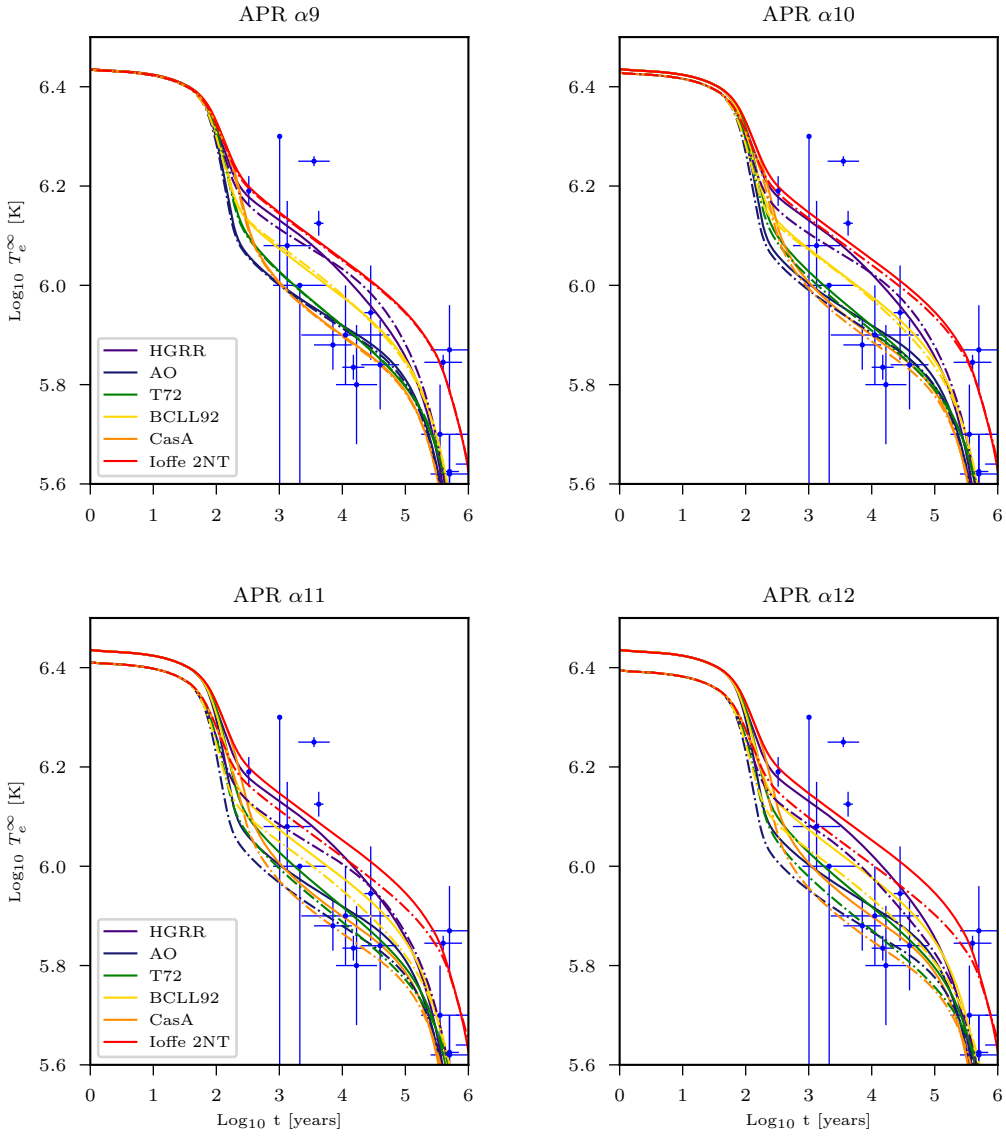

Figure 6.12: Cooling curves for the labeled $^3P_2$ neutron superfluidity models. Continuous curves: GR. Dashdotted: αX indicated at the top of each panel.

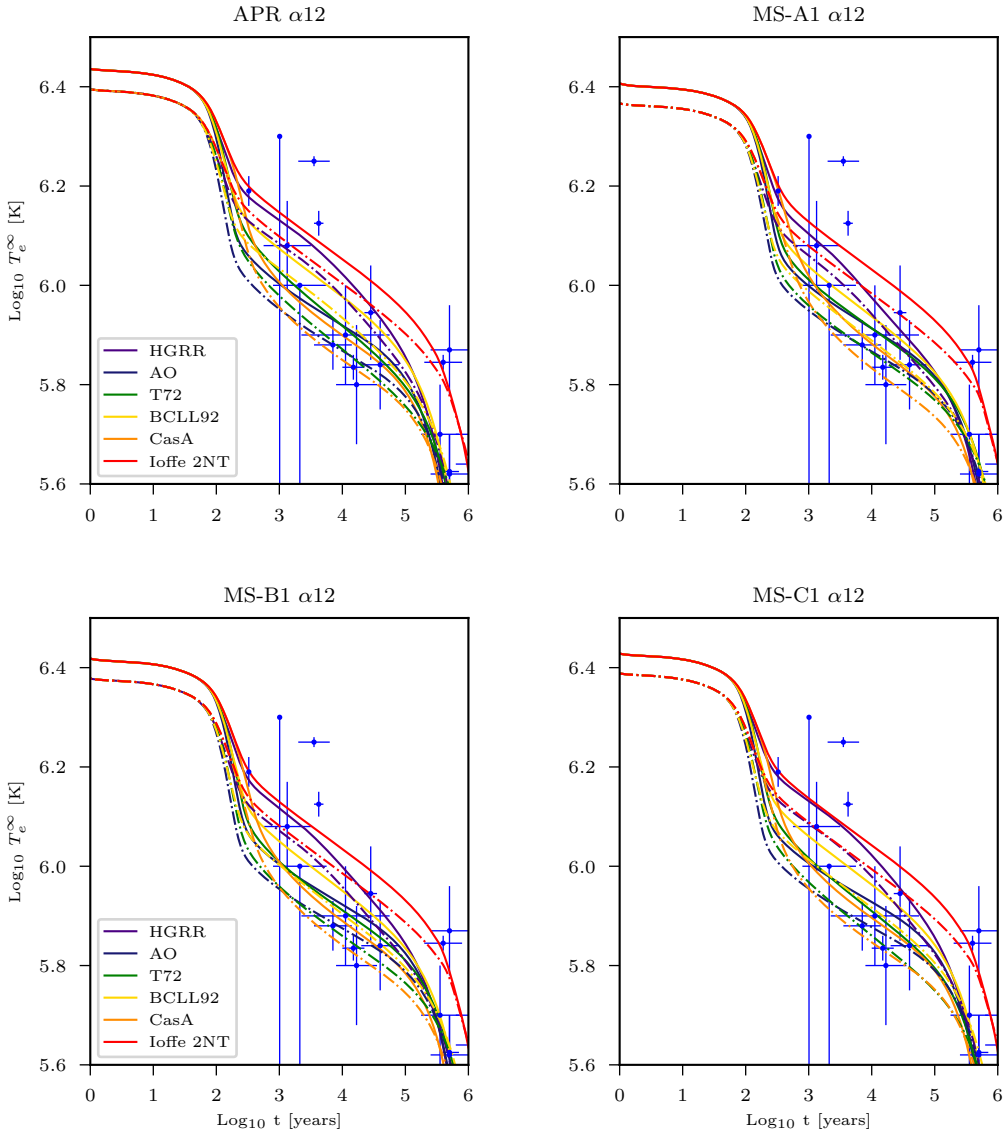

Figure 6.13: Cooling curves for the labeled $^3P_2$ neutron superfluidity models, and the EoS at the top of the panels. Continuous lines: GR. Dashdotted: α12.

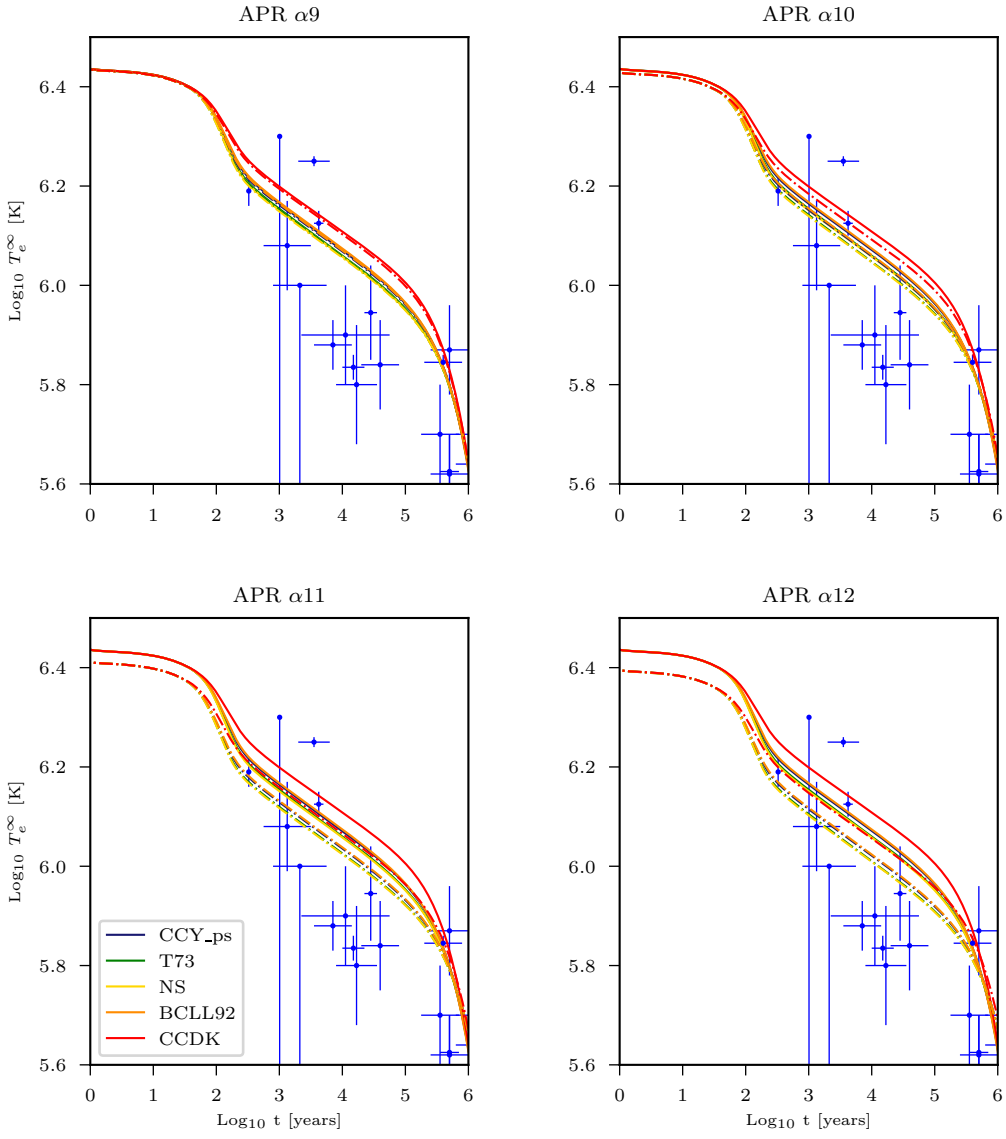

Figure 6.14: Cooling curves for the labeled $^1S_0$ proton superfluidity models. Continuous curves: GR. Dashdotted: αX indicated at the top of each panel.

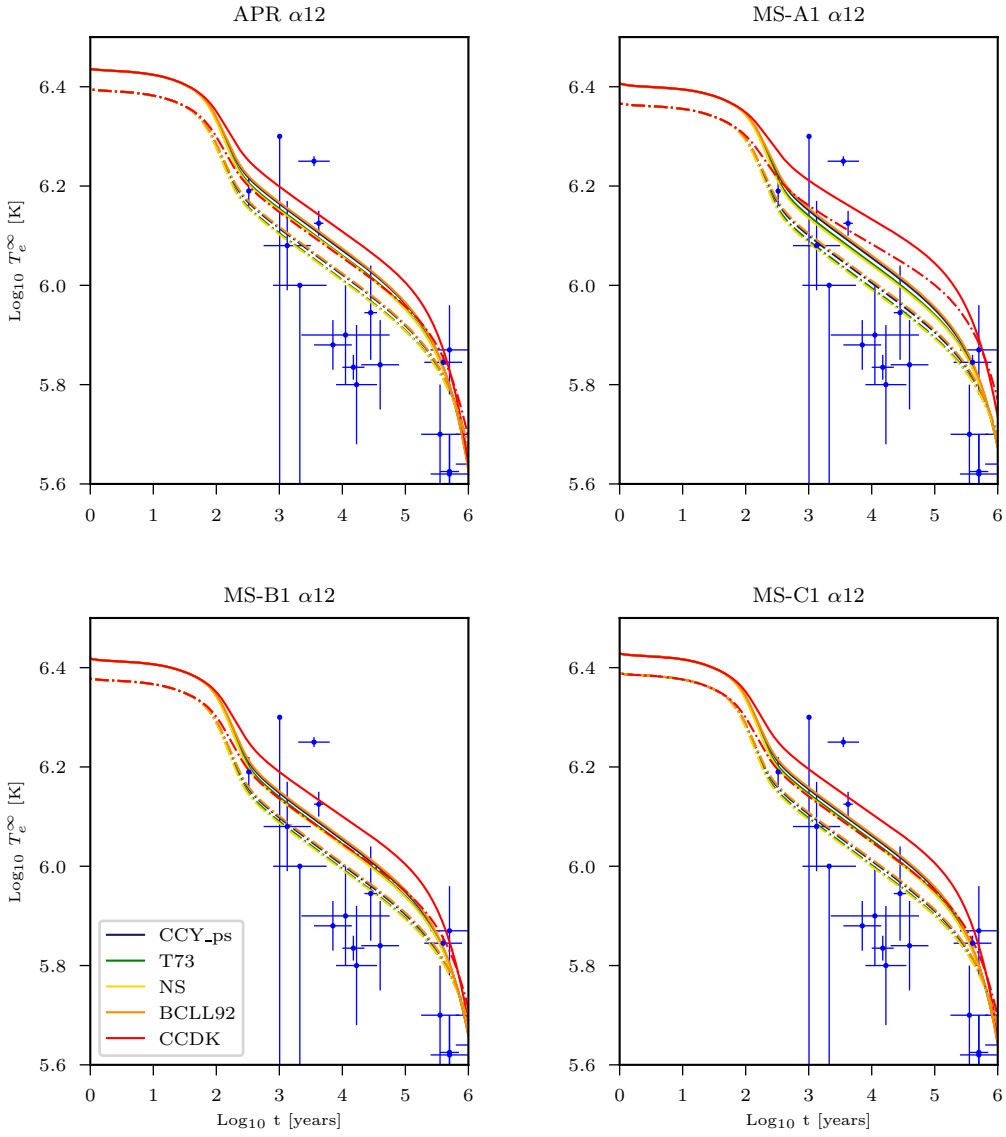

Figure 6.15: Cooling curves for the labeled $^1S_0$ proton superfluidity models, and the EoS at the top of the panels. Continuous lines: GR. Dashdotted: $\alpha 12$.

6.3.4 Experiment 4: Combined Effects

In this last experiment we present more sophisticated models that include both changes in the envelope chemical composition (see Experiment 2) and the inclusion of the effects of neutron superfluidity and proton superconductivity (see Experiment 3).

Letting both superfluidity and superconductivity to be simultaneously present, as they physically should be, one can obtain very interesting effects. The most notorious being the possibility of sudden increase in the cooling rate in models where extensive proton superconductivity (as in the model "CCDK") early suppresses neutrino emission but is followed by a late onset of superfluidity (with a relatively low values of T_c) that suddenly triggers the Cooper pair formation process. This combination results in a sudden change in the slope of the cooling curve followed by a temporal rapid cooling as was found in [67]. Such a rapid cooling was later observed in the case of the Cas A neutron star [68] and immediately interpreted as direct evidence for the occurrence of neutron superfluidity and proton superconductivity in the core of neutron stars [69, 70]. The position of the Cas A neutron star is outlined in the right panels of Fig. 6.16 where the change of the slope of the cooling curve just at Cas A's age is clearly seen. In the case superconductivity is less extended, as in the case of the "T73" models the effect of rapid cooling disappear (see the left panels of Fig. 6.16). Overall, the models of this figure show quite good agreement with most data points except the oldest ones that appear to need some extra heating to keep them warm at the late times where our theoretical cooling curves see their temperatures drop (at ages $\sim 10^6$ yrs).

In the next Fig. 6.17 we change the EoS to MS-C1, which is similar to APR, and explore the effect of changing the neutron $^3P_2$ superfluidity by comparing the "Cas A" model with the "Ioffe2NT" model which has a very low T_c. The left panels of this figure show almost identical results as in the right panels of Fig. 6.16, a natural result. In contradistinction, the right panels with the second neutron superfluidity model present completely different evolutions, most data points are missed, and the possibility of rapid cooling at the age of Cas A disappear.

Regarding the MS-A1 and MS-B1 EoSs (Figs. 6.18 and 6.19), we can notice that as a consequence of their DUrca mass threshold, it is possible to set a better constraint over the gravitational mass of the colder stars in the sample: 1.4 - 1.6 $M_\odot$ models with variable amount of light elements. Due the difference in the details of the micro-physics, the change in the slope of the cooling curves occurs later compared to the APR and MS-C1 EoSs. (However a small change in the shape of the T_c curve of the "Cas A" neutron $^3P_2$ superfluidity could shift this back in time, but such an adjustment is left for future work.) With respect to the "Ioffe2NT" model, right panels of Figs. 6.19, it explains well the oldest and warmer objects, but the rest of the sample is left out of range due to the significant gap between the 1.5 and 1.6 $M_\odot$ models.

Finally, considering the effects of modification to the theory of gravity we can see the following. A first important point is to notice that the modification of gravity we consider, αR^2, does not alter the interpretation of Cas A's rapid cooling as shown in the lower right panel of Fig. 6.16 for the $\alpha 12$ model. Overall, the many uncertain ingredients in the models, such as the EoS, the specifics of both neutrons superfluidity and proton superconductivity, as well as the uncertain chemical composition of the envelope, have much greater impacts on the cooling curves than the uncertainty on the theory of gravity. One clear effect, however, is readily seen in the case of the EoSs APR and MS-C1 in that models that undergo fast cooling with the Direct Urca process in GR turn into slowly cooling models in $\alpha 12$.

During the realization of this work, we have been aware that a recent preprint [82] has also considered the cooling process in the scalar-tensor gravity model. These authors also used `NSCool`, in its public version, but only considered simplified models of neutron stars of the type we studied in §6.3.1, i.e., without including superfluidity/superconductivity and light element envelopes. Moreover they label the models according to the surface gravitational mass, $M_{\rm surf}$: from this they claim that modified gravity effects are very large when compared to GR while once the correct total gravitational mass, $M_{\rm grav}$ which is the observable value is used as we do, the effects are small.

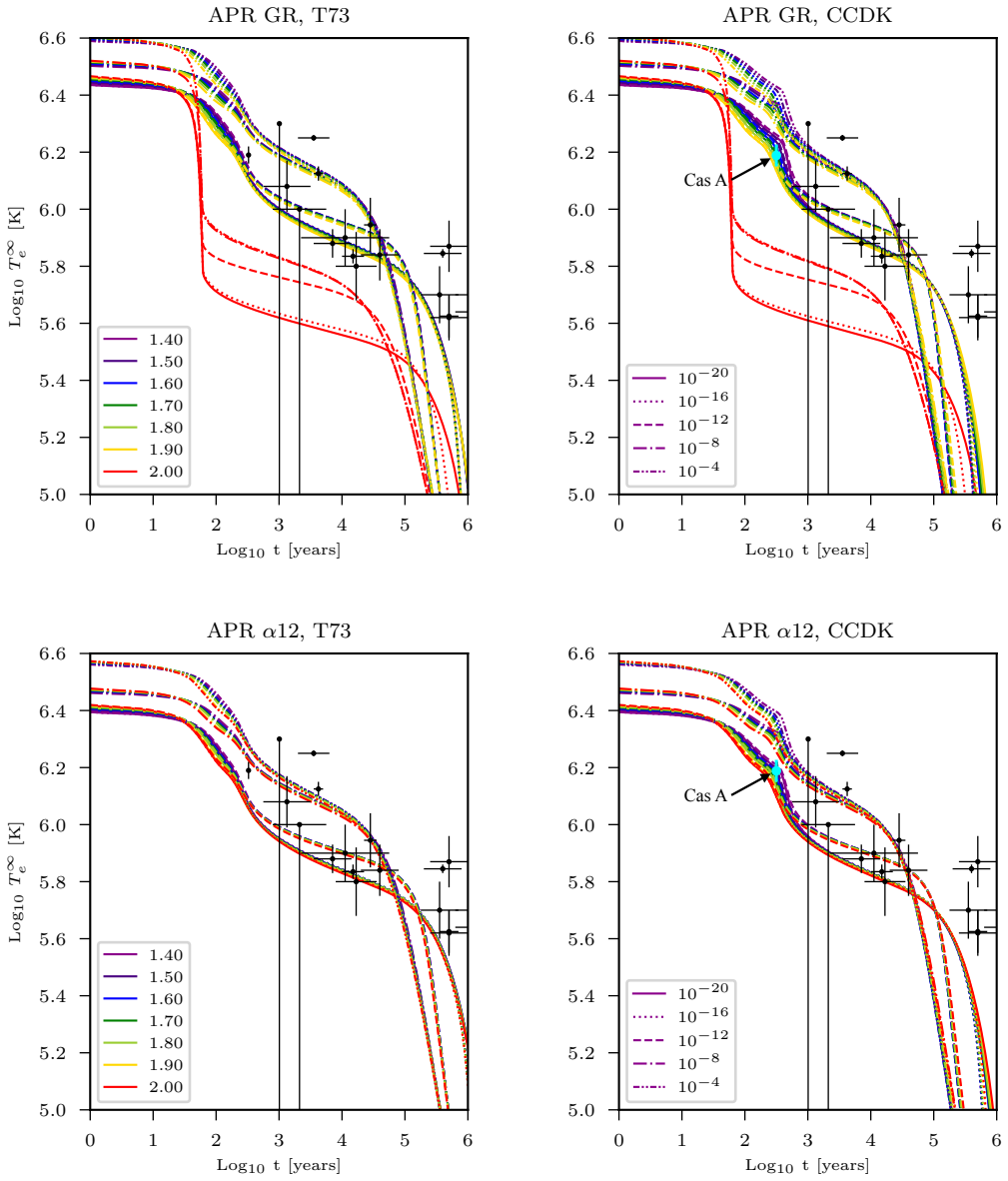

Figure 6.16: Cooling curves for APR and the indicated values of η and solar masses. Neutron superfluidity is only allowed in the $^3P_2$ channel (CasA model), and the $^1S_0$ proton superfluidity model is indicated at the top of each panel. (Upper panels) GR. (Lower panels) α12.

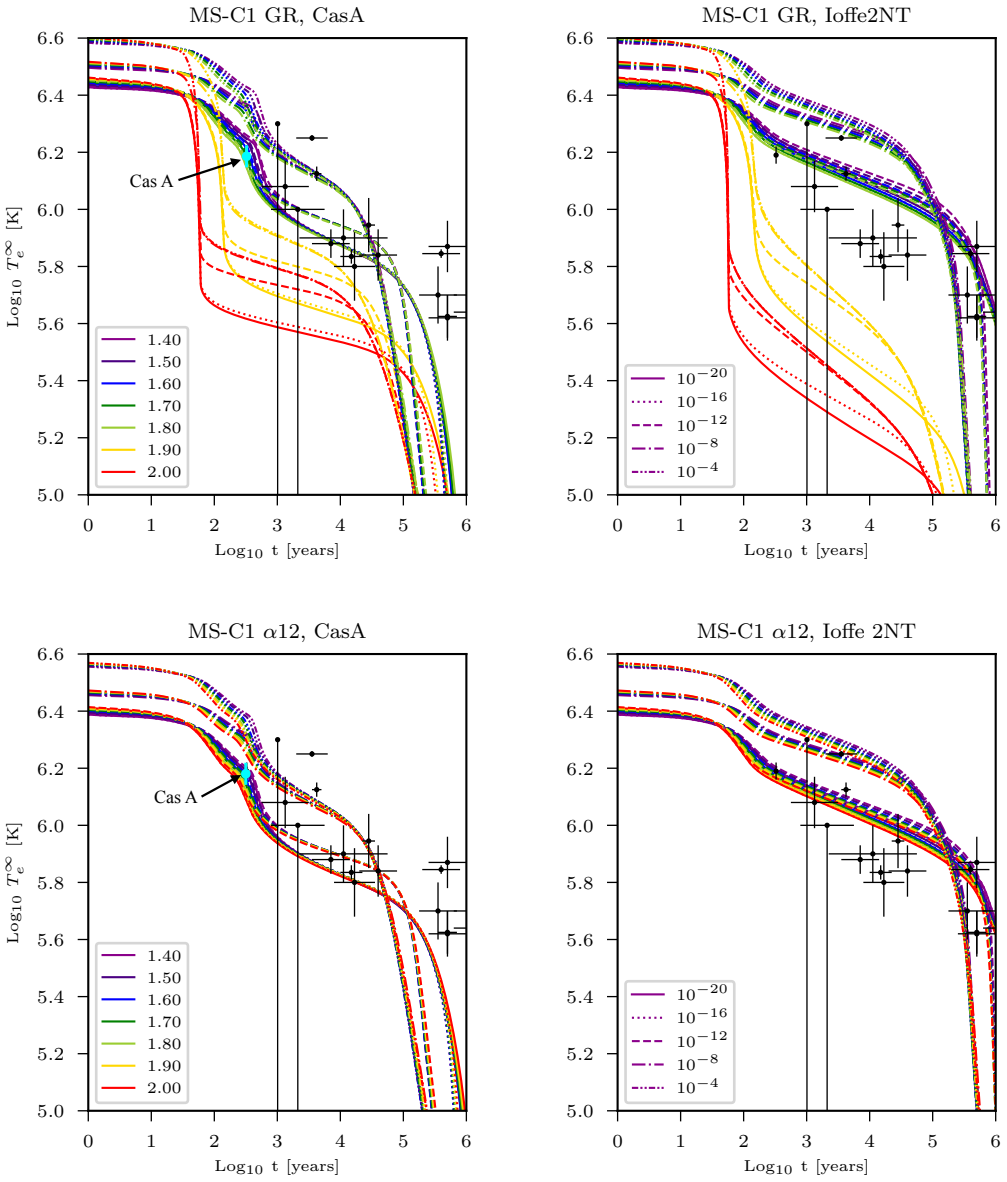

Figure 6.17: Cooling curves for MS-C1 and the indicated values of η and solar masses. Neutron superfluidity is only allowed in the $^3P_2$ channel (each model is indicated at the top of the panels), while CCDK $^1S_0$ proton superfluidity model is employed. (Upper panels) GR. (Lower panels) $\alpha 12$.

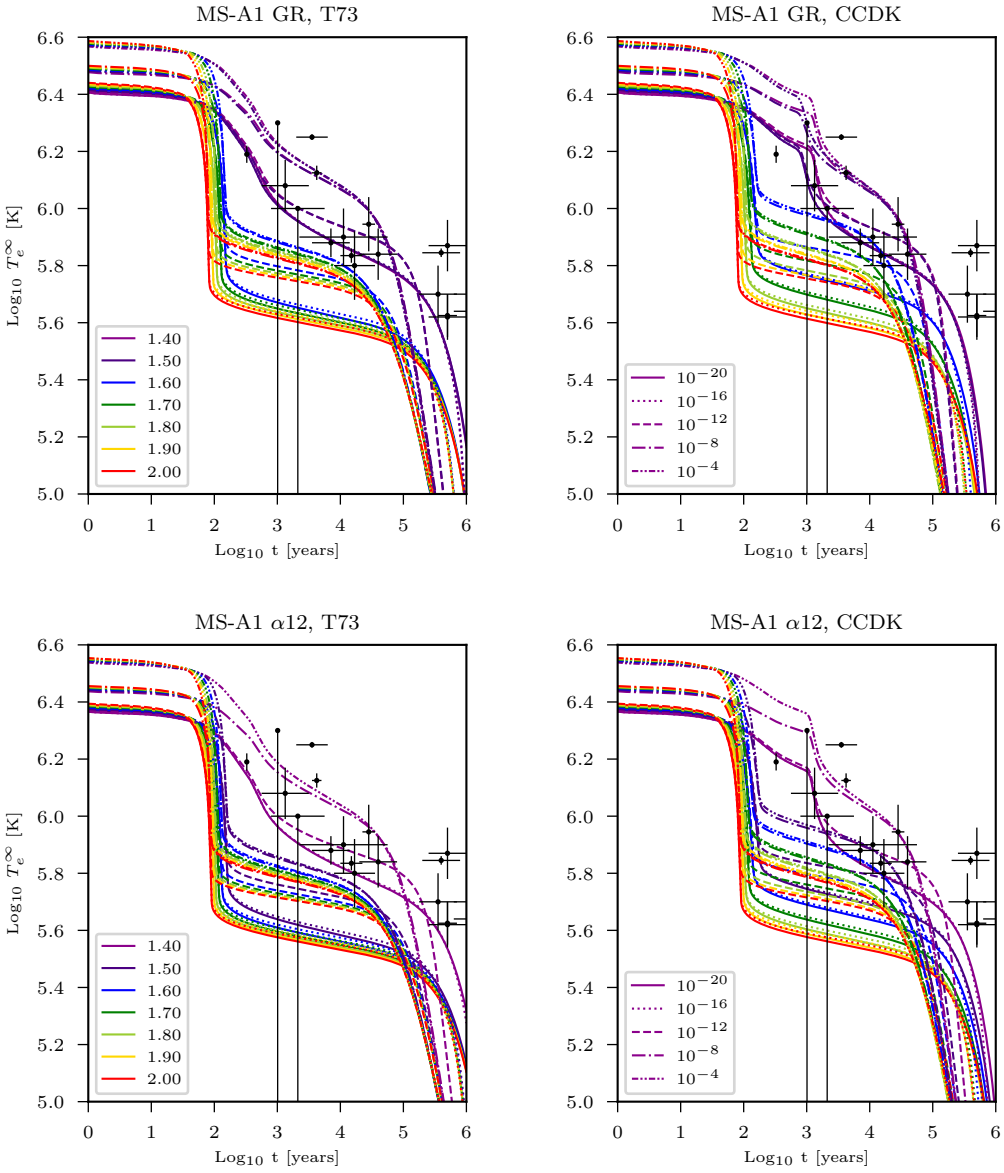

Figure 6.18: Cooling curves for MS-A1 and the indicated values of η and solar masses. Neutron superfluidity is only allowed in the $^3P_2$ channel (CasA model), and the $^1S_0$ proton superfluidity model is indicated at the top of each panel. (Upper panels) GR. (Lower panels) $\alpha 12$.

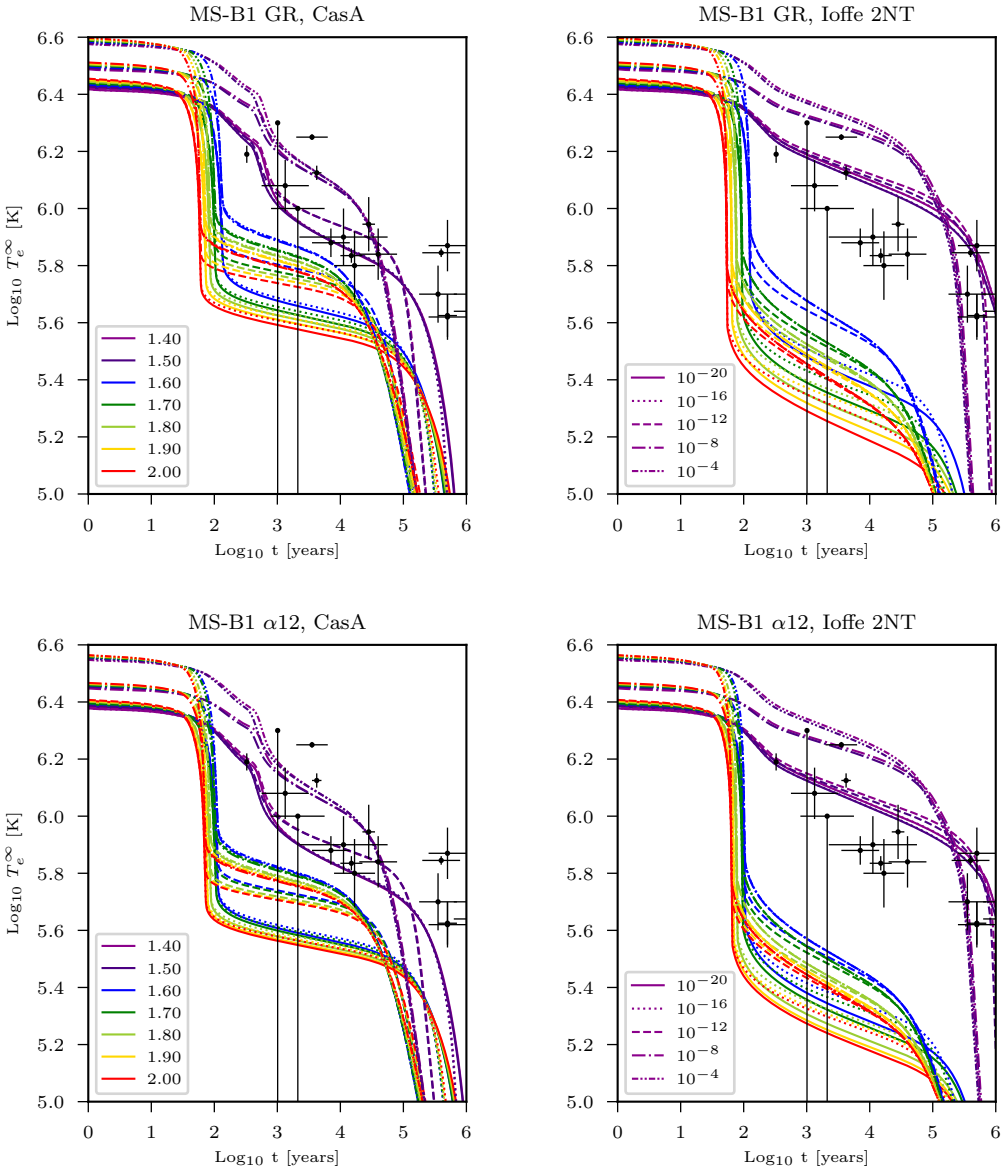

Figure 6.19: Cooling curves for MS-B1 and the indicated values of η and solar masses. Neutron superfluidity is only allowed in the $^3P_2$ channel (each model is indicated at the top of the panels), while CCDK $^1S_0$ proton superfluidity model is employed.(Upper panels) GR. (Lower panels) α12.

Chapter 7

Conclusions

"*Yes, she had had her vision*".

Virginia Woolf

Having described in detail the numerical results, it is time to discuss their implications (or simply criticize them!). As we did before, the structure of the star goes first, then the cooling.

1.A A priori, recovering Schwarzchild's metric at infinity does not seem a natural condition for the metric functions, while simple assymptotic flatness ($\Lambda, \Phi \to 0$) does. However, the quadratic model allows to recover this particular metric *at infinity* due to the vanishing of the scalar curvature and its derivatives. By combining the differential equations of the metric functions (see §3.4.1), it is clear that $\Lambda'(r \to \infty) = -\Phi'(r \to \infty)$, thus allowing a reescaling for these functions *at infinity*. Hence, the total gravitational mass recovers its status as a constant quantity, which can be significantly larger than in GR as we saw in §5.2.1. On the other hand, the differences between gravity models start to appear as we approach the surface of the star, where the gravitational sphere becomes responsible for the "extra" mass that is seen at infinity and the distinction between surface and total gravitational mass. Nevertheless, this effect would open the possibility for some EoSs whose maximum mass does not reach the 2 $M_\odot$ minimum limit (from the measured mass of the two pulsars PSR J0348+0432 and PSR J0740+6620, 2.01 $M_\odot$ [34] and 2.14 $M_\odot$ [35] respectively) to be "revived" if, for a large value of α, this limit can be reached §5.2.1. However, this is only one of several tests that such EoS should pass even in the quadratic model.

The effect of an increasing-with-distance gravitational mass, as we have seen in §5.2.1 resulting in a larger mass at infinity that at the surface of the matter distribution, is used as a candidate for explaining the huge amount of mass needed at the edge of disk galaxies in order to explain their rotation curve [11]. This suggestion deserves a careful analysis for several reasons: first, a static and spherical metric

might not be a good candidate for describing the spacetime of disk galaxies; second, development and numerical solution of the correspondent equations of motion must be performed in order to compare with existent data. Recently, a galaxy-formation simulation has been carried out employing an $f(R)$ Lagrangian [81], but the exact results and implications should be reviewed and replicated if possible, before attempting to claim that the position-dependent gravitational mass emerges as a viable explanation in these models.

1.B The invariance of the expression for the local surface gravity (see eqs. 5.25 and 5.28) when moving from GR to αR^2, have been justified with the numerical calculations of scalar curvature profiles in §5.2.2. From a theoretical (and complementary) point of view, this similarity arises due to a conclusion previously reached in perturbative approaches: *in the quadratic model, the field equations and their solutions become those of GR locally* [18], [19], [20],[13], [21].

A comparison of the ratio $M_{\rm surf}/r_*$ using the surface gravitational mass between αR^2 and GR leads to the conclusion that this modification results in *less compact* stars (see Figs. 5.11 and [80]). However, if the comparison is taken with the total gravitational mass instead, $M_{\rm grav}/r_*$, there seems to be a turning point in the compactness between models, around 1.4 $M_\odot$, see Fig. 5.12. If this is a consequence of moving from a higher density regime to a lower one remains unexplored, although it can be noted that the central pressure of the most massive GR star is greater than the most massive in αR^2, see Figs. 5.7 and 5.9.

While the redshift is very close between αR^2 and GR, see Fig. 5.13, it remains to be explored the impact of the gravitational sphere over the possibility of closed orbits in the region $[r_*, r_g]$. In principle, this would be a suitable method for exploring deviations between gravity models near the surface of the star.

Regarding the cooling process of neutron stars, there are several remarkable points to consider:

2.A The labeling of the models according with the total gravitational mass, $M_{\rm grav}$, instead of the surface one, $M_{\rm surf}$, is motivated by the fact that the former is the observed quantity at an infinite distance from the surface, not the latter. However, an observer at the surface of the star would feel a lower gravity since g_s is given by $M_{\rm surf}$ (Eq.5.28). This lower surface gravity turned out to be one of the major cause of differences in cooling behaviour found in Chapter 6.

2.B In Chapter 4, it was shown that the differential equations for the energy and heat-transport are apparently insensible to the gravity model chosen. This holds only if certain conditions are met: first, the model must admit an equivalence principle. Second, if additional scalar, vector or tensor fields are included in the lagrangian density of gravity, it must be verified that no thermodynamical consequences arise from their introduction. Third and final, if conformal transformations are invoked, one must be sure to solve both structure and thermal differential equations with the same metric functions.

Due to the invariance of the heat-transport and energy equations, the shape of the cooling curves is the same in both gravity models. However, there are slight differences between the curves of both gravity models:

2.B(a) The majority of the experiment pointed that $\alpha 9$ cooling curves are practically indistinguishable from GR's, either changing the EoS, the superfluidity model and/or the composition of the envelope. Noticable deviations between gravity models started to appear as $\alpha \to \alpha 12$.

We can infer that if future constraints over this parameter impose $\alpha \leq \alpha 9$, the cooling curves would not be a suitable candidate for spotting differences between αR^2 and GR.

On the other hand, the numerical results show that $\alpha 12$ models are in relative good agreement with observational data, thus leaving these models as viable.

2.B(b) As $\alpha \to \alpha 12$, a slight diminishing in T_e takes place, independently of the EoS, superfluidity model and composition of the envelope. This is a direct consequence of the lower surface gravity in the αR^2 model, in combination with the relationships $L \propto T_e^4 \propto g_s$ which hold at the surface of the star.

2.B(c) The increasing of light elements in the envelope translates in higher effective temperatures. This allows to explain some of the hottest stars of the sample, but this effect alone is not able to explain the coldest objects. Therefore, superfluidity is still needed to account for them.

2.B(d) The small change in the DUrca mass-threshold, for APR and MS-C1 in the $\alpha 12$ model, can be seen as responsible for the slow cooling of a 2 $M_\odot$ star, in contrast with its GR counterpart which cools much faster. However, this effect is EoS-dependent, as can be seen from the rapid cooling of MS-B1 and MS-C1 stars of the same mass (see Fig. 6.5), which allow the DUrca process in their cores (see Fig. 5.16). Here we also emphasize the fact that *the ocurrence of this process only depends on the micro-physics, not in the gravity model chosen.* The only structural difference between αR^2 and GR, related to DUrca process, is the slight increasing of the DUrca proper volume with $\alpha \to \alpha 12$. Nevertheless, this process still plays a key role in triggering the rapid cooling of NSs. More remarkable is the fact that the *Minimal Cooling scenario* remains plausible even in this gravity model, as can be seen when superfluidity enters in the modeling of thermal evolution.

Even in the presence of superfluidity the behaviour of the curves is strongly dependent in the DUrca mass-threshold. However, this mass threshold is modified when gravity is modified [**?**]. Therefore, it is important to take into account this limit for each EoS, in order to compare the constraints over mass and radius with other methods.

Finally, the presence of superfluidity, even in the quadratic model, seems to favourish the Minimal Cooling scenario. This is also confirmed from the results of Experiment 4, where considering only NSs with gravitational mass below the DUrca threshold one is capable of explaining most of the data.

Regarding further work, introducing rotation, magnetic field and accretion might be a challenge for cooling software based on the $f(R)$ equations of motion, due to the non-linearity and possibly the explicit dependence on the scalar curvature.

Appendix A

Useful theorems

A.1 Metric properties

Let ($g_{\mu\nu}, g^{\mu\nu}$,g) denote the metric tensor, its inverse and determinant. They satisfy the following properties:

1. Relation between differentials If $g_{\mu\nu}$, $g^{\mu\nu}$ are differenciable functions of their arguments, then

$$\delta g^{\nu\alpha} g_{\mu\nu} = -\delta g_{\mu\nu} g^{\nu\alpha} \tag{A.1}$$

Proof. Recall the relation between the metric tensor and its inverse,

$$g_{\mu\nu} g^{\nu\alpha} = \delta^{\alpha}_{\ \mu}.$$

Since the right hand side of the equation is a constant, the differencial of this expression yields

$$g_{\mu\nu}\delta g^{\nu\alpha} + g^{\nu\alpha}\delta g_{\mu\nu} = 0.$$

Therefore,

$$\delta g^{\nu\alpha} g_{\mu\nu} = -\delta g_{\mu\nu} g^{\nu\alpha}.$$

■

2. Derivative of the determinant Since $g_{\alpha\beta}$, $g^{\alpha\beta}$ are differentiable,

$$\delta g = g g^{\alpha\beta} \delta g_{\alpha\beta} \ . \tag{A.2}$$

3. Derivative of the square root. Under the assumption that $g_{\mu\nu}$, $g^{\mu\nu}$ and g are differentiable functions of their arguments,

$$\delta(\sqrt{-g}) = -\frac{1}{2}\sqrt{-g} g_{\mu\nu} \delta g^{\mu\nu} \ . \tag{A.3}$$

Proof. Since g is differenciable, we apply direct computation over $\sqrt{-g}$ and employ the previous property,

$$\delta(\sqrt{-g}) = -\frac{1}{2\sqrt{-g}}\delta g = -\frac{1}{2\sqrt{-g}} g g^{\alpha\beta}\delta g_{\alpha\beta} = \frac{1}{2\sqrt{-g}} g g_{\alpha\beta}\delta g^{\alpha\beta} \ .$$

Due to the fact that $g < 0$, $g = -(-g) = -\sqrt{-g}\sqrt{-g}$. Therefore,

$$\delta(\sqrt{-g}) = -\frac{1}{2}\sqrt{-g} g_{\alpha\beta}\delta g^{\alpha\beta} \ .$$

■

A.2 Propositions and theorems

Here we ennumerate and give proof for all the propositions and theorems introduced in Chapter 2.

Proposition 1: Palatini's Identity Let $R_{\mu\nu} = R^{\alpha}{}_{\mu\alpha\nu}$ be the Ricci tensor and ∇_μ the torsion-free covariant derivative. Then

$$\delta R_{\mu\nu} = \nabla_\alpha(\delta\Gamma^{\alpha}{}_{\mu\nu}) - \nabla_\nu(\delta\Gamma^{\gamma}{}_{\mu\gamma}) \tag{A.4}$$

Proof. To make calculations easier, the local flatness theorem is invoked to translate our expressions into simplified versions. Here the Riemann tensor is

$$R^{\alpha}{}_{\beta\gamma\epsilon} = \partial_\gamma\Gamma^{\alpha}{}_{\beta\epsilon} - \partial_\epsilon\Gamma^{\alpha}{}_{\beta\gamma} \ .$$

Applying variation on both sides

$$\delta R^{\alpha}{}_{\beta\gamma\epsilon} = \delta(\partial_\gamma\Gamma^{\alpha}{}_{\beta\epsilon}) - \delta(\partial_\epsilon\Gamma^{\alpha}{}_{\beta\gamma}) \ .$$

Assuming the continuity of the partial derivatives, the variation and the differentiation can be commuted,

$$\delta R^{\alpha}{}_{\beta\gamma\epsilon} = \partial_\gamma(\delta\Gamma^{\alpha}{}_{\beta\epsilon}) - \partial_\epsilon(\delta\Gamma^{\alpha}{}_{\beta\gamma}) \ .$$

For this tensorial equation to be valid in all the coordinate systems, the partial derivatives are replaced by covariant derivatives,

$$\delta R^{\alpha}{}_{\beta\gamma\epsilon} = \nabla_\gamma(\delta\Gamma^{\alpha}{}_{\beta\epsilon}) - \nabla_\epsilon(\delta\Gamma^{\alpha}{}_{\beta\gamma}) \ .$$

Finally, by contracting the first and third indices,

$$\delta R_{\beta\epsilon} = \nabla_\alpha(\delta\Gamma^{\alpha}{}_{\beta\epsilon}) - \nabla_\epsilon(\delta\Gamma^{\alpha}{}_{\beta\alpha}) \ .$$

■

Corollary 1: Palatini's Integral Let $R_{\mu\nu}$ be the Ricci tensor, ∇_μ the torsion-free covariant derivative. If $\delta\Gamma^{\mu}{}_{\alpha\beta}$ is identically zero for all μ, α, β at the boundary of some closed $\Omega \subset M$, then

$$I = \int_\Omega \sqrt{-g} g^{\mu\nu} \delta R_{\mu\nu} d^4x = 0 \tag{A.5}$$

Proof. From Palatini's identity, we have

$$I = \int_\Omega \sqrt{-g} g^{\mu\nu} \left[\nabla_\alpha (\delta\Gamma^{\alpha}{}_{\mu\nu}) - \nabla_\nu (\delta\Gamma^{\alpha}{}_{\mu\alpha}) \right] d^4x \ .$$

Since the covariant derivative of the metric tensor is zero,

$$I = \int_\Omega \sqrt{-g} \left[\nabla_\alpha (g^{\mu\nu}\delta\Gamma^{\alpha}{}_{\mu\nu}) - \nabla_\nu (g^{\mu\nu}\delta\Gamma^{\alpha}{}_{\mu\alpha}) \right] d^4x \ ,$$

$$I = \int_\Omega \sqrt{-g} \nabla_\alpha \left[g^{\mu\nu}\delta\Gamma^{\alpha}{}_{\mu\nu} - g^{\mu\alpha}\delta\Gamma^{\epsilon}{}_{\mu\epsilon} \right] d^4x \ .$$

Notice that the interior of the bracket defines a vector,

$$W^\alpha := g^{\mu\nu}\delta\Gamma^{\alpha}{}_{\mu\nu} - g^{\mu\alpha}\delta\Gamma^{\epsilon}{}_{\mu\epsilon} \ .$$

which is identically zero at $\partial\Omega$ by the hypothesis over the connection. Applying Gauss Law,

$$I = \int_\Omega \sqrt{-g} \nabla_\alpha W^\alpha d^4x = \int_{\partial\Omega} W^\alpha n_\alpha \sqrt{\gamma} d^3x = 0 \ .$$

■

Proposition 2: In a locally flat coordinate system, the 4-vector

$$W^\sigma = g^{\mu\nu}\delta\Gamma^{\sigma}{}_{\mu\nu} - g^{\mu\sigma}\delta\Gamma^{\nu}{}_{\mu\nu}$$

can be written as

$$W^\sigma = \partial^\sigma (g_{\mu\nu}\delta g^{\mu\nu}) - \partial^\mu (g_{\mu\nu}\delta g^{\sigma\nu}) \ . \tag{A.6}$$

Proof. Being a locally flat coordinate system, the first derivatives of the metric tensor and its inverse can be set to zero, but not their second order derivatives. Thus, the first term on the right hand side of the vector definition is:

$$g^{\mu\nu}\delta\Gamma^{\sigma}{}_{\mu\nu} = g^{\mu\nu}\delta \left[\frac{1}{2} g^{\sigma\alpha} \left(\partial_\mu g_{\nu\alpha} + \partial_\nu g_{\mu\alpha} - \partial_\alpha g_{\mu\nu} \right) \right]$$

$$g^{\mu\nu}\delta\Gamma^{\sigma}{}_{\mu\nu} = \frac{1}{2} g^{\mu\nu} g^{\sigma\alpha} \left[\partial_\mu (\delta g_{\nu\alpha}) + \partial_\nu (\delta g_{\mu\alpha}) - \partial_\alpha (\delta g_{\mu\nu}) \right]$$

$$g^{\mu\nu}\delta\Gamma^{\sigma}{}_{\mu\nu} = \frac{1}{2} g^{\mu\nu} \left[\partial_\mu (g^{\sigma\alpha}\delta g_{\nu\alpha}) + \partial_\nu (g^{\sigma\alpha}\delta g_{\mu\alpha}) - g^{\sigma\alpha}\partial_\alpha (\delta g_{\mu\nu}) \right] \ ,$$

$$g^{\mu\nu}\delta\Gamma^{\sigma}{}_{\mu\nu} = \frac{1}{2}g^{\mu\nu}\left[-\partial_\mu(g_{\nu\alpha}\delta g^{\sigma\alpha}) - \partial_\nu(g_{\mu\alpha}\delta g^{\sigma\alpha}) - g^{\sigma\alpha}\partial_\alpha(\delta g_{\mu\nu})\right] ,$$

$$g^{\mu\nu}\delta\Gamma^{\sigma}{}_{\mu\nu} = -\frac{1}{2}\partial^\nu(g_{\alpha\nu}\delta g^{\alpha\sigma}) - \frac{1}{2}\partial^\mu(g_{\alpha\mu}\delta g^{\alpha\sigma}) - \frac{1}{2}g^{\mu\nu}\partial^\sigma(\delta g_{\mu\nu}) ,$$

$$g^{\mu\nu}\delta\Gamma^{\sigma}{}_{\mu\nu} = -\partial^\mu(g_{\alpha\mu}\delta g^{\alpha\sigma}) + \frac{1}{2}\partial^\sigma(g_{\mu\nu}\delta g^{\mu\nu}) . \tag{A.7}$$

Now, the second term on the right hand side of the original expression is

$$g^{\mu\sigma}\delta\Gamma^{\nu}{}_{\mu\nu} = \frac{1}{2}g^{\mu\sigma}\partial_\mu(g^{\nu\alpha}\delta g_{\nu\alpha}) ,$$

$$g^{\mu\sigma}\delta\Gamma^{\nu}{}_{\mu\nu} = -\frac{1}{2}\partial^\sigma(g_{\nu\alpha}\delta g^{\nu\alpha}) . \tag{A.8}$$

By substitution of eqs. A.7 and A.8 in the definition of the vector,

$$W^\sigma = \partial^\sigma(g_{\mu\nu}\delta g^{\mu\nu}) - \partial^\mu(g_{\mu\nu}\delta g^{\sigma\nu}) .$$

■

Theorem 1: Let A be a scalar and differenciable function, $\Omega \subset M$ a closed set. If $\delta g^{\mu\nu}$, $\delta\Gamma^{\alpha}{}_{\mu\nu}$ are identically zero for all α, μ, ν at $\partial\Omega$, then

$$\int_\Omega d^4x\sqrt{-g}Ag^{\mu\nu}\delta R_{\mu\nu} = \int_\Omega d^4x\sqrt{-g}\delta g^{\mu\nu}\left[g_{\mu\nu}\partial^\sigma\partial_\sigma A - \partial_\mu\partial_\nu A\right] . \tag{A.9}$$

Proof. The integral to compute is

$$J = \int_\Omega d^4x\sqrt{-g}Ag^{\mu\nu}\delta R_{\mu\nu} = \int_\Omega d^4x\sqrt{-g}A\nabla_\sigma W^\sigma .$$

It is immediate to re-write this as

$$J = \int_\Omega d^4x\sqrt{-g}\left[\nabla_\sigma(AW^\sigma) - (\partial_\sigma A)W^\sigma\right] .$$

Applying Gauss' Law over the first summand and considering that $W^\sigma = 0$ due to our hypothesis over the variations at $\partial\Omega$, we see that

$$\int_\Omega d^4x\sqrt{-g}\nabla_\sigma\left[AW^\sigma\right] = \int_{\partial\Omega} d^3x\sqrt{\gamma}AW^\sigma n_\sigma = 0 .$$

Thus,

$$J = -\int_\Omega d^4x\sqrt{-g}\,(\partial_\sigma A)\,W^\sigma .$$

To keep things simple, we move to a locally flat coordinate system. From the previous proposition,

$$J = \int_\Omega d^4x\sqrt{-g}\partial_\sigma A\ \left[\partial^\mu(g_{\mu\nu}\delta g^{\sigma\nu}) - \partial^\sigma(g_{\mu\nu}\delta g^{\mu\nu})\right] . \tag{A.10}$$

For both summands on the right hand side, we use integration by parts. Again, there are terms that can be set to zero due to Gauss' Law and the hypothesis of nullity over $\delta g^{\mu\nu}$ and $\delta\Gamma^{\alpha}_{\ \mu\nu}$:

First term

$$\int_\Omega d^4x\sqrt{-g}\partial_\sigma A\partial^\mu(g_{\mu\nu}\delta g^{\sigma\nu}) = \int_\Omega d^4x\sqrt{-g}\left\{\partial^\mu\left[g_{\mu\nu}\delta g^{\sigma\nu}\partial_\sigma A\right] - g_{\mu\nu}\delta g^{\sigma\nu}\partial^\mu\partial_\sigma A\right\}$$

$$\int_\Omega d^4x\sqrt{-g}\partial_\sigma A\partial^\mu(g_{\mu\nu}\delta g^{\sigma\nu}) = -\int_\Omega d^4x\sqrt{-g}g_{\mu\nu}\delta g^{\sigma\nu}\partial^\mu\partial_\sigma A\ . \tag{A.11}$$

Second term

$$-\int_\Omega d^4x\sqrt{-g}\partial_\sigma A\partial^\sigma(g_{\mu\nu}\delta g^{\mu\nu}) = -\int_\Omega d^4x\sqrt{-g}\left\{\partial^\sigma\left[g_{\mu\nu}\delta g^{\mu\nu}\partial_\sigma A\right] - g_{\mu\nu}\delta g^{\mu\nu}\partial^\sigma\partial_\sigma A\right\}$$

$$-\int_\Omega d^4x\sqrt{-g}\partial_\sigma A\partial^\sigma(g_{\mu\nu}\delta g^{\mu\nu}) = \int_\Omega d^4x\sqrt{-g}g_{\mu\nu}\delta g^{\mu\nu}\partial^\sigma\partial_\sigma A\ . \tag{A.12}$$

Substitution of eqs. A.11 and A.12 in A.10 leads to

$$J = \int_\Omega d^4x\sqrt{-g}\left[g_{\mu\nu}\delta g^{\mu\nu}\partial^\sigma\partial_\sigma A - g_{\mu\nu}\delta g^{\sigma\nu}\partial^\mu\partial_\sigma A\right]\ ,$$

$$J = \int_\Omega d^4x\sqrt{-g}\delta g^{\mu\nu}\left[g_{\mu\nu}\partial^\sigma\partial_\sigma A - \partial_\mu\partial_\nu A\right]\ .$$

■

Appendix B

Identities for the SSS metric

B.1 Christoffel symbols and Einstein tensor

The following matrices contain the Christoffel symbols, arranged in the order (ct, r, θ, ϕ) from left to right and from up to down. We find this notation suitable for saving space. Here, $\partial_\beta = \partial/\partial x^\beta$.

$$[\Gamma^t{}_{\alpha\beta}] = \begin{pmatrix} 0 & \partial_r\Phi & 0 & 0 \\ \partial_r\Phi & 0 & 0 & 0 \\ 0 & 0 & 0 & 0 \\ 0 & 0 & 0 & 0 \end{pmatrix}$$

$$[\Gamma^r{}_{\alpha\beta}] = \begin{pmatrix} \exp(2(\Phi-\Lambda))\partial_r\Phi & 0 & 0 & 0 \\ 0 & \partial_r\Lambda & 0 & 0 \\ 0 & 0 & -r\exp(-2\Lambda) & 0 \\ 0 & 0 & 0 & -r sen^2\theta \exp(-2\Lambda) \end{pmatrix}$$

$$[\Gamma^\theta{}_{\alpha\beta}] = \begin{pmatrix} 0 & 0 & 0 & 0 \\ 0 & 0 & 1/r & 0 \\ 0 & 1/r & 0 & 0 \\ 0 & 0 & 0 & 0 \end{pmatrix} \quad , \quad [\Gamma^\phi{}_{\alpha\beta}] = \begin{pmatrix} 0 & 0 & 0 & 0 \\ 0 & 0 & 0 & 1/r \\ 0 & 0 & 0 & 0 \\ 0 & 1/r & 0 & 0 \end{pmatrix}$$

Regarding the Einstein tensor, the only non-vanishing components are

$$G_{00} = \frac{e^{2\Phi}}{r^2}\frac{d}{dr}\left[r\left(1-e^{-2\Lambda}\right)\right] \ , \quad G_{rr} = -\frac{e^{2\Lambda}}{r^2}\left(1-e^{-2\Lambda}\right) + \frac{2}{r}\partial_r\Phi \ ,$$

$$G_{\theta\theta} = r^2 e^{-2\Lambda}\left[\partial_r^2\Phi + (\partial_r\Phi)^2 + \frac{\partial_r\Phi - \partial_r\Lambda}{r} - \partial_r\Phi\ \partial_r\Lambda\right] \ , \quad G_{\phi\phi} = \sin^2\theta G_{\theta\theta} \ .$$

B.2 Energy-momentum tensor identity

In Chapter 4, we stated that

$$\Gamma^{r}{}_{\beta\epsilon}T^{\epsilon\beta} + \Gamma^{\beta}{}_{\beta\epsilon}T^{r\epsilon} = e^{-2\Lambda}\epsilon\partial_r\Phi + e^{-2\Lambda}P(\partial_r\Phi + 2\partial_r\Lambda) \ . \tag{B.1}$$

Proof. Since $T^{\mu\nu}$ is diagonal,

$$\Gamma^{r}{}_{\beta\epsilon}T^{\epsilon\beta} = \Gamma^{r}{}_{00}T^{00} + \Gamma^{r}{}_{rr}T^{rr} + \Gamma^{r}{}_{\theta\theta}T^{\theta\theta} + \Gamma^{r}{}_{\phi\phi}T^{\phi\phi} \ .$$

From the explicit form of the Christoffel symbols,

$$\Gamma^{r}{}_{\beta\epsilon}T^{\epsilon\beta} = e^{2(\Phi-\Lambda)}\partial_r\Phi T^{00} + \partial_r\Lambda T^{rr} - re^{-2\Lambda}T^{\theta\theta} - re^{-2\Lambda}sen^2\theta T^{\phi\phi} \ .$$

Replacing the components of the energy-momentum tensor,

$$\Gamma^{r}{}_{\beta\epsilon}T^{\epsilon\beta} = e^{2(\Phi-\Lambda)}\partial_r\Phi e^{-2\Phi}\epsilon + \partial_r\Lambda e^{-2\Lambda}P - re^{-2\Lambda}Pr^{-2} - re^{-2\Lambda}sen^2\theta r^{-2}sen^{-2}\theta \ ,$$

it follows that

$$\Gamma^{r}{}_{\beta\epsilon}T^{\epsilon\beta} = e^{-2\Lambda}\epsilon\partial_r\Phi + e^{-2\Lambda}P\partial_r\Lambda - \frac{2e^{-2\Lambda}P}{r}$$

$$\Gamma^{r}{}_{\beta\epsilon}T^{\epsilon\beta} = e^{-2\Lambda}\epsilon\partial_r\Phi + e^{-2\Lambda}P\left[\partial_r\Lambda - 2r^{-1}\right] \ . \tag{B.2}$$

Regarding the second term on the left hand side of eq.B.1, we see that

$$\Gamma^{\beta}{}_{\beta r}T^{rr} = \left[\Gamma^{0}{}_{0r} + \Gamma^{r}{}_{rr} + \Gamma^{\theta}{}_{\theta r} + \Gamma^{\phi}{}_{\phi r}\right]T^{rr} \ .$$

By substitution of Christoffel symbols,

$$\Gamma^{\beta}{}_{\beta r}T^{rr} = \left[\partial_r\Phi + \partial_r\Lambda + r^{-1} + r^{-1}\right]T^{rr} \ ,$$

$$\Gamma^{\beta}{}_{\beta r}T^{rr} = \left[\partial_r\Phi + \partial_r\Lambda + 2r^{-1}\right]e^{-2\Lambda}P \ . \tag{B.3}$$

The sum of eqs.B.2 and B.3 leads to

$$\Gamma^{r}{}_{\beta\epsilon}T^{\epsilon\beta} + \Gamma^{\beta}{}_{\beta\epsilon}T^{r\epsilon} = e^{-2\Lambda}\epsilon\partial_r\Phi + e^{-2\Lambda}P(\partial_r\Phi + 2\partial_r\Lambda) \ .$$

■

Bibliography

[1] Lattimer J. H., ARNPS 62 (2012) 485.

[2] Özel F. & Freire P, ARA&A 54 (2016) 401.

[3] Raaijmakers G. *et al* ApJ 893 (2020) id.21.

[4] Planck Collaboration, *Planck 2018 results. I. Overview and the cosmological legacy of Planck*, Astron. Astrophys. 641 (2020) A1

[5] Schutz B. *A First Course in General Relativity*, Cambridge University Press, 2000.

[6] Misner, C.W., Thorne, K.S. & Wheeler, J.A. 1973, *Gravitation* (San Franciso; Freeman).

[7] Wald, R.M. *General Relativity*, The University of Chicago Press, 1984.

[8] Hawking, S.F., Ellis, G.F.R., *The large scale structure of space-time*. Cambridge University Press, 1973.

[9] Schutz, B.F. 1970, *Phys. Rev.* D 2 2762.

[10] Brown, J.D. 1993, *Class. Quantum Grav.* 10 1579.

[11] Harko, T., Lobo, F.S.N., *Extensions of f(R) Gravity. Curvature-Matter Couplings and Hybrid Metric-Palatini Theory*. Cambridge University Press, 2019.

[12] Fisher, S.B., Carlson, E.D., 2019 *Phys. Rev. D*, 100, 064059.

[13] Stoytcho S. Yazadjiev *et al* JCAP06(2014)003.

[14] Jaime, L.G. et al, 2011, *Phys. Rev.* D 83, 024039.

[15] Capozziello, S., de Laurentis, M. Phys. Rep. 509 (2011) 167.

[16] Astashenok, A.V., Baigashov, A.S., Lapin, S.A., *Int. J. Geom. Methods Mod. Phys.* 6 (2019) 1950004.

[17] Feola, P., et al.,*Phys. Rev. D*, 101, 044037 (2020).

[18] Cooney, A., DeDeo, S., Psaltis, D. *Phys. Rev. D* 82, 064033 (2010).

[19] Arapoglu, S. et al JCAP07 (2011) 020.

[20] Astashenok, A.V. et al JCAP12 (2013) 040.

[21] Yazadjiev, S.S., Doneva, D.D., Kokkotas, K.D. Eur. Phys. J. C (2018) 78:818.

[22] Buchdahl, H.A. *On the gravitational field equations arising from the square of the gaussian curvature. Nuovo Cim* 23, 141-157 (1962).

[23] Astashenok, A.V. et al, 2017, *Class. Quantum Grav.* 34, 205008.

[24] Berry, C.P. & Gair, J.R., 2011 *Physical Review D*, 83 104022.

[25] J. Näf and P. Jetzer, *Phys. Rev. D* 81, 104003 (2010).

[26] Faraoni, V., Gunzig, E. *Einstein Frame or Jordan Frame?. International Journal of Theoretical Physics* 38, 217-225 (1999).

[27] Quiros, I., Garcia-Salcedo, R., Aguilar, J.E.M. and Matos, T., "The conformal transformation's controversy: what are we missing?". Gen, Rel. Gravit. 45, 489 (2013)

[28] Akmal, A., Pandharipande, V.R., Ravenhall, D.G., *Phys. Rev. C*, 58, 1804 (1998).

[29] Douchin, F., Haensel, P. A& A 380, 151-167 (2001).

[30] Muether, H., Prakash, M., Ainsworth, T.L. *Phys. Lett. B*, 199, 4. (1987).

[31] Müller, H., Serot, B.D., 1996, Nuc. Phys. A. 606, 508-537.

[32] Page, D., et al, 2020 ApJ 898 125.

[33] Demorest, P., Pennucci, T., Ransom, S. et al. A two-solar-mass neutron star measured using Shapiro delay. Nature 467, 1081–1083 (2010).

[34] J. Antoniadis et al., Science 340, 1233232 (2013).

[35] Cromartie, H. T., Fonseca, E., Ransom, S. M., et al. 2019, NatAs, 4, 72

[36] Thorne KS. 1977. *Astrophys. J.* 212:825–31

[37] Yakovlev, D.G. & Pethick, C.J. Ann. Rev. Astron. Astrophys. 42 (2004) 169.

[38] Lander, S.K., Andersson, N. MNRAS 479, 4207-4215 (2018).

[39] Dommes, V.A., Gusakov, M.E., Shternin, P.S., *Phys. Rev. D* 101, 103020 (2020).

[40] Migdal, A.B. 1959, *Nuc.Phys.* 13:655-74.

[41] Baym, G., Pethick, C., Pines, D. et al. Spin Up in Neutron Stars : The Future of the Vela Pulsar. *Nature* 224, 872–874 (1969).

[42] Page, D. 2009, in *Neutron Stars and Pulsars*, Astrophysics and Space Science Library, Vol. 357, ed. W. Becker (Berlin: Springer),247.

[43] Page, D., Geppert, U., & Weber, F. 2006, Nuclear Physics A, 777, 497.

[44] Page, D., & Reddy, S. 2006, Annu. Rev. Nucl. Part. Sci., 56, 327.

[45] Gudmundsson, E.H., Pethick, C.J., Epstein, R.I., Astrophys. J., 259, L19 (1982).

[46] Potekhin, A.Y., Chabrier, G., Yakovlev, D.G., Astron. Astrophys. 323, 415-428 (1997).

[47] D. Page, J. M. Lattimer, M.Prakash, & A. W. Steiner in "Novel Superfluids", vol 2, Ed. K. H. Bennemann and J. B. Ketterson, International Series of Monographs on Physics - 157, (Oxford Science Publications), p. 505-579 (2014).

[48] Yakovlev, D. G.; Kaminker, A. D.; Gnedin, O. Y.; Haensel, P., 2001 Phys.Rep. 354, 1-155.

[49] Abbott, B.P., et.al. *Phys. Rev. Lett.* 119, 161101 (2017).

[50] Press, W.H., Teukolsky, S.A., Vetterling, W.T., Flannery, B.P. *Numerical Recipes in Fortran 77. The Art of Scientific Computing. Second Edition.* Cambridge University Press, 1992.

[51] Shapiro, S. L. & Teukolsky S. A. *Balck Holes, White Dwarfs and Neutron Stars: the Physics of Compact Objects*, John Wiley & Sons, 1983.

[52] Capozziello, S., De Laurentis, M., Farinelli, R., Odinstov, S.D. *Phys.Rev. D.* 93, 023501 (2016).

[53] Yazadjiev, S.S., Doneva, D.D. *Comment on "The Mass-Radius relation for Neutron Stars in $f(R)$ gravity" by S.Capozziello, M.De Laurentis, R.Farinelli and S.Odinstov.* arXiv:1512.05711

[54] Everitt, C.W.F. et al, *Phys. Rev. Lett.* 106, 221101 (2011).

[55] Page, D. et al, 2004, ApJS 155 623.

[56] Page, D. 2016, NSCool: Neutron star cooling code. `http://ascl.net/1609.009`

[57] Schwenk, A., Friman, B., Brown, G.E., 2003, Nuclear Physics A 713, 191-216.

[58] Chen, J.M.C., Clark, J.W., Dave, R.D., Khodel, V.V., 1993, Nuclear Physics A 555, 59-89.

[59] Wambach, J., Ainsworth, T. L., & Pines, D. 1993, Nucl. Phys. A, 555, 128.

[60] Gezerlis, A., Carlson, J. *Phys. Rev. C* 77, 032801 (R) (2008).

[61] Wiringa, R.B. and Pieper, S. C., *Phys. Rev. Lett.* 89, 182501 (2002).

[62] Gandolfi, S., Illarionov, A. Y., Fantoni, S., Pederiva, F., & Schmidt, K. E., *Phys.Rev.Lett.* 101, 132501 (2008).

[63] Hoffberg, M., Glassgold, A.E., Richardson, R.W., Ruderman, M. *Phys. Rev. Lett.* 24, 775 (1970).

[64] Amundsen, L., & Østgaard, E. 1985, Nucl. Phys. A, 437, 487

[65] Lagaris, I.E., Pandharipande, V.R., 1981, Nuclear Physics A 359, 349-364.

[66] Baldo, M., Cugnon, J., Lejeune, A., Lombardo, U., 1992, Nuclear Physics A 536, 349-365.

[67] Page, D., Lattimer, J.M., Prakash, M., Steiner, A.W. Astrophys. J., 707, 1131-1140 (2009).

[68] Heinke, C. O., & Ho, W.C.G., Astrophys. J., 719, L167-L171 (2010).

[69] Page, D., Prakash, M., Lattimer, J.M., Steiner, A.W. *Phys. Rev. Lett.* 106, 081101 (2011).

[70] Shternin, P.S., Yakovlev, D.G., Heinke, C.O., Ho, W.C.G, Patnaude, D.J. Mon. Not. R. Astron. Soc. 412, L108–L112 (2011).

[71] Chao, N.-C., Clark, J. W., & Yang, C.-H. 1972, Nucl. Phys. A, 179, 320.

[72] Tamagaki, R. Prog. Theor. Phys. 39 (1968) 91-107.

[73] Takatsuka, T. Prog. Theor. Phys. 47 (1972) 1062-1064.

[74] Takatsuka, T. Prog. Theor. Phys. 50 (1973) 1754-1755.

[75] Niskanen, J. A., & Sauls, J. A. 1981, preprint, unpublished.

[76] Yakovlev, Kaminker, & Gnedin, A&A 379, L5 (2001)

[77] Kaminker, Yakovlev, & Gnedin, A&A 383, 1076 (2002)

[78] Yakovlev, Kaminker, Haensel, & Gnedin, A&A 389, L24 (2002).

[79] Beznogov, M. V., & Yakovlev, D. G., Mon. Not. R. Astron. Soc. 447, 1598–1609 (2015).

[80] Sotani, H., Kokkotas, K.D., *Phys. Rev. D* 97, 124034 (2018).

[81] Arnold, C., Leo, M., Baojiu, L. *Realistic simulations of galaxy formation in f(R) modified gravity.* Nat Astron 3, 945–954 (2019).

[82] Dohi, A. et al. arXiv:2003.12571.